Geoinformatics

Geoinformatics FCE CTU 2015

Geoinformatics

Faculty of Civil Enginnering

Czech Technical University in Prague

Volume 14, Issue 1

Geoinformatics FCE CTU, Czech Technical University in Prague **ISSN 1802-2669**

This issue was prepared from the input files supplied by the authors. No additional English style corrections of the articles were made by the compositor.

Published by Czech Technical University in Prague.

Contents

New publishing standards in Geoinformatics FCE CTU

Editorial

Dear Readers,

At the Central Library of the Czech Technical University In Prague, we were delighted to have been approached by the editor in chief of Geoinformatics FCE CTU, prof. Aleš Čepek, with a request to use our library services in the area of scientific journals publishing.

Geoinformatics FCE CTU journal (GI) presents significant research in their discipline. Numerous articles published in GI have been cited by journals covered by the citation databases Web of Science and Scopus. The cooperation with the Central library brought GI not only the implementation of new publishing standards but also new online presentation.

The first significant change was transferring the journal onto the Open Journal Systems (OJS) publishing platform. This journal management system is based on open source software designed for managing and publishing electronic journals. It offers automation of repetitive editorial activities and provides a user friendly website. OJS was developed and is further supported and freely provided within the Public Knowledge Project under the GNU General Public License.

For its readers, GI through OJS brings a clear and fast presentation of individual articles and issues with a preview of the full texts before downloading them and also an effective way to search in the archives. For the authors, OJS provides simple and transparent environment, where they can submit new manuscripts, monitor progress of the review process, upload the revised version, and upload finalized proofreading. At reviewers' disposal is a questionnaire and space for comments to the authors and the concluded comments to the editor. The editors take the advantage of the automation of individual editorial process (pre-set e-mails, automatic notification of deadlines, assigning reviewers). All these tools and functionality together enable highly transparent and effective review process.

PKP
PUBLIC KNOWLEDGE PROJECT

Open Journal Systems further provides the possibility of assigning published articles with DOI (Digital Object Identifier), an international and unique persistent identifier of an electronic document, which provides permanent link to the document. Since CTU in Prague is a member of CrossRef registration agency via the Central Library, all contributions in the GI journal are now assigned with DOIs.

Both, OJS and DOI are further connected with ORCID – a unique author's identifier; authors can specify their ORCID when registering to OJS. ORCID is used to uniquely link the work to the authors. Both, DOI and ORCID can be advantageously used in databases such as Scopus or Web of Science, and in the social networks environment, such as ResearchGate.

GI is currently indexed by DOAJ database. Evaluation to Engineering Village, an Elsevier platform, is in process. This platform helps companies keep pace with scientific and technological developments and open chances for the future.

Geoinformatics FCE CTU journal now brings its authors all publishing standards used in international journals. To the community of readers in this discipline, journal presents the high-quality articles published in an attractive and user-friendly environment.

We wish the readers and editors continuous quality improvement and much success for the future.

Iva Adlerová
Lenka Němečková
CTU in Prague – Central Library

Evaluation of the gravity field model EIGEN-6C4 in comparison with EGM2008 by means of various functions of the gravity potential and by GNSS/levelling

Jan Kostelecký[1,2], Jaroslav Klokočník[4], Blažej Bucha[5], Aleš Bezděk[4] and Christoph Förste[3]

[1]Research Institute of Geodesy, Topography and Cartography (VÚGTK) p.r.i., CZ - 20566 Zdiby
[2]Institute of Geodesy and Mining Surveying, HGF TU Ostrava
CZ – 708 33 Ostrava-Poruba, Czech Republic, kost@fsv.cvut.cz
[3]GFZ German Research Centre for Geosciences, Dept. Geodesy and Remote Sensing,
Telegrafenberg, D – 14473 Potsdam, Germany, foer@gfz-potsdam.de
[4]Astronomical Institute, Academy of Sciences of the Czech Republic, p.r.i. (ASÚ),
CZ – 251 65 Ondřejov Observatory, jklokocn@asu.cas.cz, bezdek@asu.cas.cz
[5]Department of Theoretical Geodesy, Faculty of Civil Engineering, STU in Bratislava,
SK – 81005 Bratislava, blazej.bucha@gmail.com

Abstract

The combined gravity field model EIGEN-6C4 (Förste et al., 2014) is the latest combined global gravity field model of GeoForschungsZentrum (GFZ) Potsdam and Groupe Recherches Geodesie Spatiale (GRGS) Toulouse. EIGEN-6C4 has been generated including the satellite gravity gradiometry data of the entire GOCE (Gravity and Ocean Circulation Experiment mission, November 2009 till October 2013, see i.e. Floberghagen et al., 2011 [4], Rummel et al., 2011 [13]) and is of maximum spherical degree and order 2190. In this study EIGEN-6C4 has been compared with the Earth's gravity field model EGM2008 to its maximum degree and order via gravity disturbances and the Tzz part of the Marussi tensor of the second derivatives of the disturbing potential. The emphasis is put on such areas where GOCE data (complete set of gradiometry measurements after reductions) in EIGEN-6C4 obviously contributes to an improvement of the gravity field description. GNSS/levelling geoid heights are independent data source for the evaluation of gravity field models. Therefore, we use the GNSS/levelling data sets over the territories of Europe, USA, Canada, Brazil, Japan, Czech Republic and Slovakia for the evaluation of EIGEN-6C4 w.r.t. EGM2008.

1. Theory

1.1. Gravitational potential and Marussi tensor

The disturbing static gravitational potential outside the Earth masses in spherical coordinates in spherical expansion reads

$$V(r,\varphi,\lambda) = \frac{GM}{r}\sum_{l=2}^{\infty}\sum_{m=0}^{l}\left(\frac{R}{r}\right)^{l}\left(C'_{l,m}\cos m\lambda + S_{l,m}\sin m\lambda\right)P_{l,m}(\sin\varphi) \qquad (1)$$

where GM is a product of the universal gravity constant and the mass of the Earth (known from satellite analyses as a geocentric gravitational constant), r is the radial distance of an external point where V is computed, the symbol R is for the radius of the Earth (which can be approximated by the semi-major axis of a reference ellipsoid), $P_{l,m}(sin\varphi)$ are Legendre associated functions, l and m are the degree and order of the harmonic expansion, (φ, λ) are geocentric latitude and longitude, $C'_{l,m}$ and $S_{l,m}$ are harmonic geopotential coefficients (Stokes parameters), fully normalized, $C'_{l,m} = C_{l,m} - C^{el}_{l,m}$, where $C^{el}_{l,m}$ belongs to the reference ellipsoid.

In our comparisons we will use spherically approximated **gravity anomaly** Δg, defined as

$$\Delta g = \frac{-\partial V}{\partial r} - 2\frac{V}{r} \tag{2}$$

and **Marussi tensor**.

The gravity gradient tensor Γ (the Marussi tensor) is a tensor of the second derivatives of the disturbing potential V and is computed by means of C'_{lm}, S_{lm} of the particular gravity field model known to the maximum degree $l_{\max}$

$$\Gamma = \begin{bmatrix} \Gamma_{11} & \Gamma_{12} & \Gamma_{13} \\ \Gamma_{21} & \Gamma_{22} & \Gamma_{23} \\ \Gamma_{31} & \Gamma_{32} & \Gamma_{33} \end{bmatrix} = \begin{bmatrix} \frac{\partial^2 V}{\partial x^2} & \frac{\partial^2 V}{\partial x \partial y} & \frac{\partial^2 V}{\partial x \partial z} \\ \frac{\partial^2 V}{\partial y \partial x} & \frac{\partial^2 V}{\partial y^2} & \frac{\partial^2 V}{\partial y \partial z} \\ \frac{\partial^2 V}{\partial z \partial x} & \frac{\partial^2 V}{\partial z \partial y} & \frac{\partial^2 V}{\partial z^2} \end{bmatrix} \tag{3}$$

If we use a local coordinate system in point P and basis vectors are oriented to south-north-radial direction, where r means radial direction, we can write

$$\Gamma_{33} = \frac{\partial^2 V}{\partial z^2} = \frac{\partial^2 V}{\partial r^2} = T_{zz}. \tag{4}$$

where T_{zz} is the second derivatives of the disturbing potential in radial direction. All these values were computed by software developed by Bucha and Janák, 2013 [2].

1.2. GNSS/levelling – method

A network of geodetic points with levelling heights and observable with GNSS techniques has been established on the different territories of the world. It enables a direct computation of the geoid (if we use thru ortometric heights) or quasigeoid (if we use normal Molodensky heights) undulation ξ according to a simple formula

$$\xi = h_{GNSS} - H_n + \{2\}, \tag{5}$$

where h_{GNSS} is the ellipsoidal height with respect to a reference ellipsoid (here we used GRS80 in all cases) derived from GNSS measurements, H_n is the physical (sea-level) height derived from the levelling, here the normal height according to Molodensky in the Baltic vertical datum, and $\{2\}$ are small terms of the second order, accounting for the curvature of the plumb line. The method is described in Kostelecký et al., 2012 [8].

2. The Gravity Field Model EIGEN-6C4

EIGEN-6C4 (European Improved Gravity model of the Earth by New techniques) is a static global combined gravity field model up to degree and order 2190. It has been elaborated jointly by GFZ Potsdam and GRGS Toulouse and contains the following satellite and ground data:

- LAGEOS-1/2 (deg. 2 - 30): Satellite Laser Ranging data 1985 - 2010
- GRACE, GNSS-SST and K-band range-rate data, processing according to RL03 GRGS (deg. 2 - 130): ten years 2003 - 2012
- GOCE, Satellite Gravity Gradiometry (SGG) data, processed by the direct approach including the gravity gradient components Txx, Tyy, Tzz and Txz out of the following time spans: 837 days out of the nominal mission time span 20091101 – 20120801, 422 days out of the lower orbit phase between 20120801 – 20131020. These GOCE data as well as the LAGEOS and GRACE data are the same as used for the 5th release of ESA's satellite-only gravity field model via the direct approach GO_CONS_GCF_2_DIR_R5 (Pail et al., 2011 [10] and Bruinsma et al., 2014 [1]). For EIGEN-6C4, the GOCE polar gaps were stabilized by the Spherical Cap Regularization using the combined gravity field model EIGEN-6C3stat
- terrestrial data (max degree 370): DTU12 ocean geoid data and an EGM2008 geoid height grid for the continents.

The combination of these different satellite and surface data sets has been done by a band-limited combination of normal equations (to maximum degree/order 370), which are generated from observation equations for the spherical harmonic coefficients (e. g. Shako et al., 2013 [14]). The resulted solution to degree/order 370 has been extended to degree/order 2190 by a block diagonal solution using the DTU10 global gravity anomaly data grid.

3. Models tested and differences between them

The topic and the method are well-established. We continue the work of many other authors. Here we report about our recent tests with EGM2008 (Pavlis et al., 2008, 2012 [11, 12]) and EIGEN-6C4 (Förste et al., 2014 [5]).

The models are compared by means of gravity disturbances, part of Marussi tensor elements, (for theory and examples of various applications see Kalvoda et al., 2013 [6]; Klokočník et al., 2014 [7]) and via GNSS/levelling.

Regional differences for Himalaya, Ethiopia, Egypt, Europe, and specifically for the Czech Republic are presented. Much more examples are available but cannot be presented due to the lack of space. We selected the following examples: first for an area in the Himalaya (Figs. 1 a,b,c,d) with a low quality of terrestrial data in both models (fill-in data) in a remote area with mountains, Ethiopia (Figs. 2 a,b,c,d) - one in the area with better data, outside Europe with very rich river system and erosion, Egypt – old and present Nil river (Figs. 3 a,b,c,d), for Europe (Figs. 4 a,b,c,d) and for the Czech Republic (Figs. 5 a,b,c,d). GNSS/levelling data for Europe (Figs. 6 a,b) comes from EVRS 1997 campaign, and for the Czech Republic (Figs. 7 a,b,c) and Slovakia (Figs. 8 a,b) the high quality terrestrial data

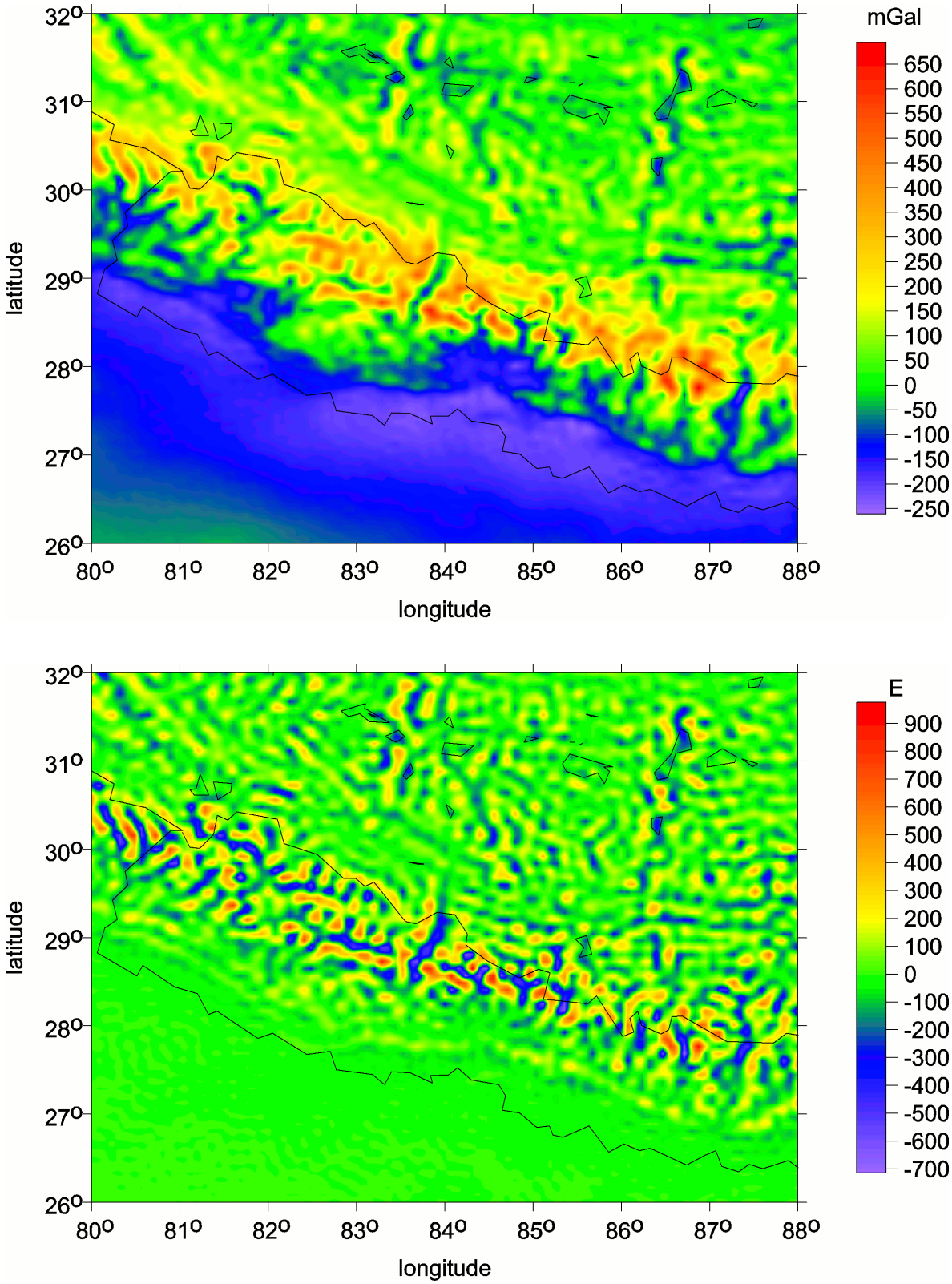

Figure 1 a, b: EIGEN-6C4, Himalaya Δg and T_{zz}

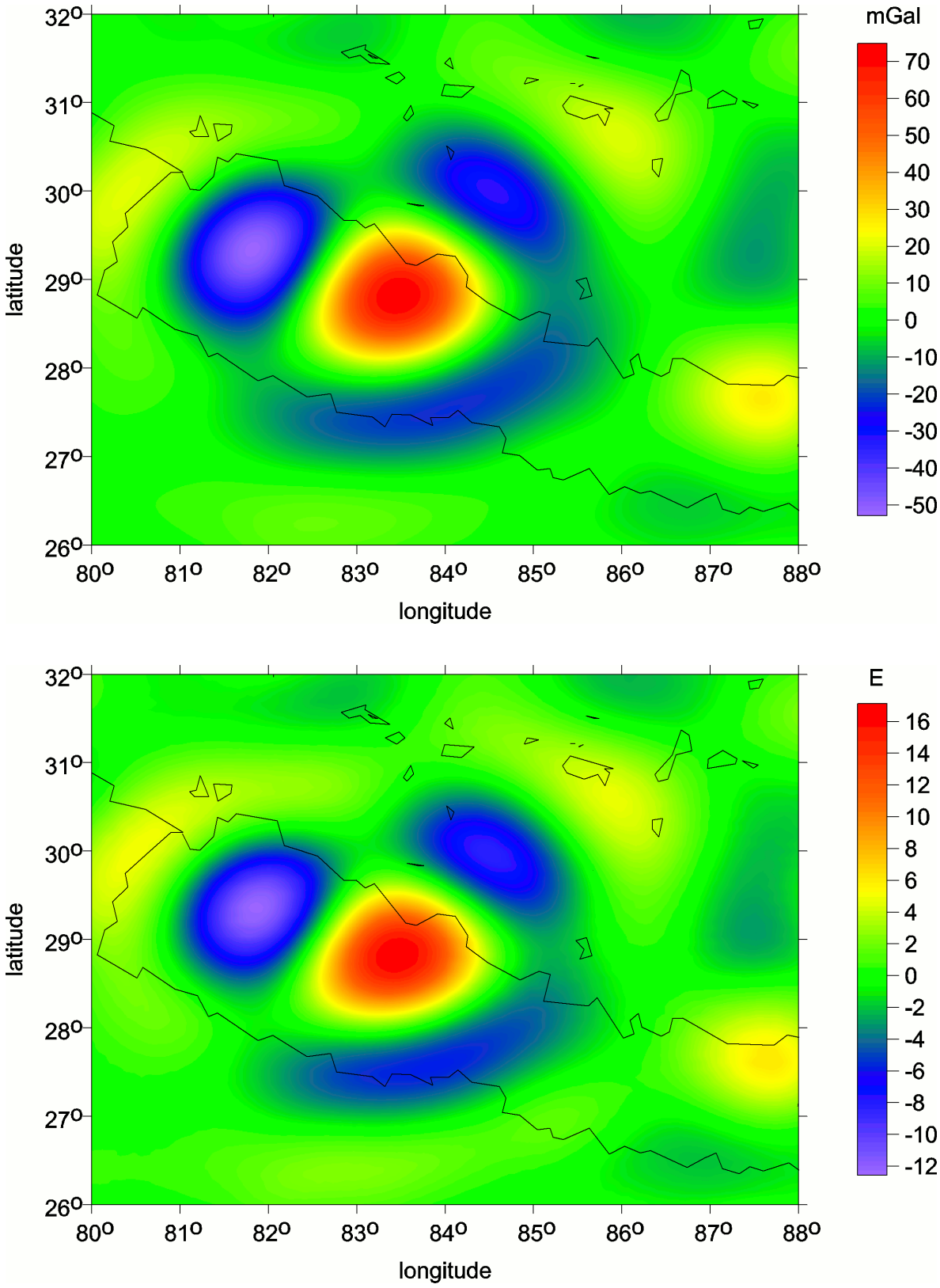

Figure 1 c, d: EIGEN-6C4 minus EGM2008, Himalaya Δg and T_{zz}

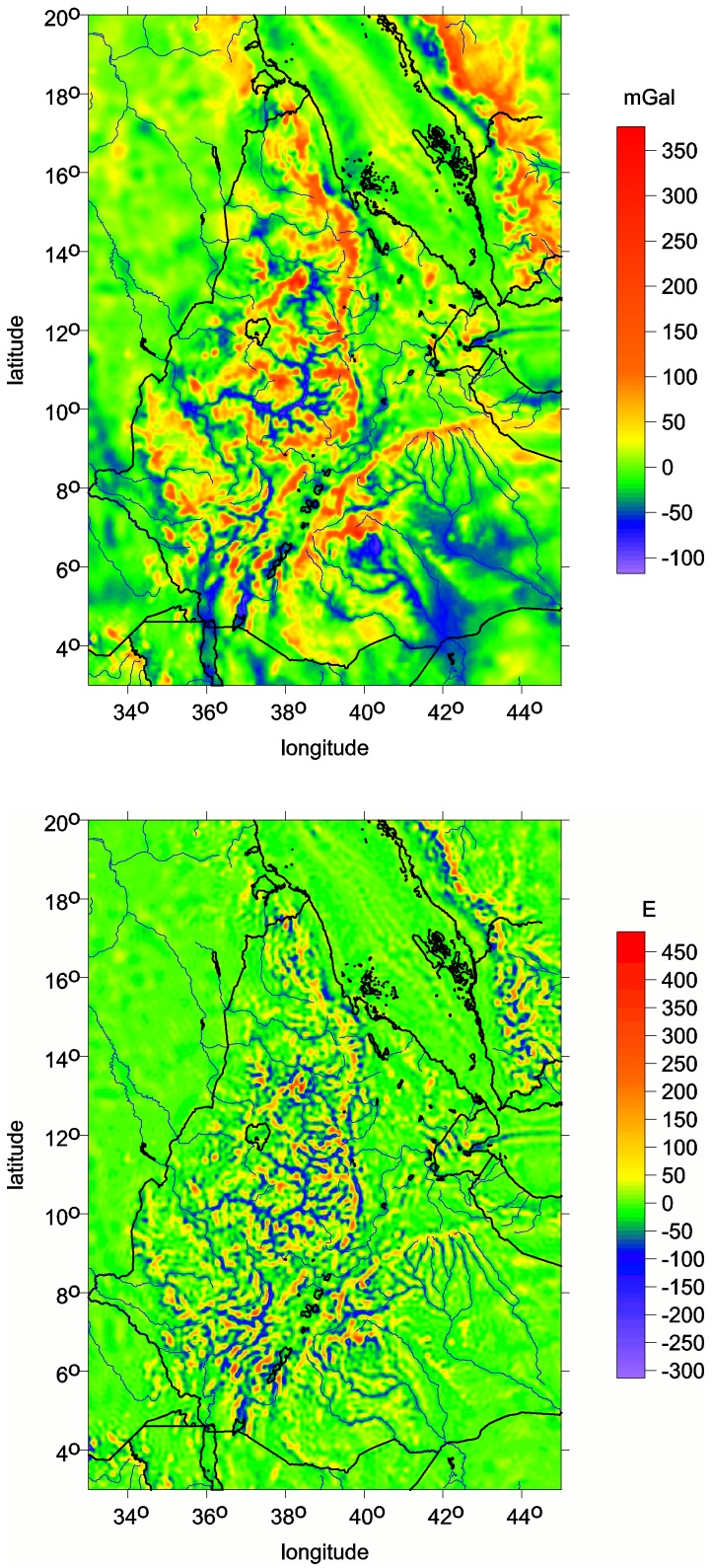

Figure 2 a, b: EIGEN-6C4, Etiopie Δg and T_{zz}

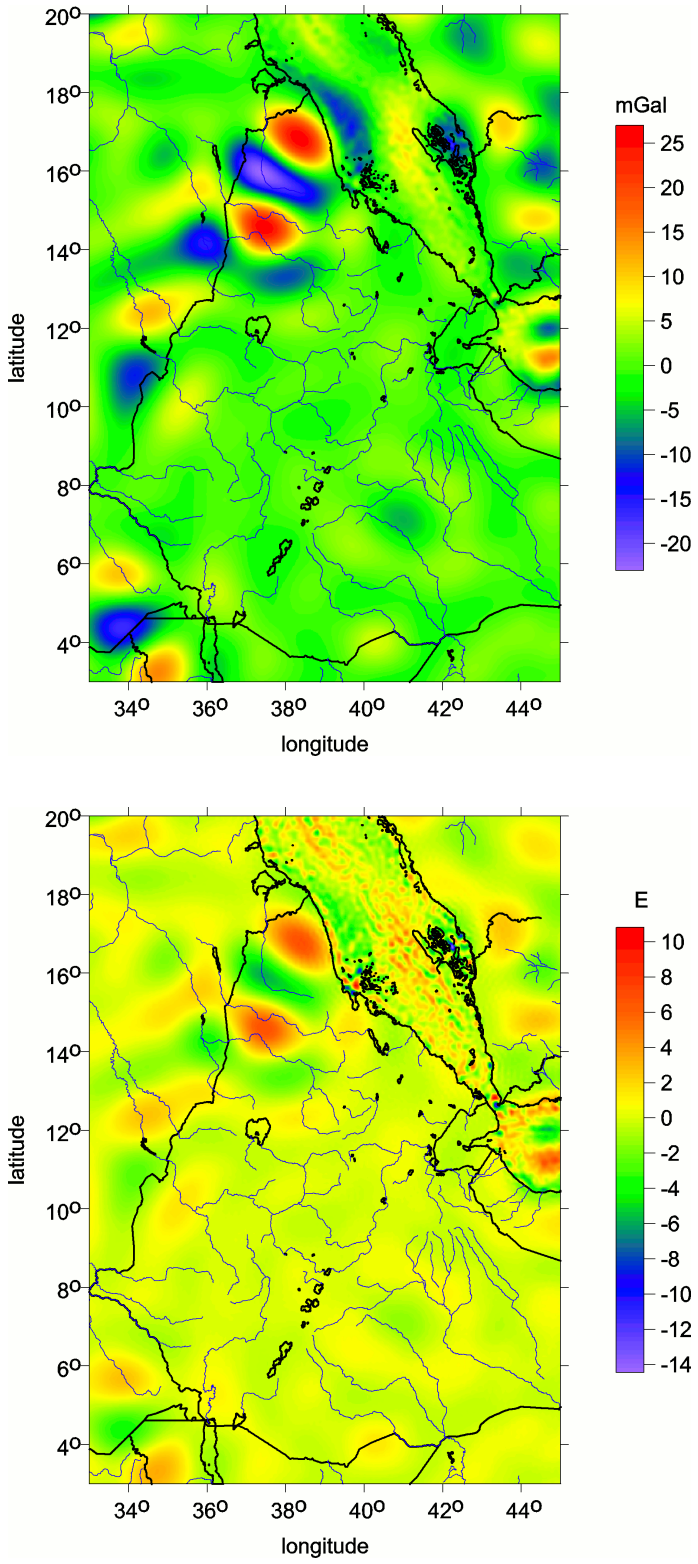

Figure 2 c, d: EIGEN-6C4 minus EGM2008, Etiopie Δg and T_{zz}

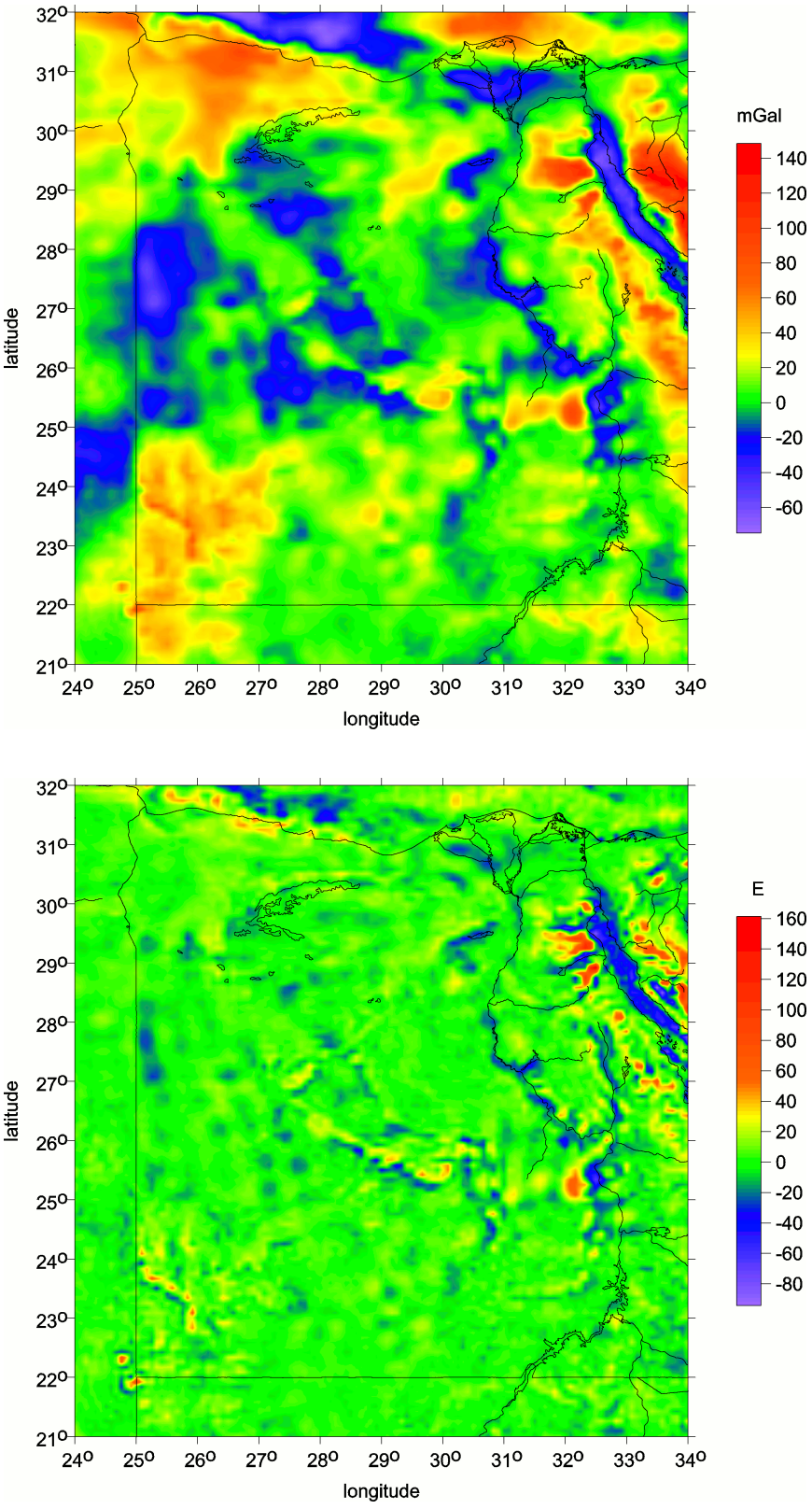

Figure 3 a, b: EIGEN-6C4, Egypt Δg and T_{zz}

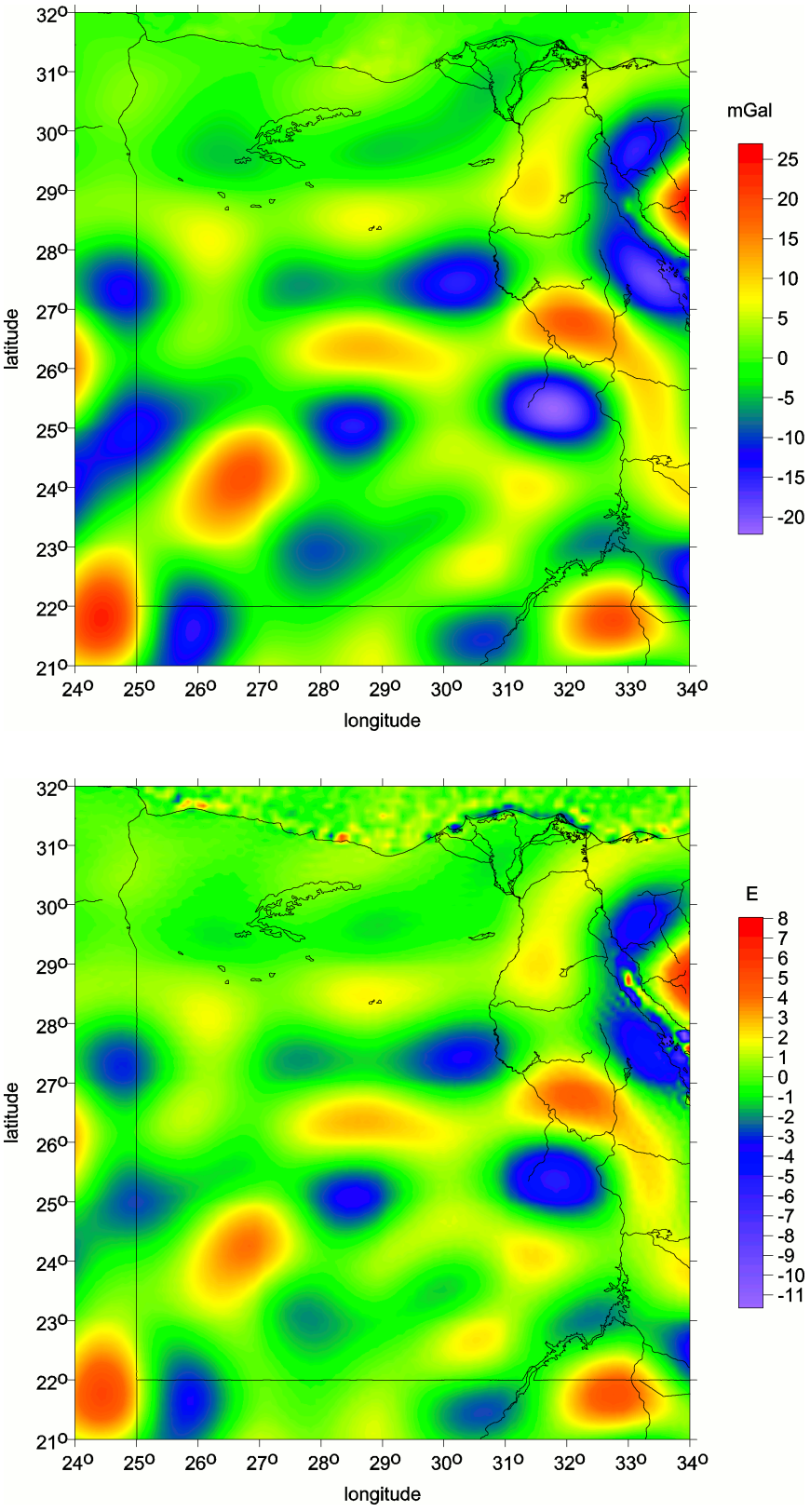

Figure 3 c, d: EIGEN-6C4 minus EGM2008, Egypt Δg and T_{zz}

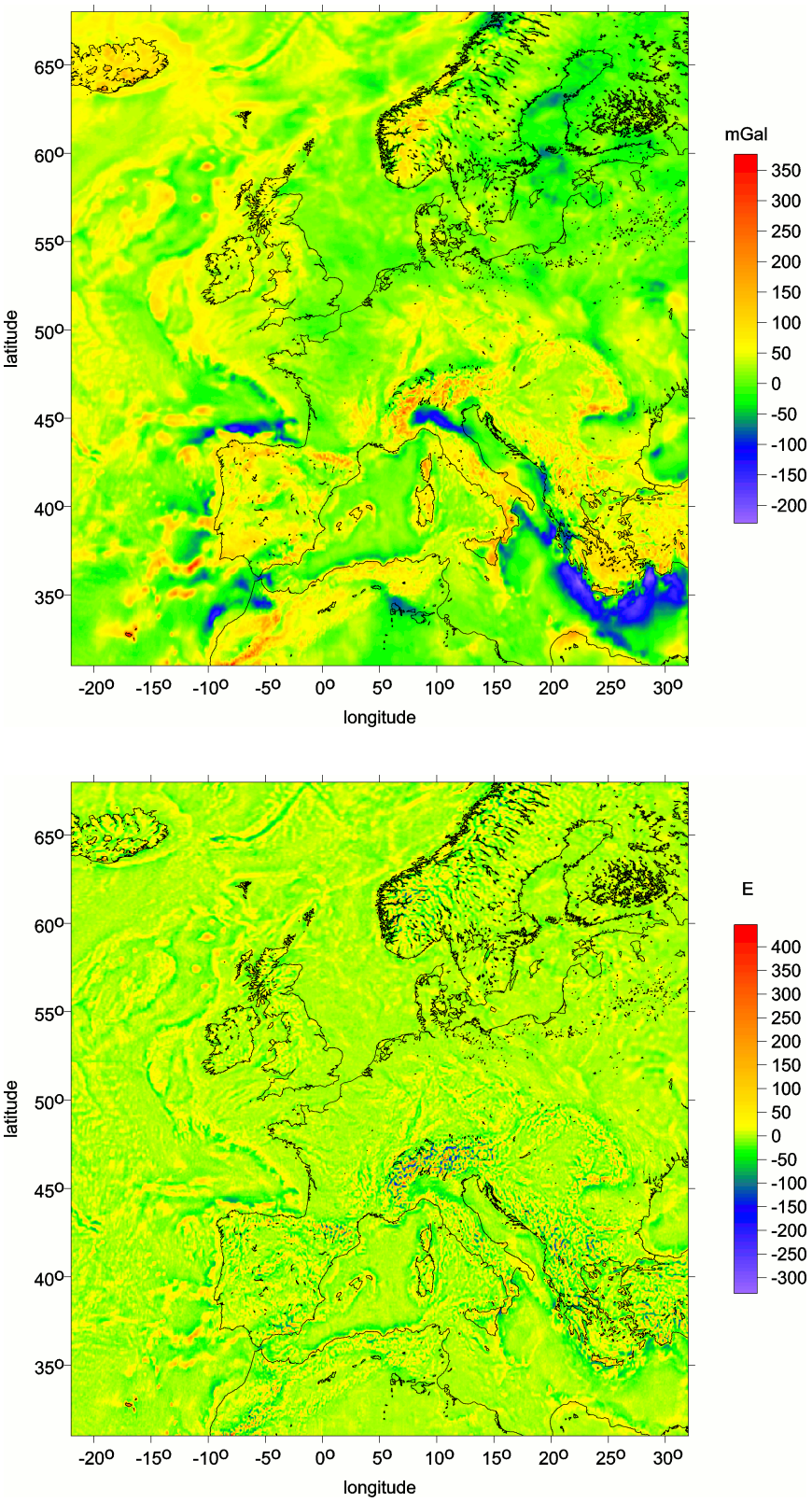

Figure 4 a, b: EIGEN-6C4, Europe Δg and T_{zz}

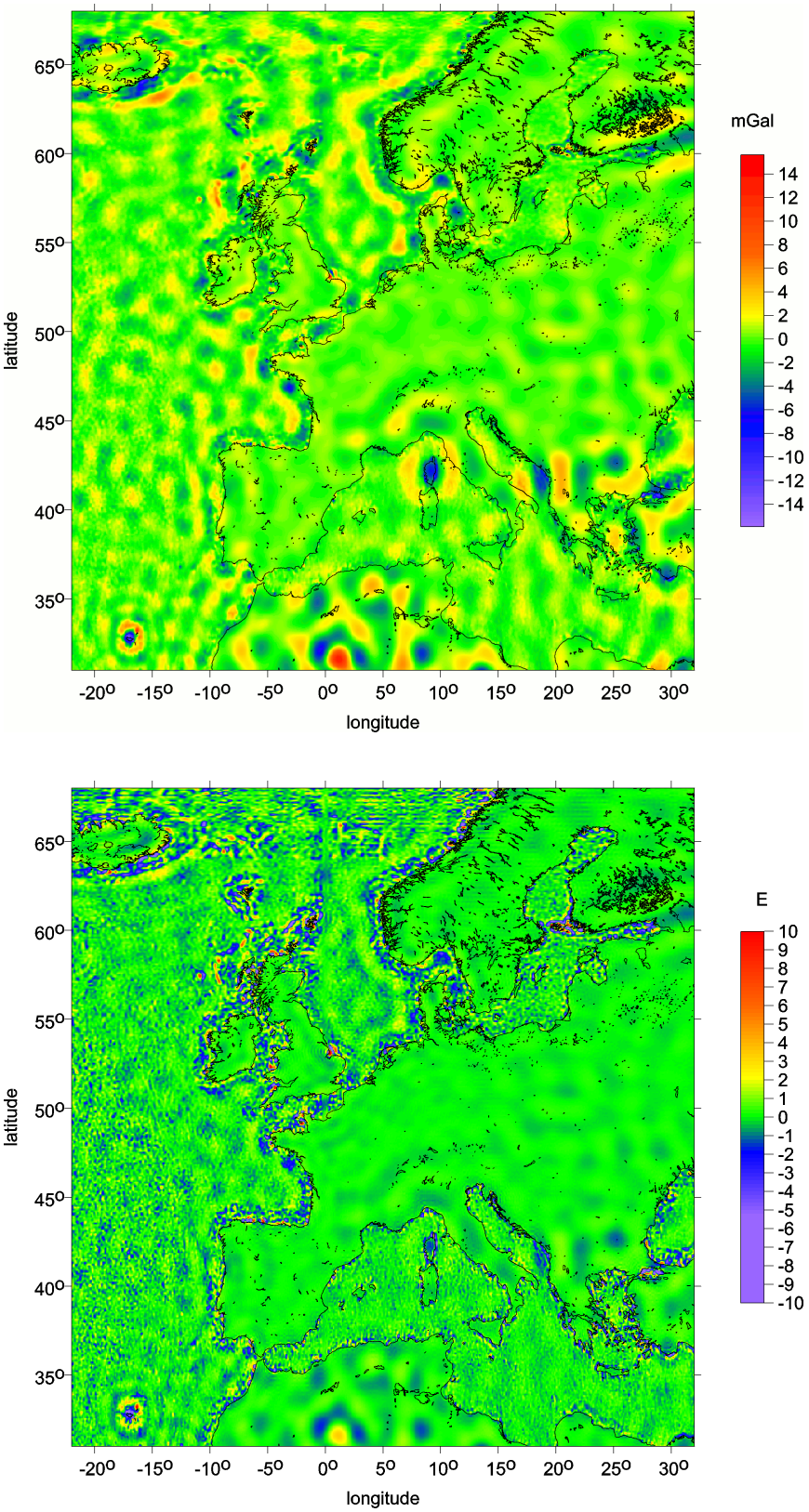

Figure 4 c, d: EIGEN-6C4 minus EGM2008, Europe Δg and T_{zz}

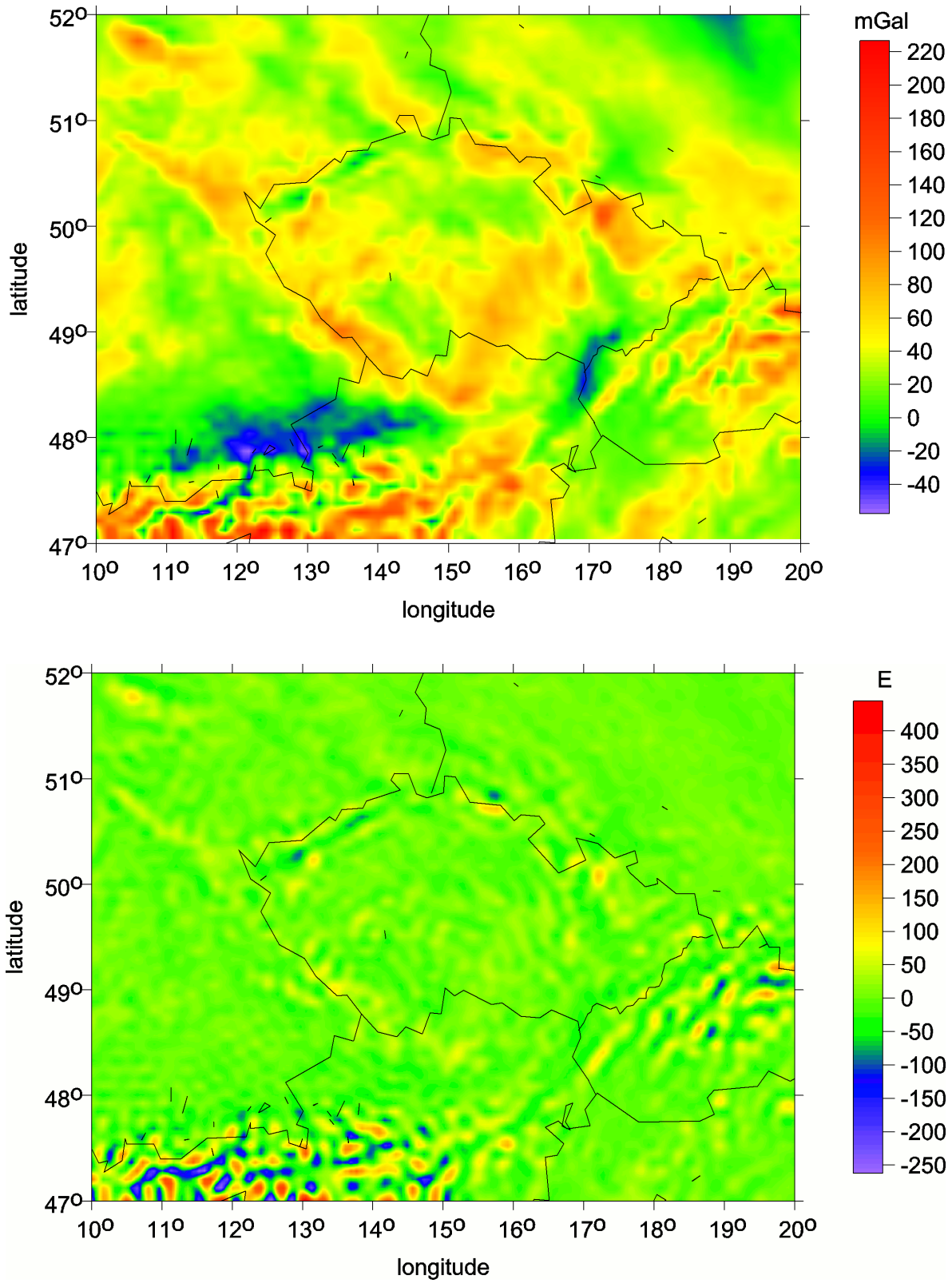

Figure 5 a, b: EIGEN-6C4, Czech Republic Δg and T_{zz}

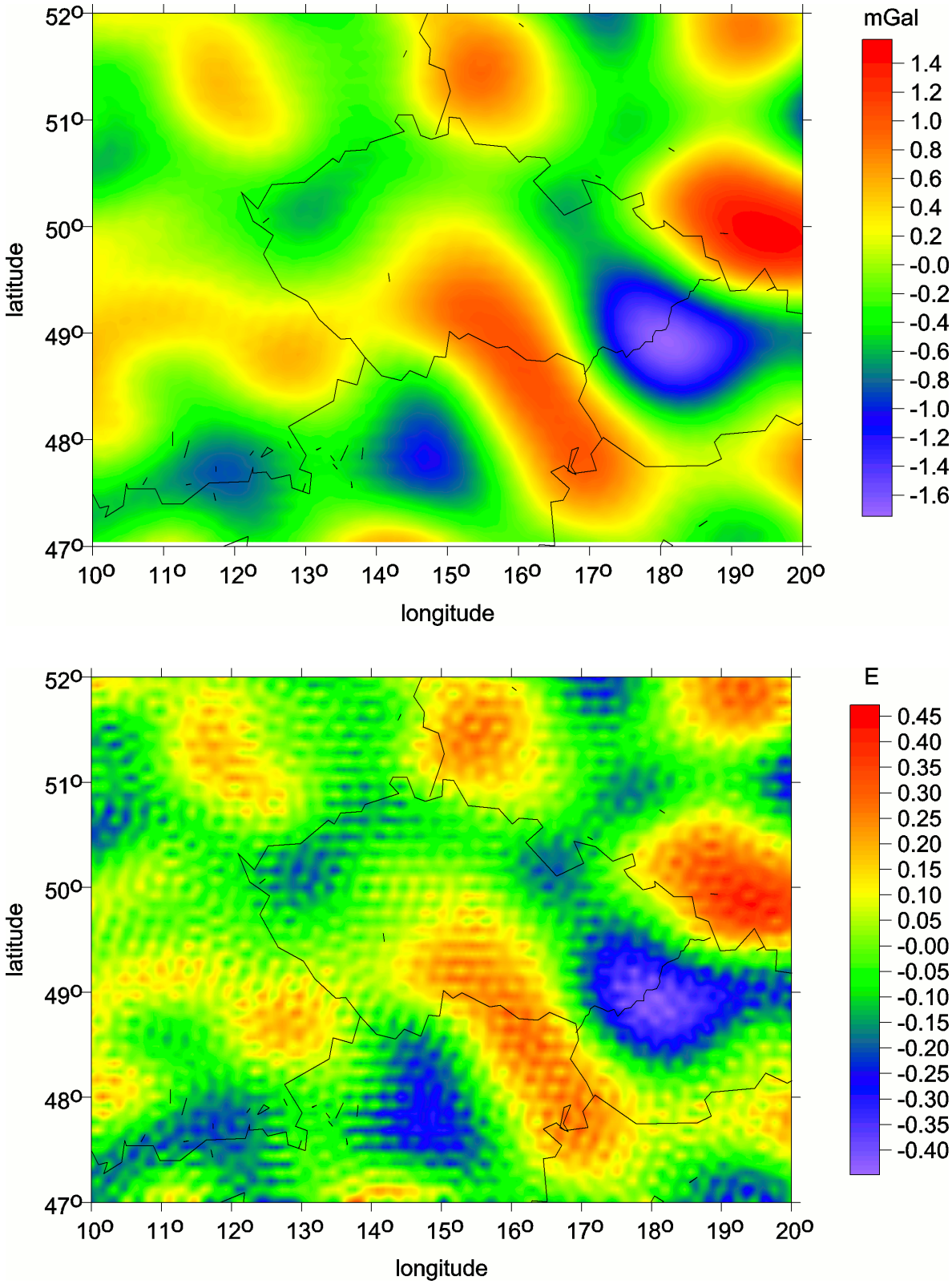

Figure 5 c, d: EIGEN-6C4 minus EGM2008, Czech Republic Δg and T_{zz}

comes from national GNSS/levelling campaigns. In the differences shown by our figures we see long wavelength discrepancies between the two models, where we anticipate a role of the GOCE data. RMS values of differences in Δg and T_{zz} are collected in Table 1, minimal and maximal values of these are visible in the figures. The differences over Europe (for Δg as well as T_{zz}) show significant values for the oceans while the differences over land are small. This is caused by the fact, that EIGEN-6C4 still contains EGM2008 over the continents while recent altimetry-based gravity data were taken for the ocean and sea area. The differences between both models for T_{zz} also show a pixelated pattern (see the figure for Czech Republic 5 c,d). We think this phenomenon is caused by noise of the GOCE data which appears more in the second radial derivative of the potential than in the gravity anomaly.

Obviously, these differences give no quantitative measure about the accuracy of the compared models. For such a purpose, independent, sufficiently precise and as spacious as possible data sets are needed. Here in our study we used GNSS/levelling data, which are independent of the models. These data are very precise but not of global coverage.

Table 1: Root mean square values of differences between EIGEN-6C4 and EGM2008

Territory	Δg (mGal)	T_{zz} (Eötvös)
Himalaya	15.4	3.5
Ethiopia	4.4	1.3
Egypt	6.6	1.6
Europe	1.3	1.0
Czech Republic	0.5	0.1

4. Tests with GNSS/levelling results

4.1. GNSS/levelling network in the Czech Republic

The GNSS/levelling network, containing 1024 points regularly covering the territory of the Czech Republic, has been surveyed by Land Survey Office with the aim to improve the gravimetric quasigeoid. Distribution of these points is visible from Figs. 7. The GNSS coordinates were measured on selected trigonometric points of the Czech Geodetic Control. The height of these points was only known from trigonometry with accuracy of decimeters; thus, the more precise heights of these points were determined by "precise geometric levelling" method using the nearest points of the Czech State Levelling Network. The accuracy of the physical heights is better than 0.5 cm with respect to the nearest points of the State Levelling Network. For all 1024 points we can then compute the geoid (quasigeoid) undulations using inversion of Eq. (1). The accuracy of the GNSS ellipsoidal heights is 1.5 – 2.0 cm. The total error of the height anomaly varies between 1.6 and 2.1 cm. see i.e. Kostelecký et al., 2012 [8].

4.2. GNSS/levelling network in Slovakia and the European gravimetric quasigeoid (EGG97)

For the territory of Slovakia the network consists of 64 points, measured by Geodetic and Cartographic Institute in Bratislava at the SLOVGERENET (SLOVak GEOdynamic REference NETtwork). The distribution of these points is visible from Figs. 8. The accuracy is approximately the same as in the Czech Republic. Since 1997, for whole Europe exists

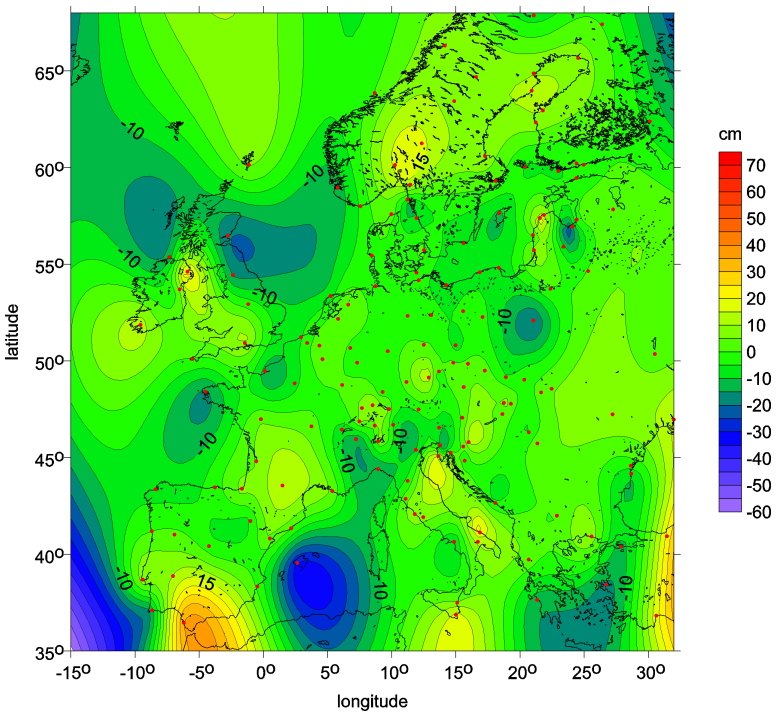

Figure 6 a: Test of EMG2008 by GPS/levelling on the territory of Europe (GPS/levelling geoid minus EGM2008 geoid; constant shift 0 cm, rmse 9.0 cm)

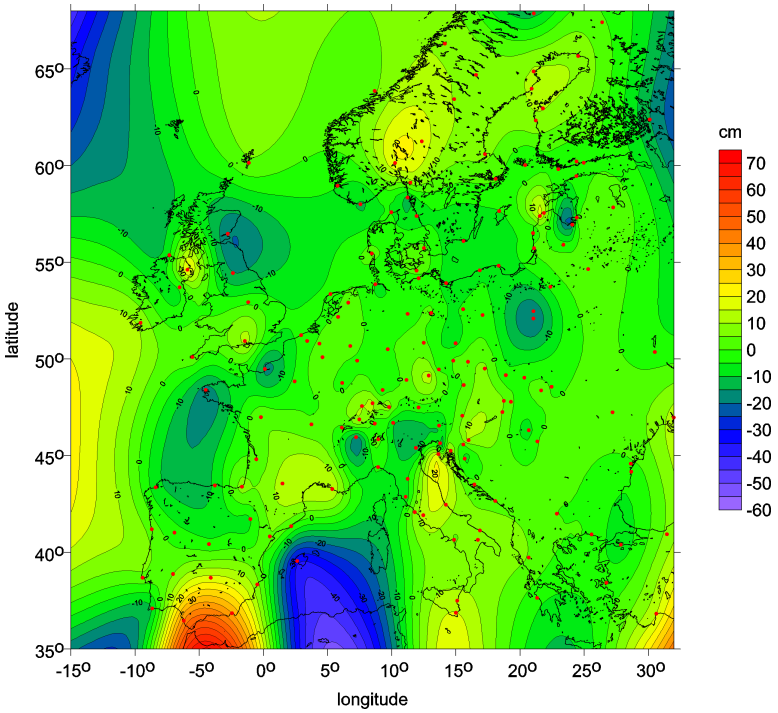

Figure 6 b: Test of EIGEN-C64 by GPS/levelling on the territory of Europe (GPS/levelling geoid minus EGM2008 geoid; constant shift 0 cm, rmse 8.6 cm)

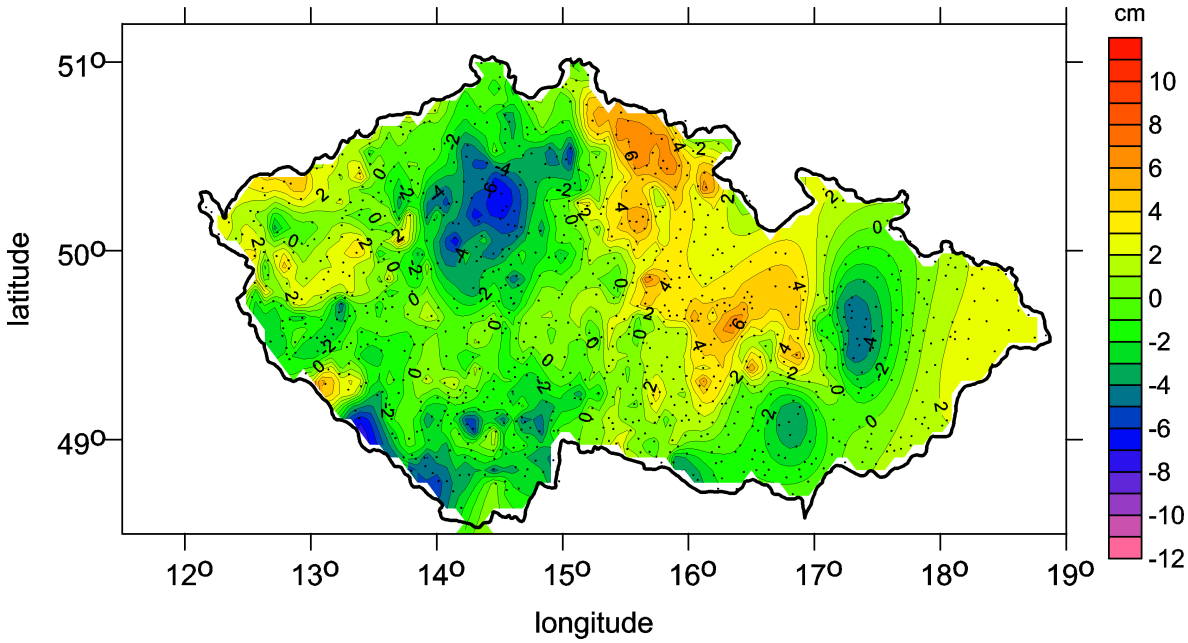

Figure 7 a: Test of EGG97 quasigeoid by GPS/levelling on the territory of the Czech Republic (GPS/levelling quasigeoid minus EGG97, substracted -14 cm, rmse 2.8 cm)

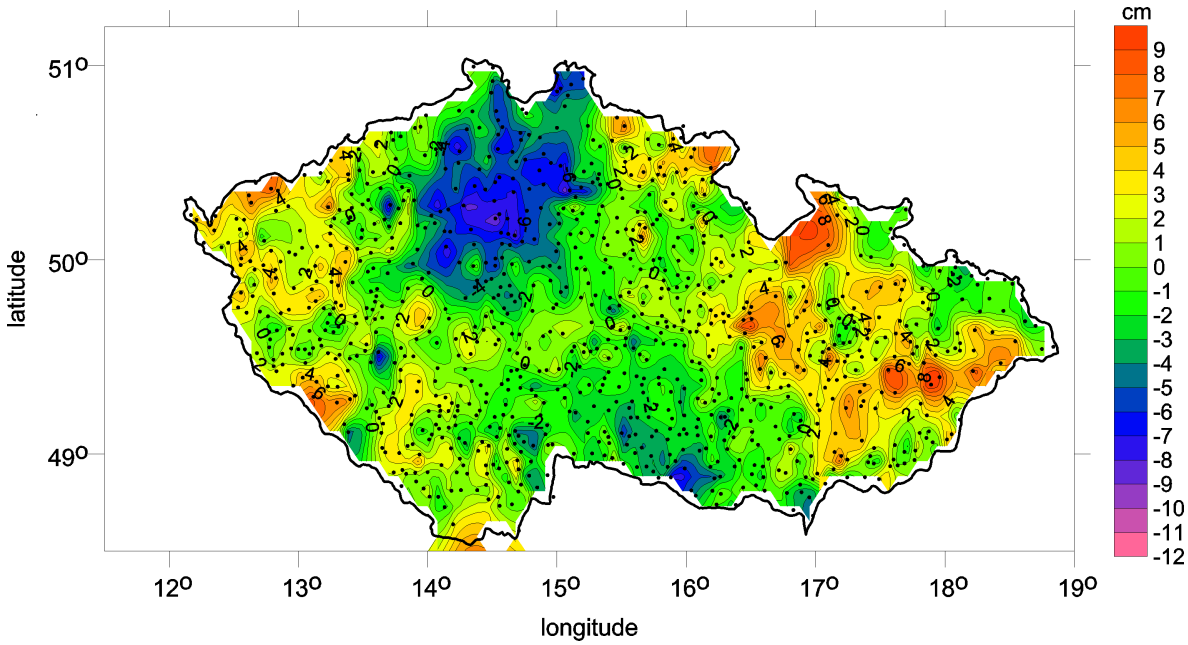

Figure 7 b: Test of EGM2008 by GPS/levelling on the territory of the Czech Republic (GPS/levelling quasigeoid minus EGM2008 geoid; substracted mean -43 cm, rmse 3.3 cm, GPS levelling point accuracy about 2 cm)

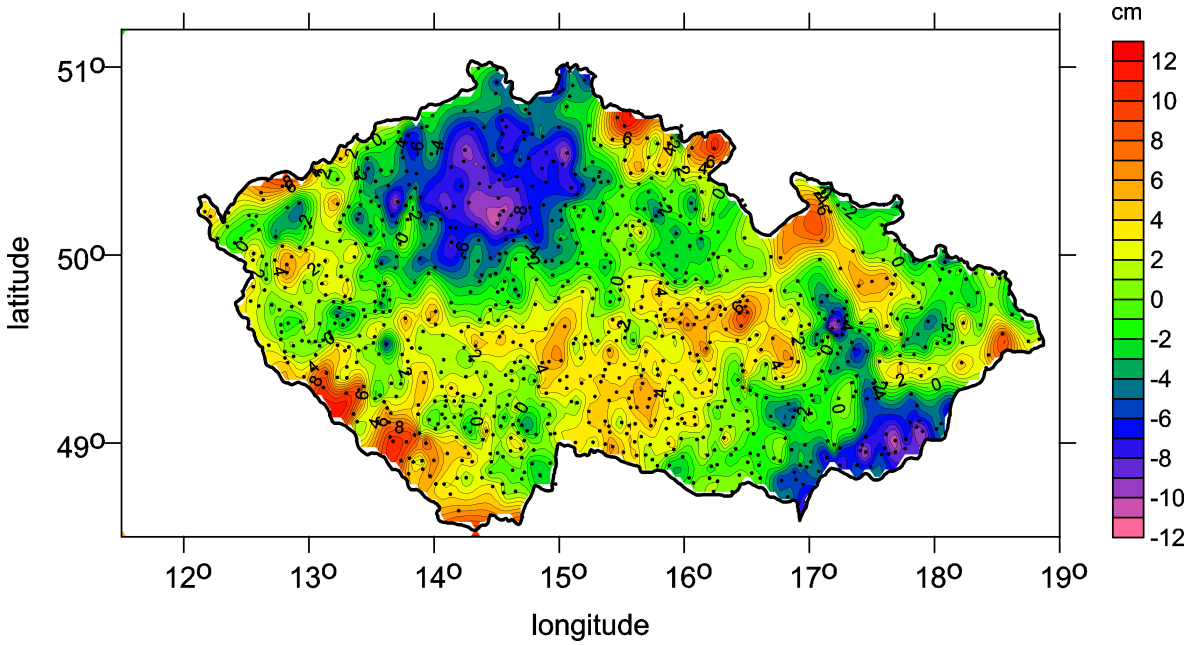

Figure 7 c: Test of EIGEN-6C4 by GPS/levelling on the territpry of the Czech Republic (GPS/levelling quasigeoid minus EIGEN-6C4 geoid; subtracted mean -46 cm, rmse 4.0 cm; GPS/levelling point accuracy about 2 cm)

a model of the European gravimetric quasigeoid (EGG97), based on gravimetric data from different sources of European countries. The accuracy of the EGG97 quasigeoid is about 3 to 5 cm per 100 km - see Denker et al., 2008 [3].

4.3. Evaluation of GNSS/levelling results

GNSS/levelling data sets (with the accuracy about 2 cm) have been used to evaluate EGM2008 and EIGEN-6C4 on the territories of the Czech Republic (CZ) and Slovakia (SK) as well as over Europe. While the Czech Republic (CZ) and Slovakia have very dense GNSS/levelling points, for Europe only data with much less density were available for us.

For GNSS/levelling heights minus geoid values from EGM2008 and EIGEN-6C4 we obtained: RMS of the differences of 3.3/4.0 cm (CZ – Figs. 7 b,c), and 5.0/4.2 cm (SK – Figs. 8 a,b) respectively. The semi-major axis of the ellipsoid used to compute the geoid from respective models is 6378136.3 m for both models. The offset (subtracted mean in the figures) about 40 cm for CZ and SK is caused by a) using different ellipsoids in the geoid and the GNSS/levelling computations (here it is used ellipsoid GRS80 with semi-major axis 6378137.0 m), b) by using different height systems of levelling heights, and c) we compare „regularized geoid“ determined from models with „quasigeoids“ from CZ, SK and Europe (differences between geoid and quasigeoid is in flat parts of Europe approximately 1 cm, in mountains it is 3 – 5 cm). For the Czech Republic (Figs. 7 a,b,c) our figures show a significant «hollow» in the northern part. We are sure that this finding is not an artifact of method or computations. To clear up this phenomenon we added Figure 7a with differences between the GNSS/levelling heights and the quasigeoid model EGG97 (Denker et al., 2008 [3]). This figure shows a systematic trend, but the differences between GNSS/levelling and the quasigeoid EGG97 are

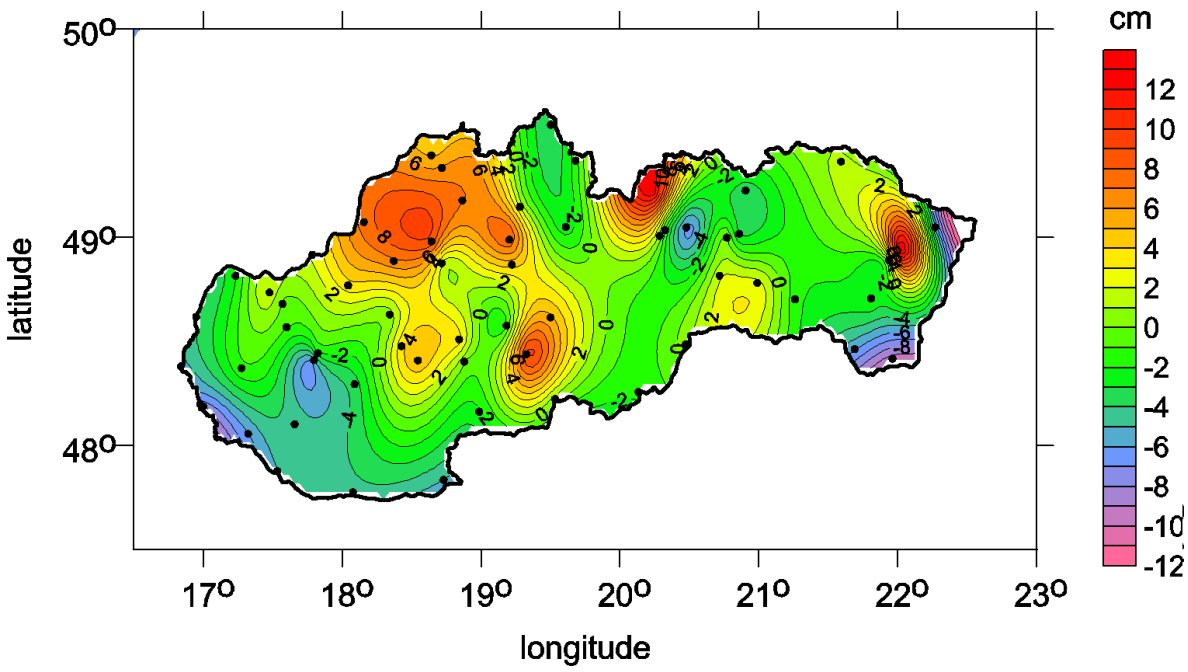

Figure 8 a: Test of EGM2008 by GPS/levelling on the territpru of Slovakia (GPS/levelling geoid minus EGM2008 geoid; subtructed mean -44 cm, rmse 5.0 cm; GPS/levelling point accuracy about 2 cm)

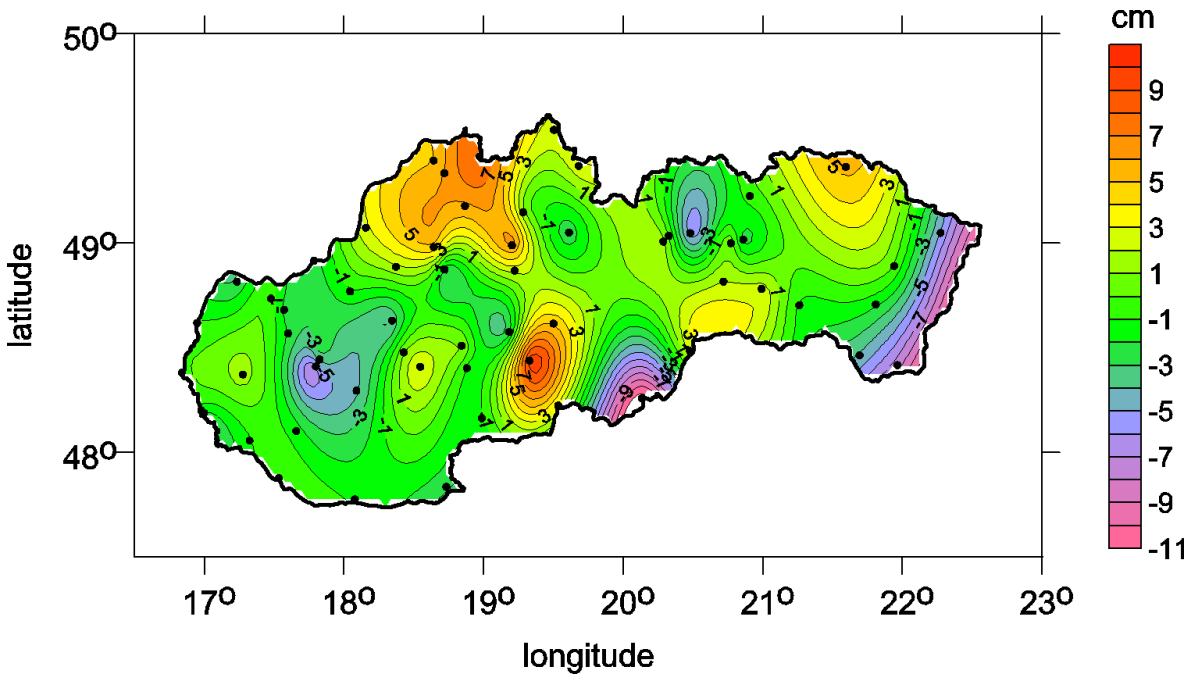

Figure 8 b: Test of EIGEN-6C4 by GPS/levelling on the territory of Slovakia (GPS/levelling geoid minus EIGEN-6C4 geoid; subtracted mean -43 cm, rmse 4.2 cm; GPS/levelling point accuracy about 2 cm)

slightly a bit lower than those for the two gravity models. This depression could be caused by a) an inaccuracy of the terrain gravity measurements and/or b) by local recent deformations (GNSS/levelling observations are from the epoch 2003 and the levelling heights are from 1986 and older, see also Zeman et al., 2007 [15]). Note also that the authors of both models estimated precision of geoid undulations computed from them in Europe to 0.10 – 0.15 m RMSE (Förste et al., 2014 [5]).

For Europe the RMS differences between GNSS/levelling height and EGM2008 or EIGEN-6C4 respectively are 9.0/8.4 cm – see Figs. 4 a,b – which means a little improvement of EIGEN-6C4 vs. EGM2008. This finding is confirmed by additional tests computed for GPS/levelling data sets for further, larger regions of Canada (M. Véronneau, Natural Resources Canada , personal communication 2003), USA (Milbert, 1998 [9]), Japan (courtesy Tokuro Kodama, Geospatial Information Authority of Japan), Australia (G. Johnston, Geoscience Australia and W. Featherstone, Curtin University of Technology, personal communication 2007) and Brazil (courtesy D. Blitzkow and A. C. O. Cancoro de Matos, Centro de Estudos de Geodesia Brazil). Again, EGM2008 and EIGEN-6C4 were taken to their maximum degree and order and RMS of differences were computed. The obtained RMS values of the geoid heigth differences after subtraction of the mean are given in Table 2. The results show an improvement of EIGEN-6C4 vs. EGM2008 for most of the tested regions which should be caused by the inclusion of the novel GOCE satellite data. Somewhat worse result for EIGEN-6C4 with comparison of EGM2008 for the Czech Republic should be statistically insignificant since the spatial extend of this region is not very large compared to the spatial resolution of GOCE and the obtained RMS values are already very small.

Table 2: Root mean square (cm) about the mean of GNSS/levelling minus model-derived geoid heights (number of points in brackets) for EGM2008 and EIGEN-6C4.

GNSS/levelling data set	EGM2008	EIGEN-6C4
Canada (1930)	12.6	12.4
USA (6169)	24.6	24.5
Australia (201)	21.5	21.1
Japan (816)	8.2	7.8
Brazil (672)	36.6	30.6
Europe (166)	9.0	8.6
Czech Rep. (1020)	3.3	4.0
Slovakia (64)	5.0	4.2

5. Conclusions

The global combined high-resolution gravity field models EGM2008 and EIGEN-6C4 have been compared by means of two functions of the disturbing gravitational potential. The main difference between both models is adding of GOCE mission data in the EIGEN-6C4 model. Here we show examples of differences in Δg and in T_{zz} for Himalaya, Ethiopia, Egypt, Europe, and namely for the Czech Republic. In our evaluation we see long wave differences between the two models in remote areas of worse terrestrial data. For these regions we assume a positive effect of the GOCE data.

GNSS/levelling data over the territories of Europe, the Czech Republic and Slovakia as well as for further larger regions has been used as an independent data source to evaluate EGM2008 (without GOCE SGG measurements data) and EIGEN-6C4 (with GOCE SGG data). These tests show an improvement for EIGEN-6C4 compared to EGM2008 for most of the included GPS/levelling data sets. The tests confirmed the declared accuracy of both models at the 10 cm level.

References

[1] Sean L. Bruinsma et al. "ESA's satellite-only gravity field model via the direct approach based on all GOCE data". In: *Geophysical Research Letters* 41.21 (2014). DOI: 10.1002/2014GL062045.

[2] B. Bucha and J. Janák. "A MATLAB-based graphical user interface program for computing functionals of the geopotential up to ultra-high degrees and orders". In: *Computers & Geosciences* 56 (2013), pp. 186–196.

[3] H. Denker et al. *The Development of the European Gravimetric Geoid Model EGG07*. Institut für Erdmessung, Leibniz Universität Hannover, Schneiderberg 50, D-30167 Hannover, Germany. 2008.

[4] Rune Floberghagen et al. "Mission design, operation and exploitation of the gravity field and steady-state ocean circulation explorer mission". In: *J Geod* 85.11 (Oct. 2011), pp. 749–758. DOI: 10.1007/s00190-011-0498-3.

[5] C. Förste et al. "The latest combined global gravity field model including GOCE data up to degree and order 2190 of GFZ Potsdam and GRGS Toulouse". In: 5th GOCE User Workshop, Paris. 25–28 November 2014. URL: http://icgem.gfz-potsdam.de/ICGEM/documents/Foerste-et-al-EIGEN-6C4.pdf.

[6] J. Kalvoda et al. "Mass distribution of Earth landforms determined by aspects of the geopotential as computed from the global gravity field model EGM 2008". In: *Acta Univ. Carolinae-Geogr.* 48 (2013), pp. 17–25. ISSN: 0300-5402.

[7] J. Klokočník et al. *Gravity Disturbances, Marussi Tensor, Invariants and Other Functions of the Geopotential Represented by EGM 2008*. Presented at ESA Living Planet Symp. 9-13 Sept. 2013, Edinburgh, Scotland. Publ. in: August 2014: J Earth Sci. Res 2, 88–101. 2014.

[8] Jan Kostelecký et al. "Realizace S-JTSK/05 (S-JTSK/05 Implementation)". In: *Geodetický a kartografický obzor* 58(100).7 (2012), pp. 145–154. URL: http://archivnimapy.cuzk.cz/zemvest/cisla/Rok201207.pdf.

[9] D.G. Milbert. *Documentation for the GPS benchmark data set of 23-July-1998*. IGeS International Geoid Service, Bulletin 8, pp 29–42. 1998.

[10] Roland Pail et al. "First GOCE gravity field models derived by three different approaches". In: *J Geod* 85.11 (Oct. 2011), pp. 819–843. DOI: 10.1007/s00190-011-0467-x.

[11] Nikolaos K. Pavlis et al. "EGM2008: An overview of its development and evaluation". In: National Geospatial-Intelligence Agency, USA, presented at conference: Gravity, Geoid and Earth Observation 2008, Chania, Crete, Greece, 23–27 June 2008.

[12] Nikolaos K. Pavlis et al. "The development and evaluation of the Earth Gravitational Model 2008 (EGM2008)". In: *J. Geophys. Res.* 117.B4 (2012). DOI: 10.1029/2011jb008916. URL: http://dx.doi.org/10.1029/2011jb008916.

[13] Reiner Rummel, Weiyong Yi, and Claudia Stummer. "GOCE gravitational gradiometry". In: *J Geod* 85.11 (Aug. 2011), pp. 777–790. DOI: 10.1007/s00190-011-0500-0.

[14] Richard Shako et al. "EIGEN-6C: A High-Resolution Global Gravity Combination Model Including GOCE Data". In: *Advanced Technologies in Earth Sciences*. Springer Science + Business Media, Nov. 2013, pp. 155–161. DOI: 10.1007/978-3-642-32135-1_20.

[15] A. Zeman et al. *Vertical component of the Earth's surface movement in the region of Central Europe (Czech Republic) from the results of satellite geodesy methods and their comparison with the results of repeated terrestrial geodetic methods*. Poster presentation at the AGU 2007 Fall meeting. 2007.

Minimal Detectable Displacement Achievable by GPS-RTK in CZEPOS Network

Martin Raška[a] and Jiří Pospíšil[b]

[a]Katastrální úřad pro Karlovarský kraj, Katastrální pracoviště Sokolov
Boženy Němcové 1932, 356 01 Sokolov, Czech Republic
martin.raska@cuzk.cz

[b]Faculty of Civil Engineering, Department of Special Geodesy
Thákurova 7, Praha 6 16629, Czech Republic
pospisil@fsv.cvut.cz

Abstract

In this paper we have made a brief study of RTK precision to estimate possibilities of network RTK using CZEPOS for purposes of geotechnic monitoring of landslides in real time. In this paper we describe a testing methodology, which resulted in estimation of point-position precision and describing minimal detectable positional change. Based on our results it is concluded that displacements could be detected with centimetre accuracy even with short-period observations.

Keywords: GNSS, network RTK, landslide monitoring

1. Introduction

The measurements with GNSS are easier than terrestrial methods for displacement monitoring of points [12]. As GNSS technology and short observation time, followed up by terrestrial observation, usually provides sufficient precision for rough position precision requirements, as shown in experimental geomorphologic analysis [9], with increasing demands on precision, usually terrestrial methods are preferred, despite their complicated and time consuming procedure [1]. Unlike to RTK, the position of observed points with permanent stations may by determined with millimetre accuracy [6].

In 2007, 27 permanent GPS reference stations comprised the CZEPOS reference system. They cover almost the whole area of the Czech Republic, however some border areas extend outside this network (see Fig. 1), 23 of them owned and maintained by the Land Survey Office, whilst the others are supported and maintained by research facilities. At the end of 2008, the whole network had been connected with surrounding networks in Germany, Austria, Poland and Slovakia, thus computing corrections in border areas of the Czech Republic has become more reliable. In December 2009, reference station in Moravský Krumlov has been relocated to Znojmo. Besides storing continuous data for post-processing computing (available through the web pages of the Land Survey Office [5]), real-time data are provided as well. Data flow could be divided into two parts - DGPS corrections (code only, for GIS applications, decimetre precision) and RTK phase based corrections (centimetre precision). In this paper only the RTK service will be discussed.

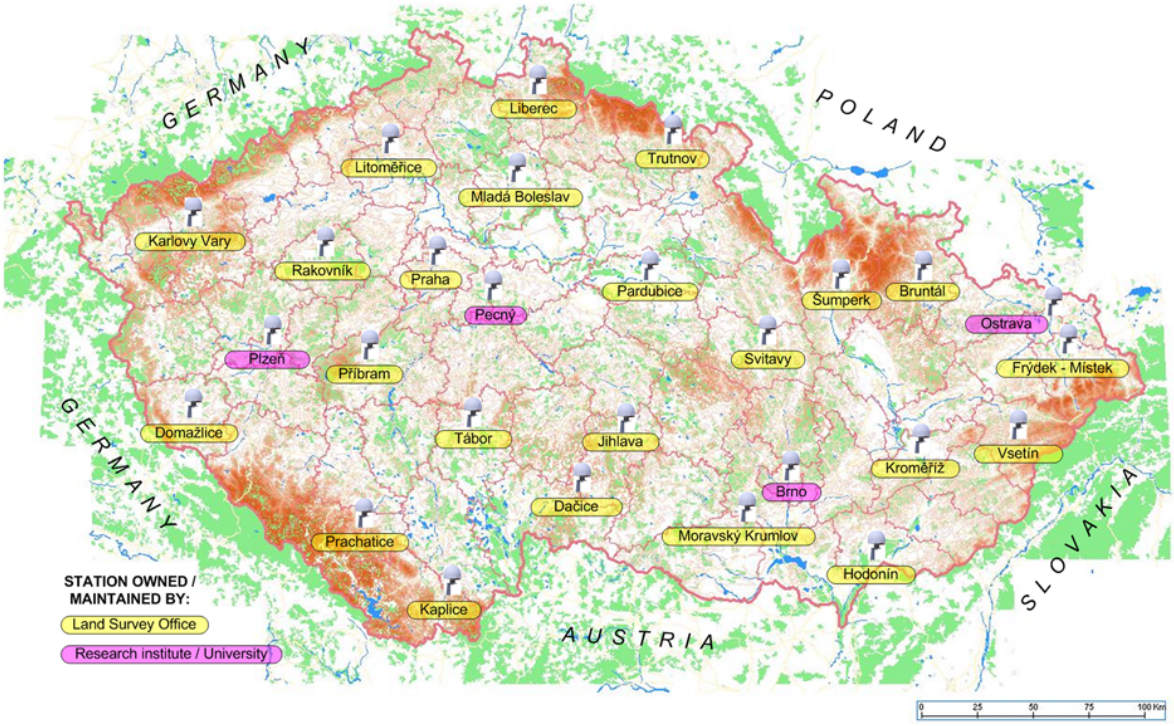

Figure 1: Reference stations of CZEPOS network

Basically, three different kinds of position solution are provided: Simple RTK, RTK-FKP and RTK-PRS. In "Simple RTK" the user chooses one of the reference stations, and corrections are then computed from that reference station only. This method is the least precise, as accuracy of baseline vector determination decreases with increasing length, as shown in [2]. Method is used only with very short baseline vector lengths or under some special circumstances (the next two solutions are computed as network solutions thus during a network solution failure, only "simple" corrections from individual reference stations are available). In "RTK – FKP", the nearest reference station is chosen automatically, but corrections are computed from modelling of the whole network area (data from all CZEPOS stations are processed). The last service provided is "RTK – PRS". In fact, PRS (pseudo-reference station) is the other name for virtual reference station (VRS), where the user gets corrections and/or observables from a virtual reference station [2], based on his initial position (NMEA) provided by a GNSS rover. Observables are computed for the reference station virtually located approximately 5 km from rover position, in the direction to the nearest reference station. Observables are created from network model of corrections, taking all observations in the whole network into account. Several experiments [10] proved that the precision of a VRS position is similar (thus being in order of 10^{-2} m) to those achieved by Simple RTK.

Corrections are received by a GPRS modem, usually integrated in a GNSS receiver, but today only the GPRS protocol is being used, while the whole area of the Czech Republic is covered by GSM signals and the GPRS data rate (theoretically with maximum at hundreds of kbps, [13]) meets the requirements for on-line data processing.

As common in such applications, the international standard Radio Technical Commission for

Maritime Services (RTCM) version 2.3 is currently used. In February 2009 the Land Survey Office introduced improved version of RTCM (version 3.1), which supports GLONASS correction transfer and has a more effective structure. With the last version of RTCM message [15], a new service "VRS3-MAX" became operational. With this service, observables and corrections for a virtual reference station are computed from a few (usually six) reference stations surrounding the rover. The closest one (called "Master") provides correction data and the others (called "Auxiliary") provide correction differences. There is an alternative service "VRS3–iMAX" for older types of receivers, where the user receives only correction data from the Master station, but Auxiliary stations data are already included in computation. Messages with corrections are sent via Networked Transport of RTCM via Internet Protocol (NTRIP) as needed for data transfer using Internet (as described in [15] and [14]).

2. Background theory

Coordinate system in the Czech Republic

For land surveying purposes, the Czech Republic uses its own national coordinate system (abr. S–JTSK). It could be described as two axes perpendicular to each other, axis +Y heading to west, axis +X heading to south. The origin is chosen so that the X–coordinate value is always greater than the Y–coordinate value, with horizontal angles measured in a clockwise direction. The height coordinate system (abr. Bpv), is a combination of levelling and gravity observations, which are used to derive heights (according to Molodensky's theory [7]).

The European continent drifts approximately 2-3 cm/year so the CZEPOS system primarily works with European Terrestrial Reference System (ETRS–89) instead of WGS84. Thus 3D–transformation from ETRS89 to S-JTSK (and Bpv) is required and is discussed below.

Datum transformation

Different solutions for transforming ETRS89 coordinates to the national system S–JTSK using universal transformation parameters already exist. The one used in Trimble GPS devices proved unusable in real applications due to distortion of the S–JTSK. This leads to very large residual vectors between "computed" (using global transformation) and "known" (computed from terrestrial observations) coordinates of points. Thus a local transformation is commonly being used. The experiment described below used a local transformation with 5 identical points (points with known coordinates in both the ETRS89 and S-JTSK system). In June 2008, Trimble introduced an improved global transformation algorithm, based on prof. Kostelecky's work [3]. Despite having a "random" characteristic of residual vector headings (compared with the original Trimble transformation), results (computed for the area surrounding city of Karlovy Vary) are better in scale by approximately one order (as we can see at Fig. 2).

The coordinates of all identical points used for a transformation, both ETRS89 and S–JTSK obtained from the Land Survey Office Database, have been used. As horizontal and vertical coordinates in national systems come from two different sources of observations and computations, local transformation from ETRS89 to S-JTSK (and Bpv) are strongly recommended to be separated into two standalone parts, horizontal and vertical (practical applications showed that using a geoid model for vertical transformation proved useful, while the geoid model

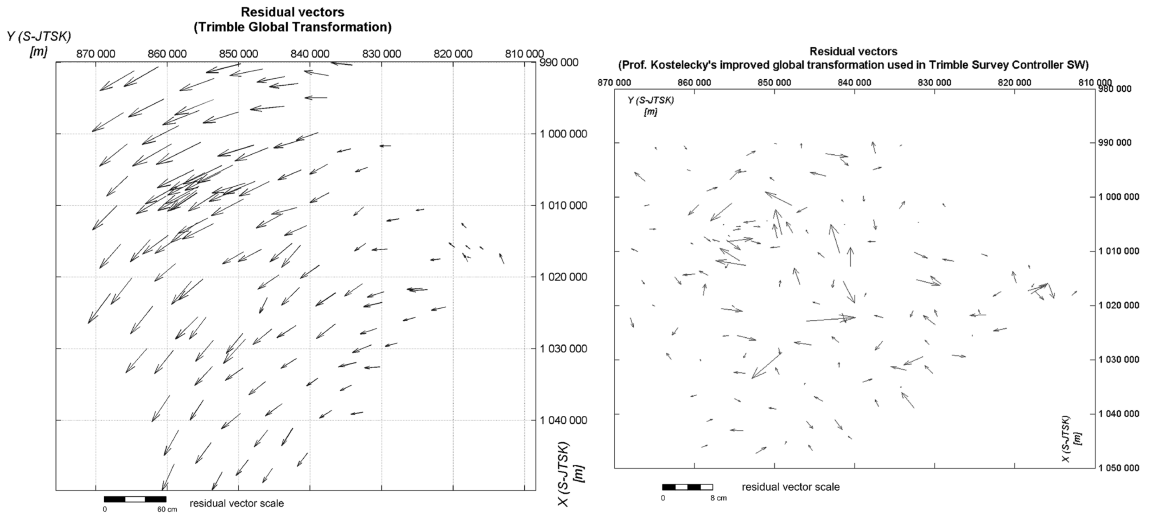

Figure 2: Comparing residual vectors of global transformation

for the Czech Republic [4] gives better results than generally used EGM96). Announced in October 2010, reference frame of the ETRS (ETRF89) is replaced by the ETRF2000.

3. Experiment overview

We chose three different sites A-C (with different terrain morphology), see Fig. 3 (represented by surveying landmark – granite stones with a diagonal cross on their top), located inside the area defined by identical-points to be used for the datum transformation. Each observation at one site included three kinds of CZEPOS data receiving (RTK only, RTK–FKP or RTK–PRS), each one for three different observation lengths (default options of receiver) periods (1 s, 5 s and approximately 180 s). For statistical analysis of the data we stored S-JTSK coordinates, as well as *a priori* accuracy characteristics. In the next step we used the entire data record for an empiric estimation of precision. During the experiment the only device used was a GPS rover Trimble R8.

Precision estimation

As the aim of this experiment was to describe the possibilities of RTK for point position change, there was no interest in deriving absolute positional accuracy in S–JTSK. Only the precision of repeatedly observed point has been tested.

As mentioned earlier, the whole data set was used for computation of positional precision estimation. During the testing procedure in three different areas (with different terrain morphology), possible systematic error (caused by specific environmental conditions) was significantly reduced. After obtaining a set of coordinates, adjustment using the least square method was used. In fact, it led to a computation of the weighted mean value for each coordinate (it was impossible to process all coordinates at one go due to their correlation; three coordinates – Y, X, H from each observation are correlated as being computed from the same set of pseudoranges).

We solved (or at least reduced) problems with different satellite constellations by introducing

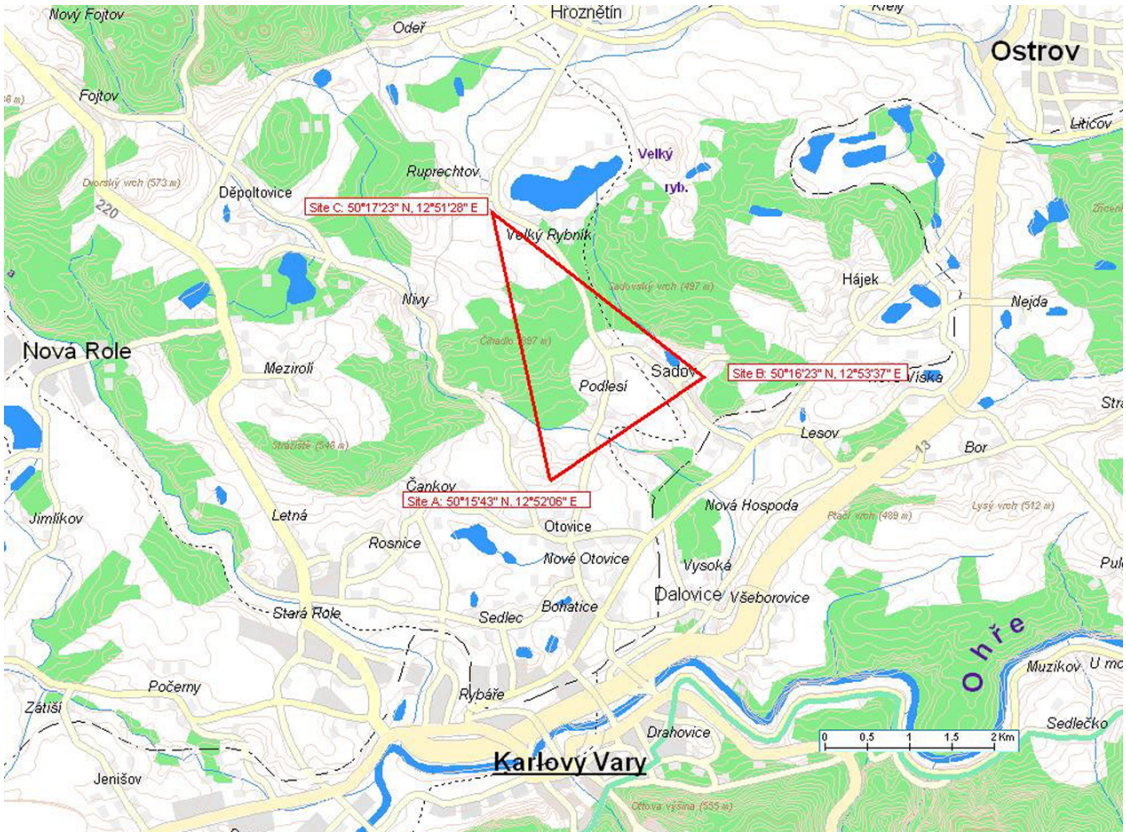

Figure 3: Geometric configuration of sites occupied during experiment

a Relative Dilution of Precision (RDOP) value for the deriving weights, as it takes into account satellite-receiver(s) geometric configuration as well as its changes during observation and observation interval [16]. Progress of RDOP value (based on model using testing site A, reference station in Karlovy Vary and 4 visible satellites) is shown at Fig. 4. It is clear, that unlike PDOP, RDOP value depends not only on instant satellite configuration, but on configuration-change during observation and observation length as well.

The next input parameter used to derive weights was the root mean square (RMS), computed during the observation. The RMS indicates the quality of the (ambiguity) solution based solely on the measurement noise of the satellite ranging observations. Using this value helped us to implement several random and systematic errors, such as multipath.

As we could derive horizontal and vertical interpretations of RDOP (called HDOP and VDOP [2]), weights for observation i can be expressed as:

$$p_{X,i} = p_{Y,i} = \frac{2}{RMS_i^2 \; HDOP_i^2} \tag{1}$$

$$p_{H,i} = \frac{1}{RMS_i^2 \; VDOP_i^2} \tag{2}$$

The next step has led to computation of residuals v, using a weighted average, and deriving a value of the "general" standard deviation (for n' as number of degrees of freedom):

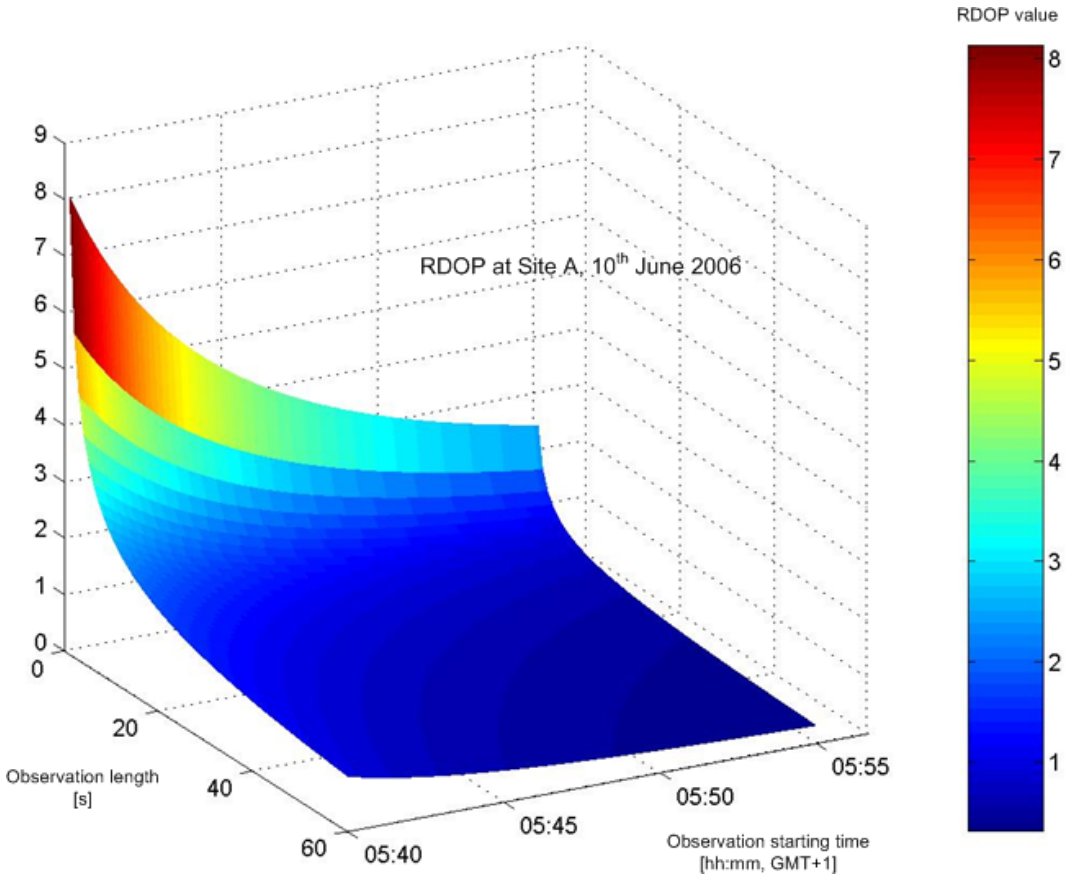

Figure 4: RDOP value modelling

The next step has led to computation of residuals v, using a weighted average, and deriving a value of the "general" standard deviation (for n' as number of degrees of freedom)

$$s_0 = \sqrt{\frac{\sum_{i=1}^{n} p_i v_i^2}{n'}} \tag{3}$$

Thus the standard deviation (used for estimation of RTK precision) can be expressed as

$$s_X = s_{X_0} \sqrt{\frac{RMS_i^2 \; HDOP_i^2}{2}} \tag{4}$$

$$s_Y = s_{Y_0} \sqrt{\frac{RMS_i^2 \; HDOP_i^2}{2}} \tag{5}$$

$$s_H = s_{H_0} \; RMS_i \; VDOP_i \tag{6}$$

Three coordinates, X, Y and H, obtained in one observation epoch, are correlated. As the correlation relations between them are unknown, a precision estimation has been performed separately for each coordinate (Table 1).

Example (1): Considering values RMS=2,7 mm, HDOP=1.26, VDOP=1.93 (mean values of all RMS and DOPs achieved during experiment performance), experimental outcome yields

Table 1: Unit factors of coordinate standard deviations.

Correction Data source	Coefficient s_{Y_0}	s_{X_0}	s_{H_0}
RTK-FKP	2.20	3.93	2.56
RTK-PRS	3.19	5.72	2.74
RTK	1.99	4.43	3.80

the resulting standard deviations for RTK-FKP service as $s_Y = 5.3$ mm, $s_X = 9.5$ mm and $s_H = 13.3$ mm.

Position change (accuracy estimation)

As we are able to estimate precision of single point coordinates, we could estimate accuracy of distance computed from 3D-coordinates of two points. Thus we could derive single point position change with its accuracy and estimate a minimum position change, which we are able to determine with a certain level of risk.

Using (4), (5), and (6) and the error propagation law, we can derive the standard deviation of such point position change

$$\Delta = \sqrt{(X_2 - X_1)^2 + (Y_2 - Y_1)^2 + (H_2 - H_1)^2} = \sqrt{\Delta_X^2 + \Delta_Y^2 + \Delta_H^2} \tag{7}$$

$$s_\Delta^2 = \frac{1}{2\Delta^2}\Big[(RMS_2^2\ HDOP_2^2 + RMS_1^2\ HDOP_1^2)(s_{X_0}^2\Delta_X^2 + s_{Y_0}^2\Delta_Y^2) + 2s_{H_0}^2(RMS_2^2\ VDOP_2^2 + RMS_1^2\ VDOP_1^2)\Delta_H^2\Big] \tag{8}$$

Indexes 1 and 2 represent two different epochs of observation at one site. If we suggest a using significance level $\alpha = 5$, we could derive the minimum detectable point displacement as:

$$\Delta_{\min} = 2\ s_\Delta \tag{9}$$

As we could see, its value is closely related to HDOP/VDOP and RMS values during observation in two epochs. This value depends on the direction of position change.

Example (2): Considering values RMS=2.7 mm, HDOP_1= HDOP_2=1.26, VDOP_1=VDOP_2=1.93, Fig. 5 shows graph describing value $\Delta_{\min}$ in relation to azimuth and elevation of point position change for service RTK-FKP.

If we plot the surface built up by minimal detectable displacement vectors, we obtain a 3D analogy of 2D Helmert's curve. To simplify (8), we could split the displacement vector into two parts, describing displacement in the horizontal plane and the vertical direction. By introducing a mean standard deviation of coordinates in horizontal plane

$$s_{X_0,Y_0}^2 = \frac{1}{2}\left(s_{X_0}^2 + s_{Y_0}^2\right) \tag{10}$$

we are able to derive minimal detectable displacements in horizontal plane and vertical direction and have a better estimation of displacement precision in horizontal plane for different data sources of corrections from the CZEPOS

$$\Delta_{\min,H_z} = s_{X_0,Y_0}\sqrt{RMS_1^2\ HDOP_1^2 + RMS_2^2\ HDOP_2^2} \tag{11}$$

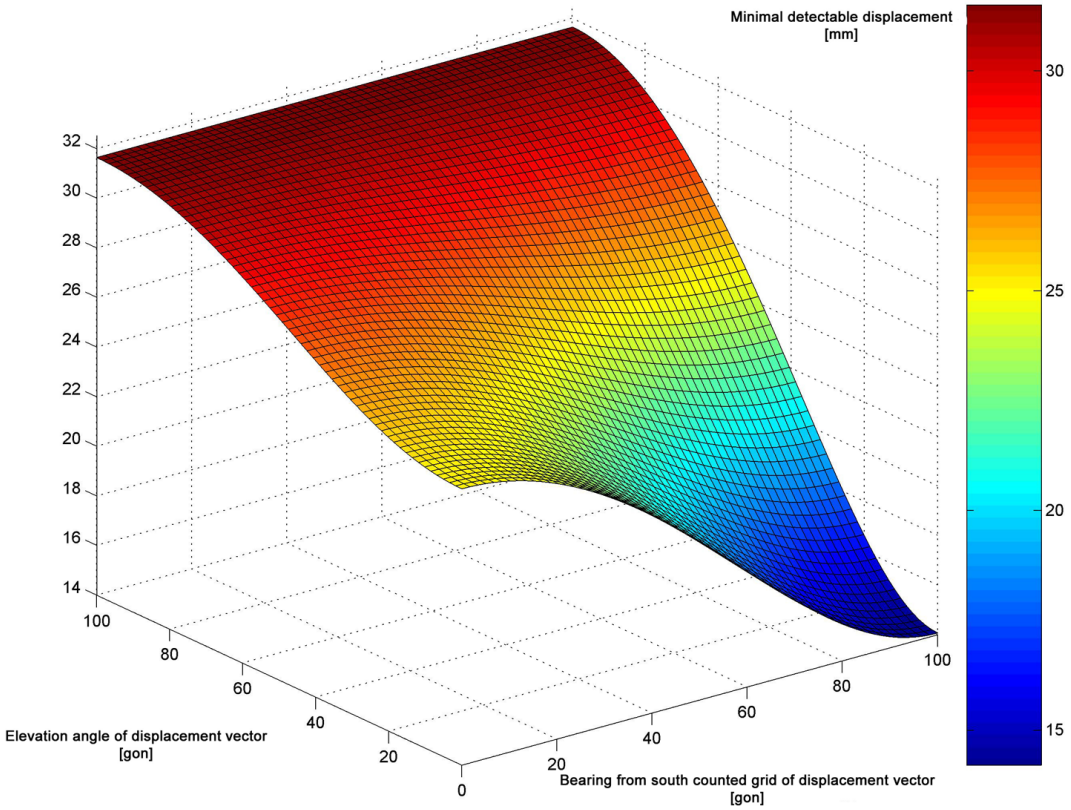

Figure 5: Minimal detectable displacement

Table 2: Unit factors of mean standard deviation in horizontal plane.

Correction Data source	s_{X_0,Y_0}
RTK-FKP	3.18
RTK-PRS	4.63
RTK	3.43

Example (3): Considering values RMS=2.7 mm, $HDOP_1$=$HDOP_2$=1.26, $VDOP_1$=$VDOP_2$=1.93 and using RTK-FKP service, threshold for reliable displacement detecting would be $\Delta_{\min,H_z} = 15$ mm and $\Delta_{\min,\text{height}} = 38$ mm.

4. Conclusions

It is obvious that a permanent reference network holds great potential for different kinds of geodetic applications, requiring real-time data. The experiment shows some possibilities of land slide monitoring with GPS-RTK technology. Within a short observation time (seconds or a few minutes), it is possible to detect centimetre displacements in real time. This precision is more than sufficient for studying earth surface morphology and its changes [8] as well as for some applications of engineering surveying, such as displacement monitoring. Conclusions of the performed experiment has been used for pilot project of landslide monitoring, in clay

quarry "Nepomyšl" [11]. However, as landslide slowed down, the need of higher monitoring precision, unachievable by GNSS/RTK emerged. Based on results of experiments it can be concluded that especially the service RTK-FKP (and its modern version RTK3) is suitable for application of GNSS technologies in the CZEPOS.

Acknowledgements

This contribution was published thanks to the financial support by Ministry of Education, Youth and Sports, the Czech Republic in the Research Program "Udržitelná výstavba" (Sustainable Construction), No. MSM 6840770005 financially supported by Ministry of Education, Youth and Sports, the Czech Republic.

References

[1] Jaroslav Braun and Pavel Hánek. "Geodetic monitoring methods of landslide-prone regions – application to Rabenov". In: *AUC GEOGRAPHICA* 49.1 (Sept. 2014), pp. 5–19. DOI: 10.14712/23361980.2014.2.

[2] Bernhard Hofmann-Wellenhof, Herbert Lichtenegger, and Elmar Wasle. *GNSS — Global Navigation Satellite Systems: GPS, GLNASS, Galileo and more*. Springer Vienna, 2008, p. 516. DOI: 10.1007/978-3-211-73017-1.

[3] Jan Kostelecký and Miloš Cimbálník. "Převod souřadnic mezi ETRS-89 a S-JTSK pomocí globálního transformačního klíče (Transformation between ETRS-89 and S-JTSK using Global Transformation Parameters)". In: *Geodetický a kartografický obzor* 53(95).12 (2007).

[4] Jan Kostelecký et al. "Quasigeoids for the Territory of the Czech Republic". In: *Studia Geophysica et Geodaetica* 48.3 (July 2004), pp. 503–518. DOI: 10.1023/b:sgeg.0000037469.70838.39.

[5] *Land Survey Office. CZEPOS website*. http://czepos.cuzk.cz/.

[6] L. Manetti, M. Frapolli, and A. Knecht. "Permanent, autonomus monitoring of landslide movements with GPS". In: *1st Europen conference of landslides. Prague, Czech Republic*. 2002, p. 6.

[7] Leoš Mervat and Miloš Cimbálník. *Vyšší geodézie 2 (Advanced Geodesy 2)*, Czech Technical University in Prague. 178 pp. 1999.

[8] J. Pospíšil and M. Raška. "Geodetic methods in a study of earth surface processes". In: *Geoscape Journal* 1 (2006), pp. 13–20.

[9] M. Raška et al. "Using geodetic techniques for geomorphologic analyses of scree slopes in low-altitude forested regions and its implication for conservation management". In: *Geographia Technica* 2 (2011), pp. 87–100.

[10] G. Retscher. "Accuracy Performance of VRS Networks". In: *Journal of Global Positioning Systems* 1.1 (2002), pp. 40–47.

[11] K. Turčin. "Landslide monitoring in quarry "Nepomyšl"". Mining surveying documentation of Sedlecky kaolin a. s.. (in Czech, company restricted material, unpublished). 2004-2011.

[12] R. Urban, M. Štroner, and K. Kovařík. "Comparison of GNSS measurement accuracy in reference stations network in territory of Prague". In: *Geodetický a kartografický obzor* 59(101).3 (2013), pp. 45–53.

[13] J. J. Westerveld. "Mobile Networks, Location Based Services lectures materials". TU Delft, Netherlands.

[14] G. Wübbena and A. Bagge. *RTCM Message Type 59 – FKP for transmission FKP, version 1.1.* Geo++® GmbH IGS Workshop, Darmstadt, Germany. 8 pp. 2006.

[15] G. Wübbena, M. Schmitz, and A. Bagge. *Real-Time GNSS Data Transmission Standard RTCM 3.0.* Geo++® GmbH IGS Workshop, Darmstadt, Germany. 26 pp. 2006.

[16] X. Yang and R. Brock. *RDOP surface for GPS relative positioning.* United States Patent No. 6057800. 2000.

Accuracy evaluation of pendulum gravity measurements of Robert Daublebsky von Sterneck

Alena Pešková, Jan Holešovský

Department of Geomatics, Faculty of Civil Engineering
Czech Technical University in Prague
Thákurova 7, 166 29 Prague 6, Czech Republic
alena.peskova@fsv.cvut.cz, jan.holesovsky@fsv.cvut.cz

Abstract

The accuracy of first pendulum gravity measurements in the Czech territory was determined using both original surveying notebooks of Robert Daublebsky von Sterneck and modern technologies. Since more accurate methods are used for gravity measurements nowadays, the work [3] is mostly important from the historical point of view. In previous works [5], the accuracy of Sterneck's gravity measurements was determined using only a small dataset. Here we process all Sterneck's measurements from the Czech territory (a dataset ten times larger than in the previous works [5]), and we complexly assess the accuracy of these measurements. Locations of the measurements were found with the help of original notebooks. Gravity in the site was interpolated using gravity model EGM08, resultant gravity is in actual system S–Gr10. Finally, the accuracy of Sterneck's measurements was evaluated on the base of the differences between the measured and interpolated gravity.

Keywords: Robert Daublebsky von Sterneck, relative pendulum measurements, gravity.

1. Introduction

Robert Daublebsky von Sterneck (* 7.2.1839, † 2.11.1910) was born in Prague, he acted as geodesist, astronomer and geophysicist. He was Head of Astronomical Observatory Institute in Vienna in 1880-1884 and also he was the first to make gravimetrical measurements in the Austria-Hungary. Although he worked in army all his life, he also did various surveying and astronomical measurements. His work was recognized and his name is famous also nowadays. The pendulum instrument built by Sterneck himself was used for gravity measurements, and its improved version was also used in other countries in Europe. Daublebsky used a relative method to measure gravity. Only the time of swing of the pendulum was measured with four implemented corrections. The initial gravity point was located in the cellar of Military Geographical Institute in Vienna, with value g = 980 876 mGal [2]. We divided Sterneck's measurements to two datasets. The first rule for division was different localities of the measurements (measurements on hilltops near trigonometrical points, and measurements in buildings in towns). The second rule was the time of measurements (there is a 3 year gap between the two datasets).

2. Localization of Sterneck's gravity measurements

The original Daublebsky's surveying notebooks [6] and a summary of results in technical report [4] were used for gravity measurement localization. The technical report contains approximate astronomical coordinates of the measurements, whereas detailed information about the measurement process and locations is given in the notebooks. From the technical report, were used these informations: year of measurement, number and title of point (Czech and Germany), latitude and longitude, elevation and the measured value of gravity. Only the details about the locations were used from the notebooks. These details were not registered for all measured points, - 15 points measured in towns haven't had any information about their location (these points were locallized only by approximate coordinates and heights). The measurements were divided into two groups: both by measurement location and by the time measurement. In 1889 – 1895, - 106 points were determined in the Czech territory, as is shown in Figure 1. The first group of points is located on hilltops close to know trigonometric points – hilltop dataset (blue circles in Figure 1). In 1889 – 1891 were determined 35 points in close trigonometric points and 6 points with differently locations in the Czech territory. In 1894 – 1895 (after a 3 year gap), the second group of 65 points was measured in buildings inside towns in the Moravian territory – building dataset (green squares in Figure 1).

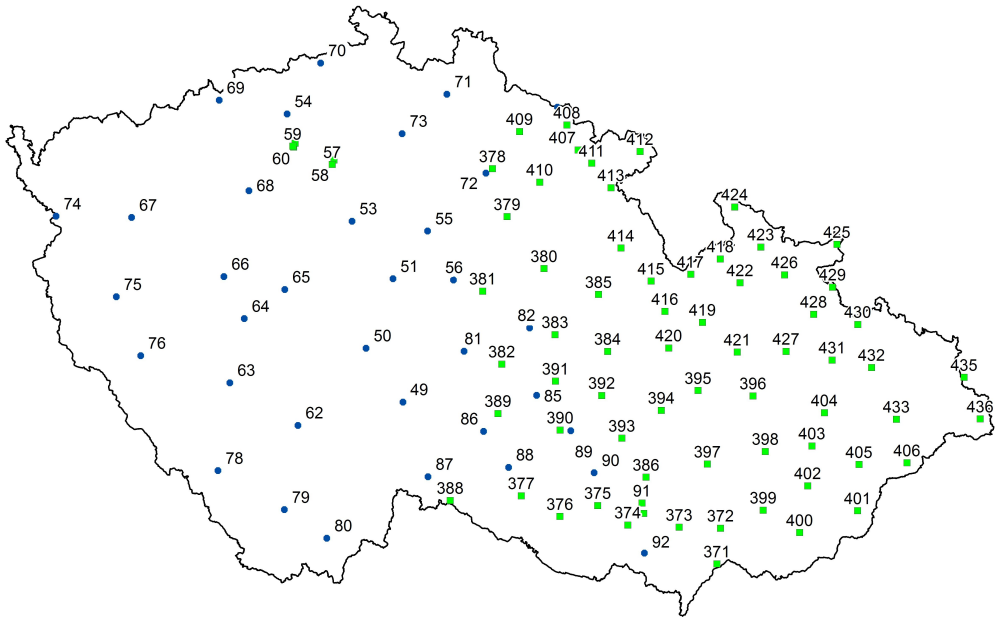

Figure 1: Locations of Sterneck's gravity measurements.

3. Determination of the gravity differences

We used the ArcMap program to determine the coordinates of the measurements with joint WMS provided by The Czech Office for Surveying, Mapping and Cadastre (ČÚZK). Coordinates of the locations with error estimates and corrections for heights (e.g. measurement in a building or on top of a lookout tower) was provided by The Department of Gravimetry, Land Survey Office (ZÚ). They intepolated the complete Bouguer anomaly using the methods of ordinary kriging. The results of interpolation are the most probable values of gravity for the

referenced locations, given with their upper and lower estimate limits. The gravity value is found in this interval with 95% probability. The limits are affected by the uncertainty in elevation and position. The estimated interval isn't symmetrical and it is different for each of the measured points. Throughout this work, only the most probable gravity values were used. The gravity differences are calculated as the difference between Sterneck's measured gravity and the interpolated gravity. These differences were used to evaluate the accuracy of Daublebsky's pendulum gravity measurements.

4. Data analysis

The differences between the measured and interpolated gravity values are distinctly different for the hilltop and the building dataset. The differences gravity in the building dataset show a systematical offset +21.7 mGal, shown in Figure 2. This displacement represents a 72 meters error in elevation. The cause of this displacement isn't known, therefore both datasets were processed separately. A surprising fact about building dataset is that the gravity differences for points without precise location information (only approximate coordinates and heights) and points with these information weren't significantly different. This is illustrated in Figure 3.

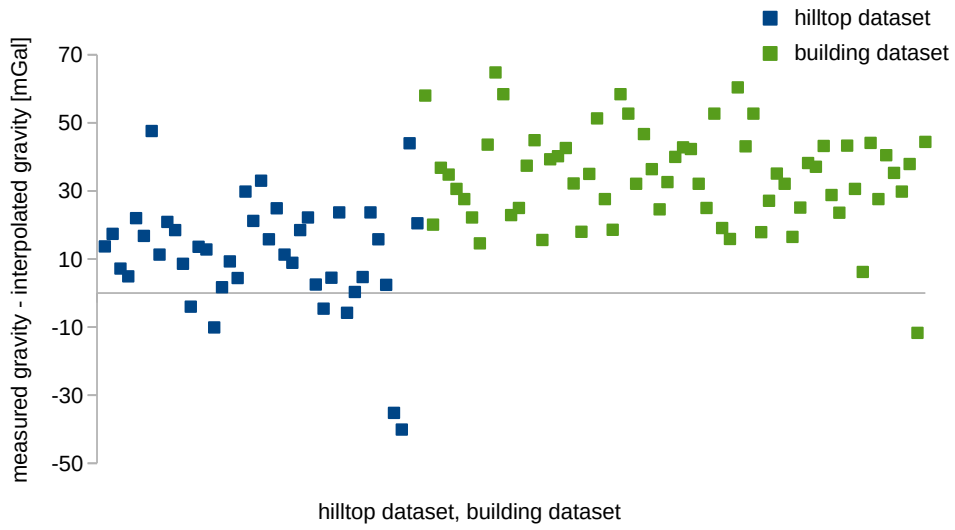

Figure 2: Differences between measured and interpolated gravity for both datasets.

The datasets were tested for data quality. Dependencies between various quantities were tested for this purpose using hypothesis verification. The computed correlation coefficient was compared with its critical value. The tested hypotheses are: gravity falls with growing elevation – (H1), gravity grows with growing latitude – (H2), and gravity and longitude are independent – (H3). All three hypotheses were verified for the hilltop dataset. In the building dataset, H2 and H3 were also verified, but H1 not. Because all of the tested quantities in the building dataset are all right, we think that the elevation values are also affected by an error different from Gaussian noise. Still, the building dataset was used in other processing.

The accuracy of Sterneck's measurements was evaluated by several methods. First, we deter-

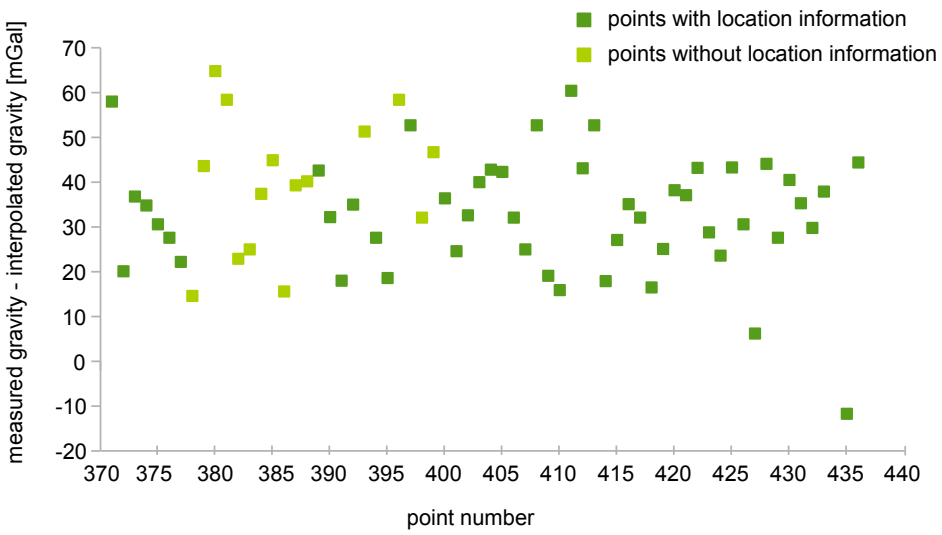

Figure 3: Differences between measured and interpolated gravity for the building dataset.

mined the value mean gravity difference. This value shows the magnitude of the difference between Sterneck's measured gravity and the interpolated gravity. The hilltop dataset has mean gravity difference +11.6 mGal, and +33.3 mGal is for the building dataset. These means are apparently affected by an unknown displacement of the used gravity systems. However, the computed differences are only valid with the assumption of null displacement between the gravity systems. If we want to compare the accuracy of the past and recent measurements, we must calculate the mean difference from absolute value of gravity difference. The datasets are characterized by the mean absolute value of gravity difference of 12.9 mGal for the hilltop dataset and 33.3 mGal for the building dataset. The second method is to evaluate the precision of the measurements using standard deviation of the mean gravity difference. This value shows precision of the measurement method and removes the systematic displacement between the two datasets. Both datasets have identical value of standard deviation equal to 10.3 mGal. The conclusion is that both datasets have identical measurement accuracy, although they were determined with different conditions and in a different environment.

5. Discussion and conclusion

Sterneck's measurements were divided into two dataset differing by both the type of the measurement locations and the time of their acquisition. The statistical processing and evaluation was done separately because of these differences. The building dataset is displaced systematically by about +21.7 mGal from the hilltop dataset (mean gravity difference 11.6 mGal for the hilltop dataset and 33.3 mGal for the building dataset). The cause of this systematic displacement is unknown. The building dataset was determined after 3 year gap. During this time some parameters of the pendulum instrument or some changes in way of calculating corrections could be changed. These changes probably can cause the systematic displacement between both of datasets. Therefore the accuracy of Sterneck's measurements is better assessed by standard deviation of the mean difference. That is 10.3 mGal and is identical for both datasets. This value can be compared with Sterneck's precision estimate of

10 mGal [4]. The mean of gravity difference 11.6 mGal for the hilltop dataset and 33.3 mGal for the building dataset can be compared to measurements in Hungary where the errors of Sterneck's measurements are up to ±20 mGal [5], (but the difference for some points is up to 25 mGal [1]).

Acknowledgement

The authors thank the employees of The Department of Gravimetry, Land Survey Office (ZÚ) in Prague; Martin Lederer, who borrowed the original surveying notebooks of Robert Daublebsky von Sterneck and Otakar Nesvadba, who interpolated the gravity values.

References

[1] Alexandr Drbal and Milan Kocáb. "Významný rakouský generálmajor Dr.h.c. Robert Daublebsky von Sterneck". In: *Geodetický a kartografický obzor* 56(98).2 (2010), pp. 40–46. URL: http://archivnimapy.cuzk.cz/zemvest/cisla/Rok201002.pdf.

[2] Martin Lederer. "Historie kyvadlových měření na území České republiky". In: *Geodetický a kartografický obzor* 58(100).6 (2012), pp. 129–133. URL: http://archivnimapy.cuzk.cz/zemvest/cisla/Rok201206.pdf.

[3] Alena Pešková. "Hodnocení přesnosti kyvadlových tíhových měření R. Sternecka". Master thesis. Czech Technival University in Prague, 2015. URL: http://geo.fsv.cvut.cz/proj/dp/2015/alena-peskova-dp-2015.pdf.

[4] Zdeněk Šimon. *Kyvadlová měření v letech 1956 - 1962*. Tech. rep. Geodetický a topografický ústav v Praze, 1962.

[5] V. B. Staněk and J. Potoček. "Vývoj a způsob měření intensity tíže v Čechách a na Moravě". In: *Zeměměřičský obzor* 1(28).6 (1940), pp. 81–87.

[6] Robert Sterneck. "Měřické sešity 1889 - 1895". Vojenský zeměpisný ústav ve Vídni. Unpublished.

Table 1: Input – Part 1

Year of measurement	Number of point	Latitude [° ’]	Longitude from Ferro [° ’]	Altitude [m]	Measured gravity [mGal]
1889	49	49 24	32 38	738	980 856
	50	49 36	32 20	712	980 887
	51	49 55	32 27	545	980 938
	52	50 44	33 24	1602	980 762
	53	50 08	32 08	356	981 016
	54	50 33	31 36	835	980 924
	55	50 08	32 39	213	981 070
	56	49 57	32 51	470	980 952
	57	50 22	31 57	205	981 076
	58	50 23	31 57	459	981 019
	59	50 25	31 40	202	981 060
	60	50 26	31 41	417	980 998
	61	50 25	31 41	250	981 055
1890	62	49 14	31 58	624	980 846
	63	49 22	31 29	585	980 851
	64	49 39	31 31	842	980 855
	65	49 48	31 45	659	980 911
	66	49 49	31 20	716	980 893
	67	50 01	30 40	822	980 922
	68	50 12	31 25	534	980 983
	69	50 34	31 08	921	980 920
	70	50 48	31 47	748	980 963
	71	50 44	32 39	1010	980 915
	72	50 25	32 59	430	981 016
	73	50 32	32 23	565	980 989
	74	49 58	30 10	939	980 862
	75	49 40	30 39	537	980 937
	76	49 26	30 52	724	980 877
	78	49 00	31 29	1362	980 663
	79	48 52	31 57	1084	980 716
	80	48 46	32 15	869	980 760
1890	81	49 39	32 59	709	980 849
	82	49 47	33 24	662	980 895
1891	85	49 30	33 30	693	980 881
	86	49 19	33 11	732	980 873
	87	49 05	32 51	731	980 819
	88	49 10	33 22	710	980 861
	89	49 22	33 45	639	980 841
	90	49 11	33 56	513	980 846
	91	49 05	34 16	201	981 004
	92	48 52.0	34 19.0	550	980 853

Table 2: Input – Part 2

Year of measurement	Number of point	Latitude [° ’]	Longitude from Ferro [° ’]	Altitude [m]	Measured gravity [mGal]
1894	371	48 51.3	34 47.7	160	980 943
	372	49 00.6	34 47.8	193	980 917
	373	48 59.7	34 31.5	226	980 943
	374	48 58.9	34 11.3	181	980 957
	375	49 03.0	33 58.8	246	980 961
	376	48 59.1	33 44.5	355	980 937
	377	49 03.3	33 28.5	465	980 925
1895	378	50 26.3	33 01.3	273	981 057
	379	50 14.5	33 09.5	228	981 068
	380	50 02.3	33 26.8	214	981 076
	381	49 54.6	33 03.5	263	981 054
	382	49 36.5	33 14.7	428	980 946
	383	49 45.7	33 34.3	569	980 935
	378	50 26.3	33 01.3	273	981 057
	379	50 14.5	33 09.5	228	981 068
	380	50 02.3	33 26.8	214	981 076
	381	49 54.6	33 03.5	263	981 054
	382	49 36.5	33 14.7	428	980 946
	383	49 45.7	33 34.3	569	980 935
	384	49 42.9	33 55.9	555	980 955
	385	49 57.3	33 49.7	287	981 030
	386	49 11.7	34 16.5	235	980 962
	387	49 02.3	34 17.1	191	980 979
	388	48 59.9	33 01.0	506	980 911
1895	389	49 23.7	33 15.5	514	980 940
	390	49 21.3	33 40.7	425	980 955
	391	49 33.7	33 36.6	574	980 922
	392	49 31.4	33 55.5	554	980 942
	393	49 21.0	34 05.3	270	980 999
	394	49 29.3	34 19.7	396	980 969
	395	49 35.4	34 33.3	410	980 953
	396	49 35.4	34 55.3	225	981 026
	397	49 16.7	34 40.0	254	981 001
	398	49 21.5	35 02.3	200	980 983
	399	49 06.3	35 03.7	209	980 958
	400	49 01.4	35 18.8	248	980 932
	401	49 08.4	35 40.7	390	980 892
	402	49 13.7	35 20.2	231	980 959
	403	49 24.0	35 20.5	316	980 972
	404	49 32.9	35 24.2	256	981 010
	405	49 20.4	35 39.7	340	980 954

Table 3: Input – Part 3

Year of measurement	Number of point	Latitude [° ’]	Longitude from Ferro [° ’]	Altitude [m]	Measured gravity [mGal]
1895	406	49 21.9	35 58.5	510	980 906
	407	50 33.8	33 34.9	415	981 052
	408	50 39.8	33 29.1	610	981 045
	409	50 36.7	33 10.4	462	981 052
	410	50 24.3	33 21.0	335	981 039
	411	50 30.8	33 41.0	359	981 097
	412	50 35.2	33 59.9	405	981 085
	413	50 25.1	33 49.8	337	981 069
	414	50 09.9	33 56.6	321	981 014
	415	50 02.2	34 10.0	368	981 007
	416	49 54.8	34 16.8	387	981 002
	417	50 05.1	34 25.6	567	980 972
	418	50 09.8	34 36.8	536	980 969
	419	49 53.0	34 32.3	301	981 000
	420	49 45.5	34 19.9	350	981 002
	421	49 46.3	34 47.3	235	981 025
	422	50 04.2	34 45.6	489	981 005
	423	50 13.9	34 52.5	441	981 023
	424	50 23.5	34 40.4	339	981 043
	425	50 16.5	35 22.9	238	981 081
	426	50 07.4	35 03.1	519	981 003
	427	49 47.7	35 06.6	550	980 944
	428	49 58.0	35 16.2	550	980 999
	429	50 05.4	35 22.7	313	981 041
	433	49 32.9	35 52.9	406	980 973
	435	49 45.1	36 18.3	308	980 972
	436	49 34.7	36 26.0	386	980 973

Geodetic surveying as a tool for discovering the prehistoric settlement in Sudan (the 6th Nile cataract)

Jan Pacina

J. E. Purkyně University in Ústí nad Labem
Czech Republic

Abstract

Surveying is an important part of any archaeological research. In this paper we focus on the archaeological research in north Sudan (6th Nile cataract) and the surveying methods applicable under the local conditions. Surveying in the Third World countries is affected by the political situation (limited import of surveying tools), local conditions (lack of fixed points, GNSS correction signal), inaccessible basemaps and fixed point network. This article describes the methods and results obtained during the three archaeological seasons (2011 – 2014). The classical surveying methods were combined with KAP (Kite Aerial Photography) to obtain the desired results in form of archaeological maps, detailed orthophoto images and other analyses results.

Keywords: Sudan, 6th Nile cataract, surveying, KAP, methods

1. Introduction

The Czech Institute of Egyptology has conducted research on archaeological concessions in Sudan (6th Nile cataract) since 2009 (Lisá et al., 2011; Suková – Cílek, 2012; Suková – Varadzin, 2012). This archaeological concession is located approximately 80 km downstream of Khartoum. It covers nearly 40 km of the west bank of the Nile and includes the whole western part of the Sabaloka Mountains and the zone is *ca.* 10 km in breadth extending from the riverbank towards the west and north-west (see Fig. 1). The interdisciplinary exploration of this area is aimed at a better understanding of the occupation of the Sabaloka Mountains and its vicinity during the Mesolithic and Neolithic periods (8th–4th millennia BC) and its interaction with the (changing) environment.

An integral part of the archaeological research is documentation by a variety of geodetic methods. The total station in combination with GPS measurements and Kite Aerial Photography was used for the surveying of the archaeological sites and features and topographic elements (such as terrain, settlements, paths). The results of the surveys are plans and archaeological maps, which supplement the satellite images of the research areas. Due to the absence of a fixed geodetic network and the GNSS correction signal, the survey was performed in a local coordinate system and even standard surveying procedures had to be adjusted from time to time to suit the local conditions. The objective of this article is to present the surveying methods applied in the extreme conditions of the Sudanese desert and the results achieved.

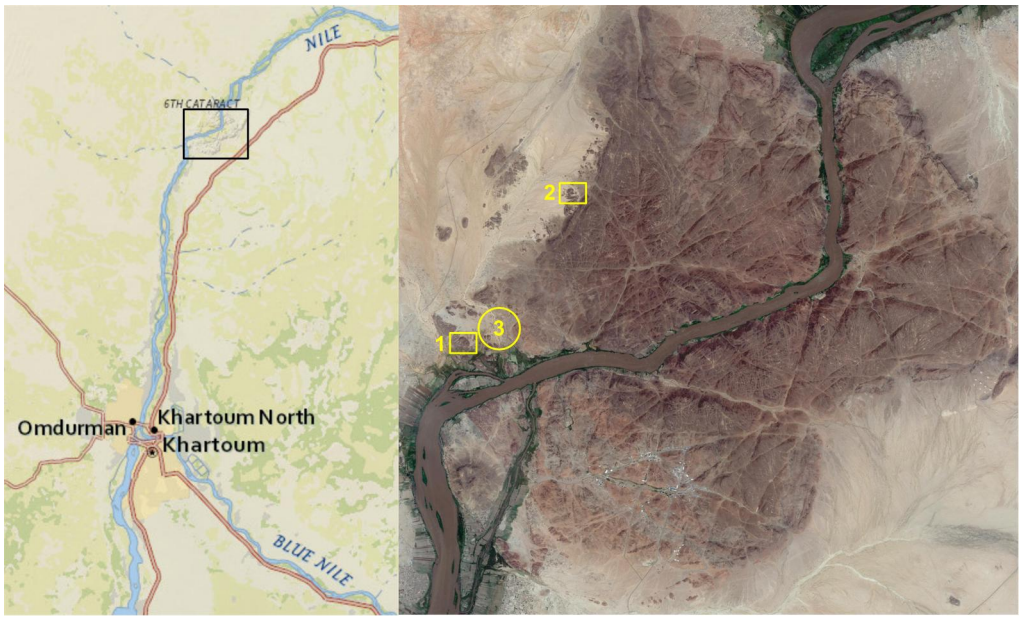

Figure 1: Area of interest overview (Sabaloka game reserve): 1 - the Fox Hill locality, 2 - the Sphinx Locality, 3 - prehistoric lake in the Lake Basin (basemaps: left – ESRI, right – Google).

2. Surveying conditions in Sudan

2.1. Importing surveying equipment

The Republic of South Sudan became independent in spring 2011. Since this period, the Republic of Sudan has applied very strict rules for the import of all surveying equipment (and many more things). All of the equipment (total station, GPS receivers, walkie-talkies) is subjected to special taxes. Permission issued by the Surveying Department in Khartoum allowing the usage of imported equipment may be required. The price of the permission depends on the type of imported equipment. Importing walkie-talkies (for long distance surveying) is not recommended as an additional permission from the Ministry of Communication is required.

2.2. Basemaps and satellite imagery

All of Sudan is, according to (Ali, 2009), covered by the Anglo-Egyptian Sudan Map Series, scale 1:250 000, created in the period of 1936-1951 by the United Kingdom Directorate of Overseas Survey. These maps are stored at the Survey department in Khartoum and they contain topographic layers together with approximate position of benchmarks and triangulation points. Other topographical maps available in our area of interest are maps 1:200 000, made by the Soviet Union in 1971. A more detailed map, is the one issued by the Sudan Survey Department in scale 1:100 000 – this map series was prepared in cooperation with the United Nations Development Program and it covers selected areas of the country (see Fig. 2).

There are no large scale maps available for the areas of interest, thus satellite imagery was used to identify terrain objects, possible settlement areas and for navigation purposes. The

Figure 2: Area of interest presented on a 1:100 000 map.

WorldView 2 panchromatic (spatial resolution in nadir 0.46 m) and multispectral (resolution 1.8 m) imagery were chosen as a suitable data sources for research purposes. The data obtained, were further processed using the *pansharpening* method. With respect to the price of the data, only the core areas were covered by the WorldView 2 imagery at the Sabaloka site.

The entire area of the research site at Sabaloka (covers nearly 40 km of the west bank of the Nile and includes the entire western part of the Sabaloka Mountains and the zone ca. 10 km in breadth extending from the riverbank towards the west and north-west) was covered by satellite imagery accessible by Google Earth, handpicked and saved directly from the application. All the images were stitched together using a panorama stitching software into a seamless image. The produced image is not registered to any coordinate system.

Navigation in an unknown terrain required an easy way how to transfer registered satellite imagery into a rugged Garmin GPS receiver. The new Garmin BirdsEye Satellite Imagery was used in this case, it offered the same quality as it is accessible in Google Earth for our areas of interest. This was very helpful while moving within the Sabaloka mountains.

2.3. Coordinate system and geodetic control network

In Sudan, one can encounter many different coordinate systems – Adindan, 1942 or WGS84. Adindan is a geodetic datum suitable for use in Eritrea, Ethiopia and Sudan. Adindan

references the Clarke 1880 (RGS) ellipsoid and the Greenwich prime meridian (GeoRepository, 2015). The 1942 coordinate system is used in the Russian maps 1:200 000 and WGS84 is used worldwide for the GPS NAVSTAR.

The coordinates of the archaeological sites were obtained from NCAM (Sudan National Corporation for Antiquities and Museums) in the Adindan coordinate system without any metadata. This coordinate system was identified in ArcGIS (ESRI corp.) as Adindan_UTM_Zone_36N and the data could be properly transformed into WGS 84 and used for navigation using a common Garmin GPS.

The geodetic control network at the Sabaloka locality was explored in the Survey department in Khartoum, but the closest benchmark and triangulation point on the west bank of the Nile is located in Obdurman (ca. 70 km upstream). Fixed points on the east of the Nile were closer, but located in a highly secured military area. Based on these facts, local coordinate systems were established.

2.4. The local geodetic control network

The absence of a geodetic control network at Sabaloka resulted in the creation of a local geodetic network covering all areas of interest – the total area where the surveying tasks were performed is larger than 400 ha. The terrain at Sabaloka is very complex, with hills, large rocky structures and flat desert planes making the surveying difficult.

Figure 3: Points used as ground control points in the KAP survey (left), discrete fixed points (right).

The archaeological research begun in autumn 2011 at the Fox Hill locality (SBK.W-20/B) (Suková – Cílek, 2012; Suková – Varadzin, 2012) and here the beginning of the local coordinate system was situated. The coordinate system was initially meant to be used only for Fox Hill and the close neighborhood. The imprecise GPS measurements made it impossible to compare the elevation characteristics of the other archaeological sites within the Czech concession – thus the same coordinate system was "transferred" into all areas of interest.

Altogether 21 fixed points were established within the Fox Hill and the Sphinx (SBK.W-60) localities. All measurements performed in this area were based on these fixed points. The fixed point establishment was performed in 2012 by colour painting on selected rocks as the hills in the surroundings are made of friable granite. In the beginning of 2014, almost no fixed

Figure 4: Fox Hill locality and the surroundings.

points were identified as the extreme weather conditions destroyed the paint. The renewal of the local geodetic network was a crucial part of the 2014 expedition as incorporating the measurements from the past seasons with the current results was highly desirable.

3. Surveying instruments and tools

The most important imported surveying tool was the total station Leica TCR 303 (see Fig. 5). Two types of GPS receivers were used during the archaeological research – GPS Trimble Juno ST and Garmin GPSMap 62s. Despite of the lack of the GNSS correction signal, GPS usage was limited. GPS is mainly used for marking points of interest (settlement marks, important objects, terrain formations) discovered during the archaeological research in the wide area of the Sabaloka Mountains, marking the geodetic control network points as it is not easy to identify them in the rocky area, navigation to archaeological sites defined by NCAM and for navigation in the unknown terrain.

Figure 5: Surveying at the Sphinx locality (photo: L. Varadzin).

Figure 6: The Picavet suspension used on the Rhombus kite.

Kite Aerial Photography (KAP) was applied during the last archaeological season (autumn 2014). Small Format Aerial Photography is produced by KAP (Aber et al, 2010) which is usable for 3D models and orthophoto creation. KAP may be used as a supplement for UAVs (drones) in regions where their usage is forbidden. KAP has been successfully used in archaeological research in Africa many times (Bitteli, 2001; Brůna, 2013; Chagny – Hesse, 2007; Żurawski, 1993, 2005)

The one-string kite Elliot Rhombus Mega Power Sled, 300 × 170 cm, string length ca 200m, wind range 2 – 5 Bft and reinforcements GFK 2mm was used for the KAP survey. The same kite system was used with great success at archaeological sites at Abusir, Egypt (Brůna, 2013). The Picavet suspension (Verhoeven et al., 2009) is used to carry the camera used for SFAP (see Fig. 6). The camera holder was originally designed for a Canon Power Shot D10 camera with a mechanical trigger shooting images every 10 seconds. The 10 second shooting interval made this camera inappropriate for surveying large areas. A GoPro Hero 3+ camera was used instead. GoPro is a wide-angle, watertight camera with a 12MPix sensor and electronic shutter allowing time lapse images at a defined interval (2 second interval was used in this case). This camera is not primarily designed for SFAP (as it is equipped with a rolling shutter), but concerning its weight/pixel count/durability and based on our previous tests, this camera best served our needs in the KAP survey.

Other integral parts of the archaeological documentation are the simple measuring equipment which effectively support the surveying instruments. These are measuring tapes on a wheel of length 20 m and 50 m, tape rules (2 m or 5 m), folding rules (2 m), plummets, surveying stakes, strings for the delimitation of an archaeological squares, etc.

3.1. Surveying methods and precision

The total station Leica TCR 303 in combination with a surveying prism on a telescopic pole was used for the most of the mapping tasks. The range of the TCR 303 is maximally 2500 m and the longest sight lines within the archaeological mapping did not reach 1500 m. The total station is equipped with a program for computation of the free station method, measurements of minor geodetic points and indirect distance measurements. The methodology of “surveying

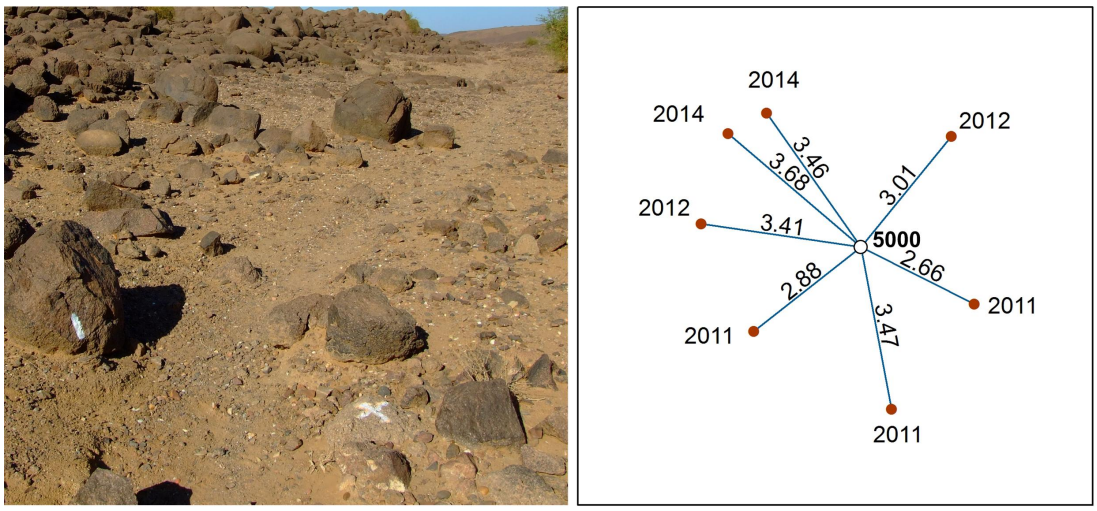

Figure 7: The initial point 5000 of the local coordinate control network (left). The control measurements on point 5000 during the archaeological seasons 2011, 2012 and 2014. The calculated distances are in cm (right).

in the desert" was many times proven during other archaeological expeditions in Egypt. See Brůna (2013) for more details.

The surveying conditions are much different from well-known European standards. The lack of a geodetic control network makes the surveying even more complicated and standard surveying workflows can't always be followed. Another factor is time stress – despite the expedition's time schedule and the surveying tasks time demandingness, all of the tasks had to be performed on the first attempt. This was a problem when making long-distance measurements. Long distance measurements are used while transferring the local coordinate control network to other archaeological sites in the area of interest. The measured distances were ca. 1000 m long and communication between the surveyor and the telescopic pole operator is problematic. Walkie-talkies normally used in Western countries, but are forbidden in Sudan – thus special flag signals (in combination with binoculars) are used to check whether the surveyor or the pole operator is ready to perform the measurement.

There are also several facts as well that may influence surveying precision. The imported total station may be stored in a custom warehouse for several days. Based on our experience, the goods stored in the custom warehouse were not always gently handled. The total station had to be checked and some basic calibration performed prior to surveying in the field.

Other facts influencing precision are the total station and the telescopic pole centering uncertainties - the fixed points are (with respect to the granite stones and rocks) marked by ca. 4 cm thick lines (see Fig. 7). Points established by the iron pipes (see Fig. 3, left) were built at the end of the 2014 season to preserve the points for further use. The vertical position of the telescopic pole is another crucial factor of the measurement but the set for the three-tripod system, suitable for long-distance measurements and fixed point establishment, is impossible to import into Sudan.

While transferring the coordinate system into other localities an oriented traverse is used.

Under standard conditions, such a long traverse should be oriented and connected on both ends to preserve the measurement precision. In the desert, we were forced to make the traverse only one side oriented and connected. Using this method will secure a sub-decimeter precision in the Z coordinate in-between the archaeological sites required for the Nile flood modelling. Transferring the coordinate system from Fox Hill to the Sphinx locality was the biggest surveying task. The traverse was almost 5 km long and 7 change points were used. This measurement lasted two days due to the rough terrain in which all the equipment couldn't be transported by a car.

The precision of the surveyed points was regularly checked by the control measurements on the established fixed points[1]. During every archaeological season, these measurements are performed to check the accuracy of the reconstructed fixed point network. An example is presented in Fig. 7, where the control measurements were performed on the initial point of the local geodetic control 5000 [1000, 1000, 377.87]. The measured coordinates are presented in Tab. 1. The RMS errors calculated based on these measurements are the following:

$$m_x = 0.020; \qquad m_y = 0.021; \qquad m_{xy} = 0.030.$$

Archaeologists required surveying precision (under these conditions) up to 5 cm, which was fully achieved.

Table 1: Point 5000 coordinates as measured during archaeological seasons 2011, 2012 and 2014.

Year	X 1000.000	Y 1000.000	Z 377.870
2011	999.977	999.982	377.876
2011	1000.023	999.988	377.863
2011	1000.006	999.965	377.876
2012	1000.019	1000.023	377.880
2012	999.966	1000.004	377.874
2014	999.980	1000.028	377.873
2014	999.972	1000.024	377.877

Another task was to compute the KAP derived models accuracy. The results derived from the KAP survey are Digital Surface Models (DSM) and orthophotos. Here we may want to know the accuracy of the resulting 3D model. The derived raster DSM is compared with the points surveyed during the 2011 and 2012 season (see the Fox Hill case study chapter). The resulting differences should evaluate the quality of the data. All of the tested DSMs have differences of no larger than +/- 5 cm from the reference data. The larger differences are caused by the sparse surveyed points which do not describe all of the rocks and stone formations in detail.

4. General conditions

The general conditions are much different from Western World standards. The whole archaeological expedition is living in the same conditions as the locals, accommodated in a rented

[1] While measuring archaeological data, the points of the (local) fixed geodetic network in the surroundings are measured as unknown points to evaluate the measurement accuracy.

house near the archaeological site. The house is built of bricks dried in the sun and usually contains of two large rooms, a hall and a large back-yard (used as an open-space bedroom). Food is obtained from local sources and prepared by a hired Sudanese cook. Nile water is used for washing and cooking and bottled water for drinking. Electricity has been available since 2013, so the diesel generator used for charging all the equipment is no longer used.

Sunrise is about 6am and sunset about 6pm. Work starts usually at 7am and there is a lunch break from 12.30 pm to 3pm, as the weather is very hot during midday. High temperatures (over 50°C) are not suitable for the surveying equipment. Stronger winds sometimes bring dust and sand in the air and these conditions are not suitable for long distance measurements.

The local people are mostly friendly and hospitable, but the fixed points have to be marked in a very discrete way as a cross made on the stones by the *foreigner* means that there is gold hidden underneath. This has led to the destruction of fixed points on several occasions.

5. The Fox Hill locality (SBK.W-20/B)

The Fox Hill locality is the most important prehistoric site located within the Czech archaeological concession in the Sabaloka region. The site is structured on 16 terraces and platforms, the total surface area of which is 11,650 m^2 (Fig. 8). The terraces and platforms are well delimited by the exposed bedrock and boulders and vary in size, elevation and ease of access. The settlement is dated back to the Mesolithic (ca 9000 – 5000 BC) and Neolithic (5000 – 3000 BC) periods (Suková – Varadzin, 2012).

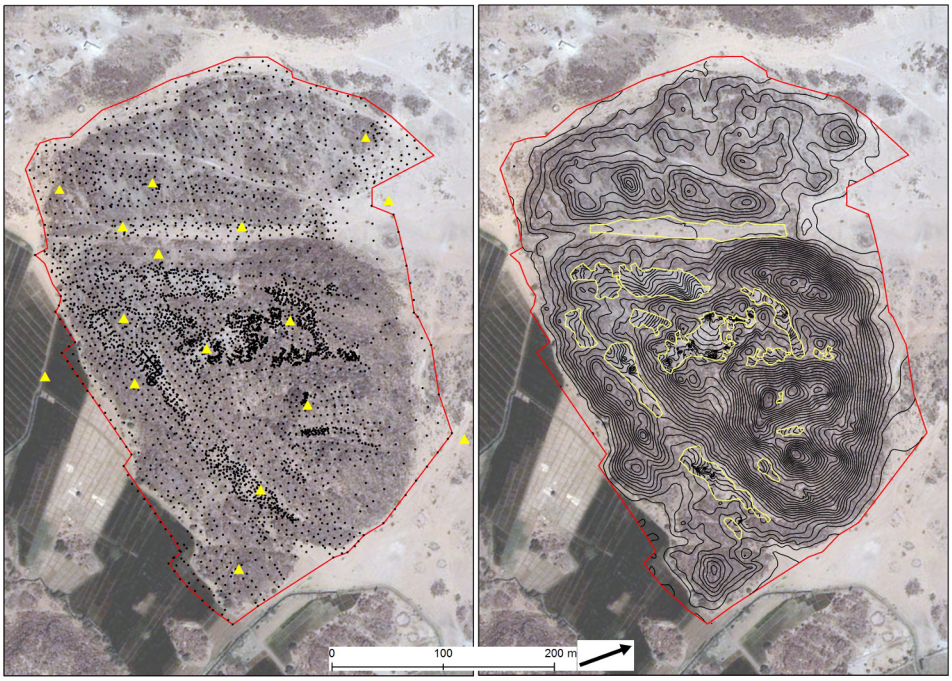

Figure 8: Surveyed points at the Fox Hill locality with marked fixed points (left). Contour lines generated from the DEM generated based on the surveyed points and the delineated occupation terraces (right). (Basemap: Google)

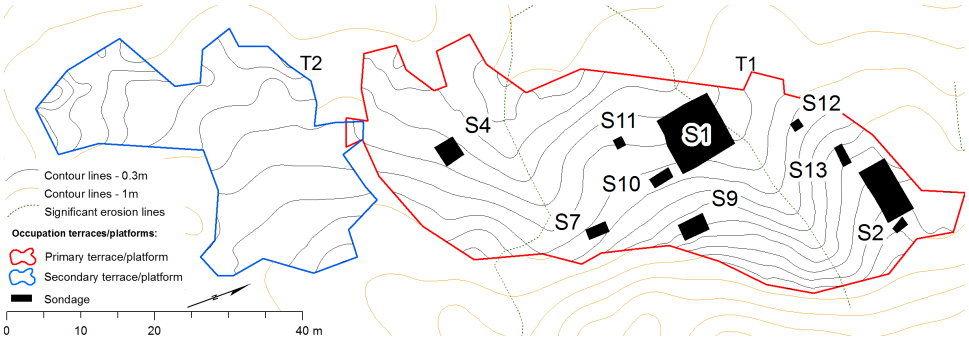

Figure 9: Detail of Terrace 1 and Terrace 2 at the Fox Hill locality.

At Fox Hill, 17 geodetic control points were established and more than 4500 points were measured. The occupation terraces are covered by a 1x1m point network and the rest of the area by a 5x5 m network, supplemented by points of erosion lines, ridges and significant stone structures.

Every site has its own specific environment, thus the choice of a proper interpolation method is required (Karel, 2006; Pacina, 2013). Based on previous results and tests, interpolation methods implemented in the ArcGIS (Topo to Raster) were used for producing a DTM of the localities.

Contour lines of a 0.3m interval for the occupation terraces and a 1m interval for other areas were derived from the interpolated DTM. See Fig. 8. The contour map may describe the spatial relationships between adjacent areas in the locality, material transportation caused by erosion (the archaeological soundings started in the areas that are not affected by erosion), and possible connections between the settlement areas and their elevation.

Delimitation of the occupation terraces at Fox Hill must be done by an archaeologist, as they recognize the boundaries of the terrace. An example of the delineated terrace, together with archaeological soundings is shown in Fig. 9. Fig. 11 shows objects excavated at Terrace 1 (T1), Sounding 2 (S2) in detail.

6. The Sphinx locality (SBK.W-60)

The Sphinx locality, positioned on a granite outcrop in the Rocky Cities area is the second most important site in the Czech concession. The outcrop features only one platform of 940 m^2 situated ca 15 m above the surrounding terrain. The surface finds at Sphinx attest to the occupation of this site only during the Mesolithic period (Suková – Varadzin, 2012).

Despite of the distance between the two localities it was decided to make a local coordinate system at Sphinx as well. The archaeologist requested a sub-meter precise comparison of the altitudes of these two localities in connection with the possible local flooding by Nile. A test using the Garmin GPS receiver was performed to define the altitude of the two known points previously measured with the total station. Altitude calibration was performed on one of the points and the other point several hundred meters away was then measured. The result was unsatisfactory – the difference in the altitude was almost 10 m. It was decided to put the Sphinx locality in the same local coordinate system as Fox Hill. This was performed by a *one*

Figure 10: Fox Hill - Terrace 1, Sounding 2 - excavated circular objects.

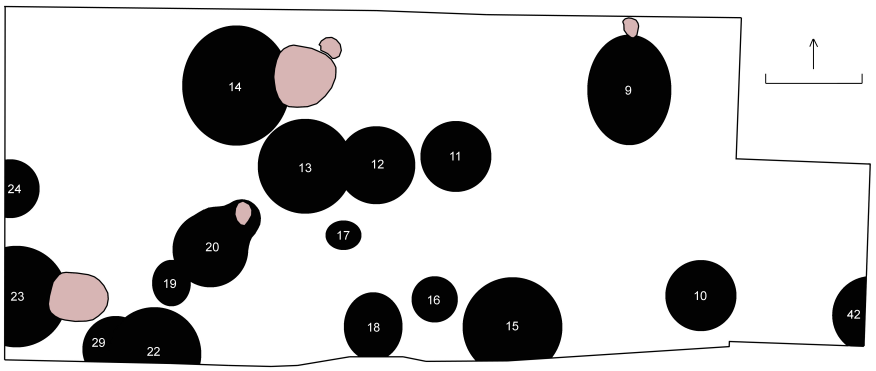

Figure 11: Objects excavated at Terrace 1, Sounding 2 – compare with Fig. 10.

point oriented traverse (7 points, 4.7 km length). Based on previous precision tests performed in this area; we may consider the precision of the applied method satisfactory.

Within the Sphinx locality, about 400 points on settlement terrace of ca. 900 m^2 (see Fig. 12) were surveyed. The resulting archaeological map is presented in Fig. 14 and the sounding excavated in season 2012, in Fig. 13. The archaeological map has a detailed orthophoto used as the basemap. This orthophoto was created using KAP and the Small Format Aerial Photography. Altogether more than 1300 images were taken during the KAP survey. The camera on the kite swung and thus only a small amount of the imagery could be considered horizontal and used for further processing. Only 60 images were used for creating the 3D model of the Sphinx locality and the derived orthophoto (presented in Fig. 14). Image processing was per-

Figure 12: The Sphinx locality with marked occupation terrace.

Figure 13: The Sphinx locality - research at Sounding 2 (2012).

formed using PhotoScan (Agisoft LLC) software. Detailed processing workflow is described i.e. in (Verhoeven et al., 2012).

7. Discovering a prehistoric lake – the Lake Basin locality

The Lake Basin area adjoins the massif of Jebel Sabaloka from the south west and extends over ca. 2.2 km x 1.5 km. This microenvironment is closely connected to the Nile, the waters of which used to submerge the lower reaches of this area during the annual floods in prehistoric times. This landscape type is formed of more than 20 mostly granite rock outcrops which vary in their size and in the number of natural terraces and platforms suitable for occupation (see Fig. 15). The former occupation sites are arranged around a depression where the remains

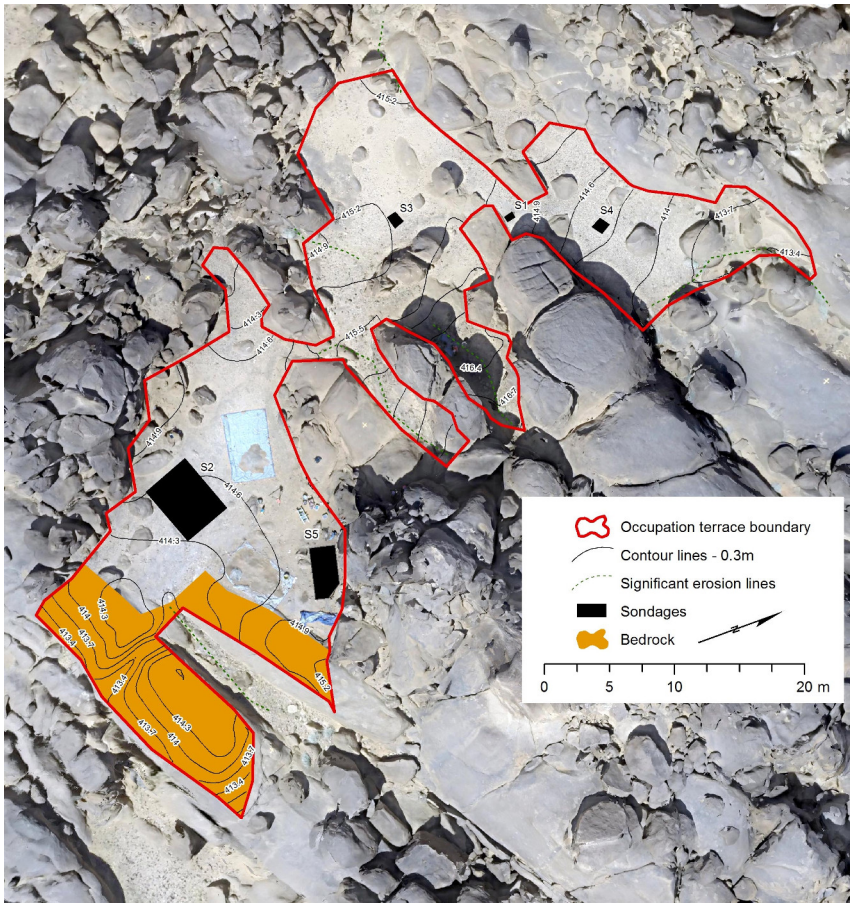

Figure 14: Archaeological map of the Sphinx locality.

Figure 15: Lake Basin with granite rock outcrops.

Figure 16: KAP in the Lake basin (Photo: J. Novak).

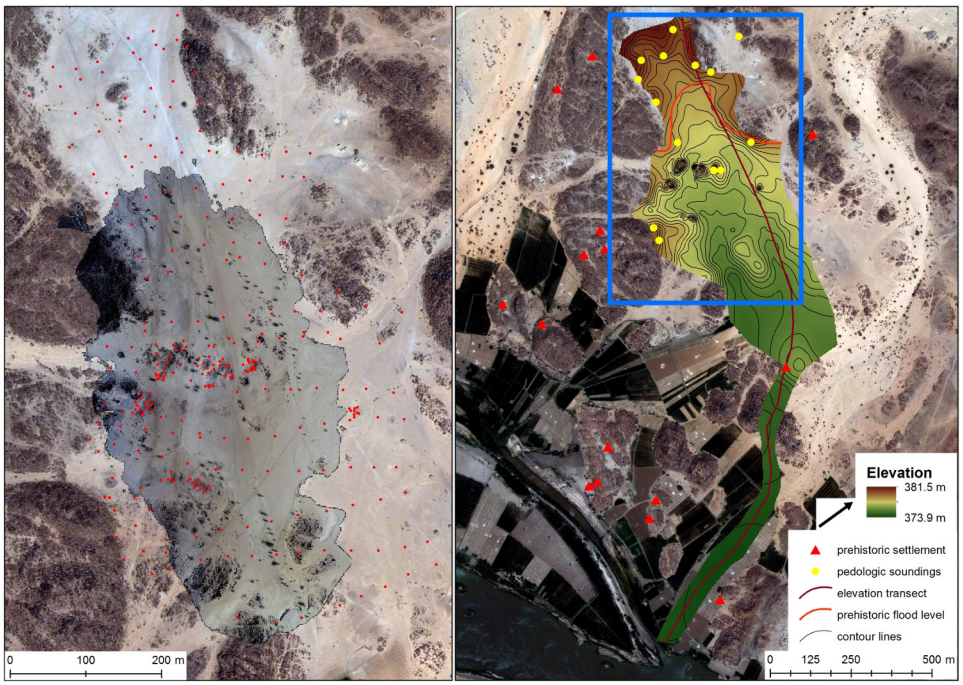

Figure 17: Point surveyed within the Lake Basin area and orthophoto derived from the KAP survey (left). The created DTM of the prehistoric lake bottom with locations of identified archaeological sites and sediment soundings. (Basemap: Google)

Figure 18: Orthophoto image created based on the KAP survey – marked sounding at the tumulus foot.

of a prehistoric lake were identified (Suková – Varadzin, 2012).

Since the 2012 season, it was desired to create a 3D model of the prehistoric lake bottom and prove the relationship with the Nile water level and potential prehistoric flooding. With respect to the natural conditions in the Sabaloka region, it is not easy to visually estimate elevations and distances. The lake bottom reconstruction has been done using several methods. In 2012, two transects were surveyed proving that this area could be flooded by the Nile. More effort was used to work on this topic in the 2014 season. The whole bottom of the potential lake (ca. 25 ha) was covered with a regular 25 x 25 m point grid and surveyed with the total station densified in the areas with a more complex terrain.

The KAP survey was used in the areas where the sediment samples were taken. The area of interest was surveyed twice as during the first attempt a very strong wind caused an uncontrollable kite fall resulting in camera damage. The second attempt went well, but it was proven that the KAP method is not suitable for covering such large areas, using the equipment used so far. The camera swings on the kite and a longer observation at one point is required to obtain horizontal images – this can be achieved in smaller localities but impossible at a 25 ha area. The oblique images in different directions "break" the point cloud computed by the Structure from Motion algorithms. More than 1600 images were taken during this survey and only 200 were finally used for the 3D model and orthophoto creation.

The area surveyed by the KAP method and covered with surveyed points is presented in Fig. 17. Based on all the obtained data, the DTM representing the former lake bottom was created. In Fig. 17 (right) the prehistoric settlement sites (occupation terraces) in the Lake Basin surroundings are identified. The altitude of these sites varies from 378 to 380 m.

Based on field research, it was determined that these settlement sites were (probably) not flooded during the seasonal Nile floods and thus this elevation value was used for modelling the level of prehistoric floods. Details of the resulting orthophoto image of the Lake Basin (with 3 cm/pixel resolution) are presented in Fig. 18. In the figure, the soil profile containing the original prehistoric lake sediments, protected from erosion by the tumulus is marked.

8. Conclusions

The modern methods of spatial data collection offer fast and quality data. Surveying in developing countries is a little different as new methods can't be imported (UAV) or properly used (GNSS correction signal). The surveying methods applied in the Sudanese desert are not absolutely fitting into Western standards but still offer the best possible results under these extreme conditions. In this paper, spatial data collection methods are presented used within the archaeological research that offer a new point of view on archaeological sites and findings. One interesting data collection method is Kite Aerial Photography that is used as an UAV supplement. We were capable of creating orthophoto and 3D models of the sites. 3D models created during the 2014 season are presented at https://sketchfab.com/jan.pacina/folders.

References

[1] James S. Aber, Irene Marzolff, and Johannes B. Ries. *Small-Format Aerial Photography: Principles, Techniques and Geoscience Applications*. Amsterdam – London: Elsevier Science, 2010. ISBN: 978-0-444-53260-2.

[2] Abdullah Elsadig Ali. "Current Status of GIS in the Sudan". In: *Eighteenth United Nations Regional Cartographic Conference for Asia and the Pacific, Bangkok*. United Nations E/CONF.100/CRP.10, Oct. 2009.

[3] G. Bitelli, M. Unguendoli, and L. Vittuari. "Photographic and photogrammetric archaeological surveying by a kite system". In: *Proceedings of the 3rd International Congress on Science and Technology for the Safeguard of Cultural Heritage in the Mediterranean Basin*. Ed. by Jesús Alpuente et al. Alcala de Henares: Servicio de Publicaciones de la Universidad de Alcala, July 2001, pp. 538–543.

[4] Vladimír Brůna. "Využití KAP (Kite Aerial Photography) při dokumentaci výzkumu v Abúsíru". In: *Pražské egyptologické studie, UK Praha* XI (2013), pp. 37–43.

[5] B-N. Chagny and A. Hesse. "Soudan 1994–2006: Photographies archéologiques sous cerf-volant avec Francis Geus". In: *Mélanges offerts à Francis Geus. Égypte-Soudan, Lille: Université Charles de Gaulle-Lille*. Ed. by Brigite Gratien. Cahiers de recherches de l'Institut de papyrologie et d'egyptologie de Lille 26, pp. 47–59.

[6] *GeoRepository, Geodetic Datum used in Africa - Eritrea, Ethiopia and Sudan*. http://georepository.com/datum_6201/Adindan.html. Oct. 2015.

[7] W. Karel, N. Pfeifer, and C. Brueser. "DTM quality assessment". In: *ISPRS Technical Commission II Symposium, Vienna*. Ed. by W. Kainz and A. Pucher. 2006, pp. 7–12.

[8] Lenka Lisá et al. *Sabaloka a Šestý nilský katarakt*. Novela Bohemica, 2012. ISBN: 978-80-904573-6-2.

[9] J. Pacina et al. "Detailed analysis of georelief development in the lake Most surroundings". In: *Ad Alta: Journal of Interdisciplinary Research* 3.2 (2013), p. 44.

[10] L. Suková and V. Cílek. "The Landscape and Archaeology of Jebel Sabaloka and the Sixth Nile Cataract, Sudan". In: *Interdisciplinaria Archaeologica – Nat. Sciences in Arch.* 3.2 (2012), pp. 189–201.

[11] Ladislav Varadzín and Lenka Suková. "Preliminary report on the exploration of Jebel Sabaloka (West Bank), 2009-2012". In: *Sudan & Nubia* 16.1 (2012), pp. 118–131. ISSN: 1369-5770.

[12] Geert J. J. Verhoeven et al. "Helikite aerial photography - a versatile means of unmanned, radio controlled, low-altitude aerial archaeology". In: *Archaeological Prospection* 16.2 (Apr. 2009), pp. 125–138. DOI: 10.1002/arp.353.

[13] G. Verhoeven et al. "Mapping by matching: a computer vision-based approach to fast and accurate georeferencing of archaeological aerial photographs". In: *Journal of Archaeological Science* 39.7 (July 2012), pp. 2060–2070. DOI: 10.1016/j.jas.2012.02.022.

[14] Bogdan Żurawski. "Low altitude aerial photography in archaeological fieldwork: the case of Nubia". In: *Archaeologia Polona* 31 (1993), pp. 243–256.

[15] Bogdan Żurawski. "Miracles of Banganarti. Polish archaeological discoveries in Sudan". In: *Focus on Archaeology* 5.1 (2005), pp. 20–23.

An investigation into the possibilities of BIM and GIS cooperation and utilization of GIS in the BIM process

Pavel Tobiáš

Department of Geomatics, Faculty of Civil Engineering
Czech Technical University in Prague
Thákurova 7, 166 29 Prague 6, Czech Republic
pavel.tobias@fsv.cvut.cz

Abstract

In the coming years we will most probably watch a significant increase of the BIM (building information model) utilization in the AEC (Architecture/Engineering/-Construction) sector even in the Czech Republic. Therefore, it would be reasonable to consider possible utilization of the well-established geographic information systems within the building information modelling process. This paper is based on the currently existing literature and is focused on the interrelationship between BIM and GIS. The main goal is to reveal potential fields of cooperation and to find possible utilization of GIS in BIM. To provide a theoretical framework, this article briefly introduces and defines the term of BIM and deals with the most important semantic models in AEC and 3D GIS – IFC and CityGML. The paper also contains examples of specific efforts recently dealing with the BIM and GIS collaboration.

Keywords: BIM, Building Information Modelling, IFC, GIS, CityGML

1. Introduction

In recent years we can hear more and more about building information modelling. However, the employment of a shared information model during the whole building lifecycle is still not very common, especially if we speak about the Czech Republic. On the other hand there already exist several scientific papers which are focused on the interrelationship between this relatively new field and the well-established field of geographic information systems (GIS). Martin Černý's dissertation thesis "GIS analysis in building information models" [6] can be a very good example and one of the first academic theses in our country which deal with BIM.

The main goal of this paper is to reveal main areas where BIM and GIS can benefit from their cooperation. This could not be achieved without a theoretical framework. Therefore, the paper first explains the term of BIM and introduces the most important AEC and GIS standards, mainly the IFC and CityGML semantic models. The most important part of the paper is focused on the BIM and GIS relationship and describes main fields of cooperation, the most serious obstacles and above all introduces particular efforts to integrate BIM and GIS.

2. The basics of building information modelling

The term BIM was used in AEC for the first time in 2002 [5]. There are more ways how to interpret this acronym: it can mean building information model, building information modelling or even building information management. In the Czech Republic all these terms are translated into Czech and explained in the BIM reference book by the Czech BIM Council (czBIM) [5] which can be considered as a fundamental source for the Czech environment. Nevertheless, because this paper is written in English, it would not be appropriate to translate all definitions back in English. Therefore, original English definitions found are listed hereafter.

According to Isikdag et al. [17] building information modelling can be described as "a new way of creating, sharing, exchanging and managing the information throughout the entire building lifecycle."

> BIM is a computable representation of all the physical and functional characteristics of a building and its related project/life-cycle information, which is intended to be a repository of information for the building owner/operator to use and maintain throughout the life-cycle of a building.
>
> *NBIMS (The National BIM Standard—United States)*

> BIM is a data-rich, object-oriented, intelligent and parametric digital representation of the facility, from which views and data appropriate to various users' needs can be extracted and analysed to generate information that can be used to make decisions and improve the process of delivering the facility.
>
> *AGC (Associated General Contractors of America)*

> BIM is a three dimensional database designed specifically for built facilities. BIM integrates a digital description of a building with all the elements that contribute to its on-going function such as air conditioning, maintenance, cleaning or refurbishment along with describing the relationship between each element.
>
> *CRC (Cooperative Research Centre for Construction Innovation)*

It is apparent from the mentioned definitions that building information model is an information database which comprises all information about a building throughout its whole lifecycle (design, construction, operation and maintenance, demolition/renovation). Building information modelling/management[1] is then the comprehensive process of sharing and exchanging information about the building.

The word "building" in the acronyms can be understood as the specific type of structure above ground surrounded by walls, roof, etc. but also as the general construction process of arbitrary structures. It is important to realize that BIMs can also be used for different structures than buildings (e.g. road or railway structures – roads, bridges, tunnels. . .).

In BIM, shapes and dimensions of buildings are always described three-dimensionally. However, it is of utmost importance that the 3D model alone (i.e. only 3D geometry) cannot still be called building information model. The geometrical model is only one of more ways of

[1] There is another term with this meaning used in the USA: VDC – virtual design and construction [25].

representation of stored information. "The 3D geometry is only one of the properties, at the same level as the name of the vendor, cost, etc." [27].

Considering the mentioned, BIM can be understood as an object-oriented parametric modelling of a building. Parameters (i.e. non-graphic and additional information about particular elements) express structural and material properties of elements, positions in the construction schedule, inspection and exchange schedules or investment and operating costs. A comprehensive model of a real building can be created using parameters and this model can be used for the construction preparation, the construction itself and further for the facility management and analyses.

BIM should also enable the N-dimensional modelling. Time is considered as the fourth dimension whereas cost information, energy consumption or facility management information can create another dimensions of BIM [5].

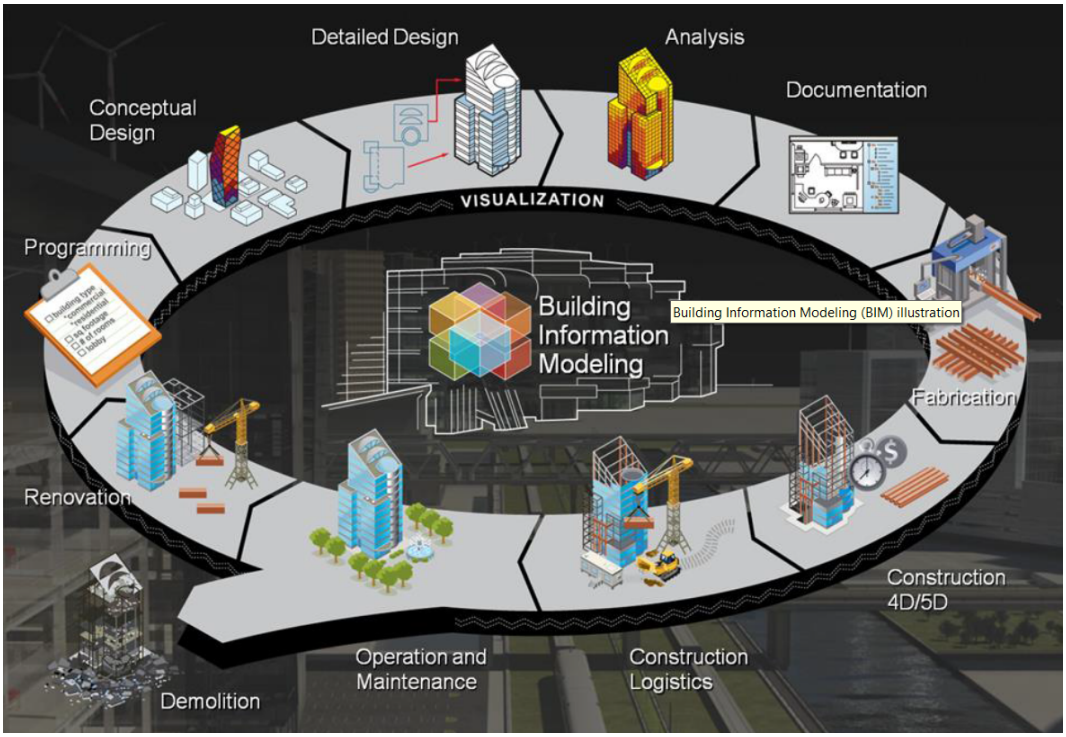

Figure 1: The life cycle of a building [25]

3. Existing standards

Today's BIM standards are the successors of older exchange formats such as DXF. The most mentioned standards are currently Industry Foundation Classes (IFC) and CIMSteel Integration Standards (CIS/2). These semantic models describe buildings using the EXPRESS language which is a part of STEP (STandard for the Exchange of Product model data, ISO 10303) [17, 8]. Standards are not only being developed to describe the geometric model. United States Army Corps of Engineers file format COBie (Construction Operations Building Information Exchange) is mainly focused on non-geometric data and can be used for the facility management [25].

The up to date 3D GIS file formats are often based on XML. An example is the COLLADA format which is used together with the OGC[2] standard KML for the geometry representation in Google Earth (within KMZ files) and Trimble SketchUp. Another important OGC standards are GML (Geography Markup Language, ISO 19136) and its application schema CityGML (see below). The CityGML standard is widely used as an interface within the process of transformation from BIM (IFC) into the geospatial environment. On the other hand, ESRI shapefile may be called de-facto standard "due to its wide acceptance by users and software vendors" [27]. This format is quite important because in most cases it is the target destination of BIM to GIS transformations although the conversions often employ CityGML as an intermediate format. This is no surprise considering the worldwide spread of the ESRI products. The ESRI Multipatch geometry type is used to model the three-dimensional shell of objects within shapefile or ESRI geodatabase [10].

3.1. The Industry Foundation Classes data model

IFC (Industry Foundation Classes) is an open data model and file format developed and managed by buildingSMART International (formerly the International Alliance for Interoperability). The data model was introduced in 1997 as the first standard by this alliance. In 2005 IFC became an ISO standard (ISO 16739). The most up to date version is currently IFC4 which is still not widely supported by software vendors. Therefore, IFC 2x3 TC1 is now the most widespread version [6, 5, 27, 18].

It was already mentioned afore that the most common model description method in IFC is the EXPRESS language. However, there also exist an XML implementation – ifcXML. Both EXPRESS and XML model descriptions are stored as a text file and are human-readable. The ifcZIP file format can be used for the data compression.

There are two basic types of objects in IFC: spatial structure elements (site, building, building storey, space) and building elements (walls, columns, doors, windows...). Important thing is that neither spatial structure elements, nor building elements have to have geometry defined and a model can be purely semantic (which is consistent with the BIM focus on all kinds of information, not only on geometry). On the other hand, IFC supports many ways of geometry representation: Compound Solid Geometry (CSG), swept geometry (sweep volume, sweeping) as well as Boundary Representation (B-Rep) which is common in 3D GIS [6, 8].

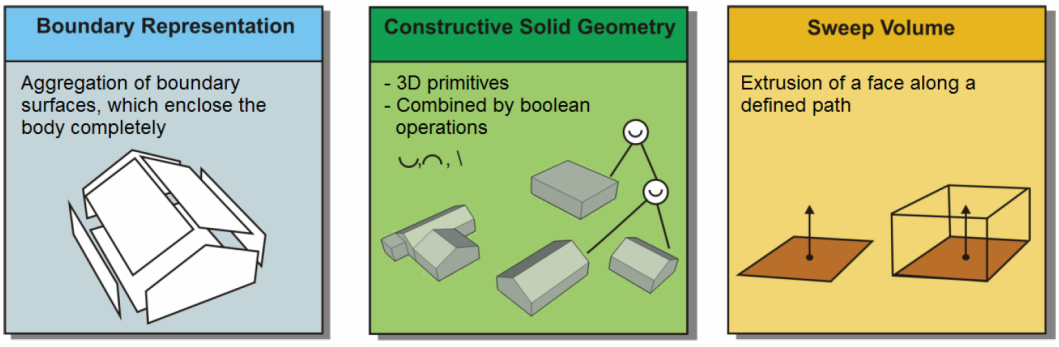

Figure 2: The ways of geometry representation in IFC [8]

[2] Open Geospatial Consortium: http://www.opengeospatial.org/

3.2. CityGML - between the worlds of BIM and GIS

CityGML is an open data model and file format based on XML which can be used for storing and sharing virtual 3D city models. It is an application schema of GML 3.1.1. CityGML was originally developed by SIG3D (Special Interest Group 3D GDI-DE[3]) and first successful implementation was performed in 2005 within the Pilot 3D project. In 2008 CityGML became an adopted OGC standard. At present the most up to date version is 2.0.0. CityGML is currently used as a standard for 3D models of cities in many countries in Europe (Germany, France, the Netherlands, Monaco, Switzerland or Denmark) and worldwide (Turkey, Qatar, Japan, Malaysia) [7].

The standard defines the way of description of geometry, semantics, topology and appearance for the most important objects in cities. Its focus on semantics is very similar to the BIM (IFC) approach. The geometric-topological model is adopted from GML3, employs the ISO standard 19107 Geographic information – Spatial schema and represents geometry using the Boundary Representation method. The semantics is described by the thematic model which contains classes for the most important objects in modern cities. Currently there are fourteen modules in the CityGML thematic model – CityGML core and thirteen thematic extension modules: Appearance, Bridge, Building, CityFurniture, CityObjectGroup, Generics, LandUse, Relief, Transportation, Tunnel, Vegetation, WaterBody, TexturedSurface [7].

Different applications of CityGML require various detail of three-dimensional city models. Therefore, different levels of detail (LOD, 0 – 4) can be used. Every city object can have more geometric representations in one CityGML dataset (one for each LOD). In addition, explicit generalisation associations between city objects can be defined. This enables aggregation of objects in a lower LOD.

Considering that building information models attempt to depict structures in the greatest detail possible, the most detailed CityGML LOD4 is closest to BIM. In LOD4 buildings are portrayed as architectural models with their surfaces categorised as walls, roofs or openings and with details such as balconies, chimneys, dormers or antennas. Interiors are also modelled and buildings are divided into rooms with interior installation (stairs, railings, radiators or pipes) and furniture (tables, chairs). Other structures than buildings (tunnels, bridges) are modelled in LOD4 in a similar way. However, even in LOD4 CityGML data model is not sufficient and has to be extended to be better compatible with BIM (IFC) models (see 5.2) [7].

4. BIM and GIS cooperation

4.1. Fields of cooperation

Isikdag states in his article [14] that an implementation of BIM in the geospatial context can be useful for site selection analyses, simulations to determine energy consumption and lighting requirements in buildings, fire response management operations and N-dimensional analyses at the urban level.

Donkers [8] indicates possible utilization of building models for cadastral applications (3D cadastre), environmental analyses, determination of solar potential, architectural applications (count and distribution of windows according to the location of a building, assessment of

[3] GeoDaten Infrastruktur Deutschland

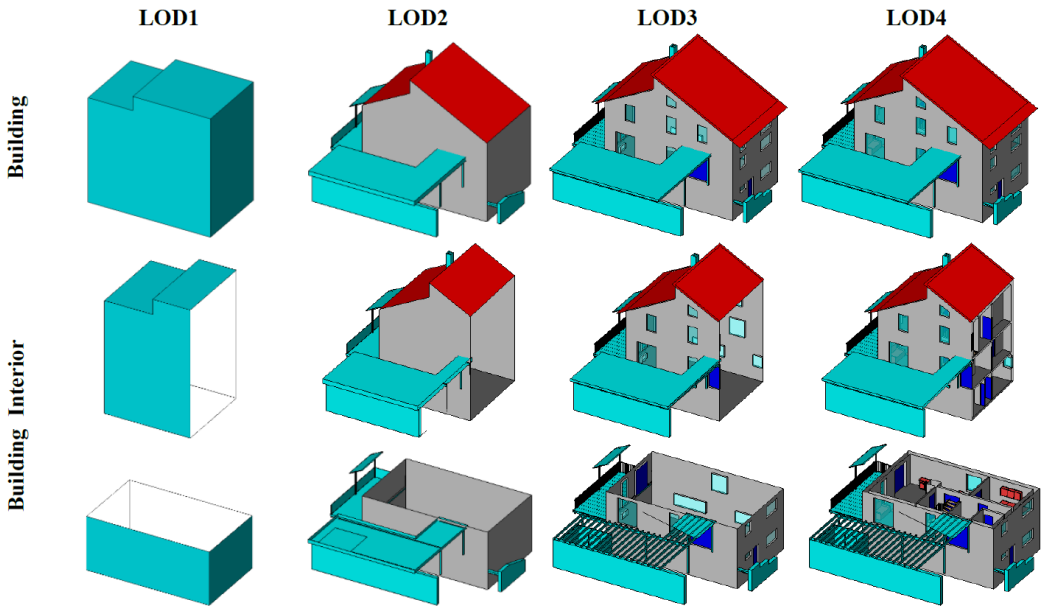

Figure 3: A building model in CityGML LOD1 – LOD4 [7]

interaction between neighbouring buildings and their surroundings – noise and heat transfer) or for real estate agents (searching houses with specific features).

Laat and Berlo [23] describe the mutual benefits of BIM and GIS cooperation when BIM can be an important data source for models of urban areas in GIS and conversely, GIS can serve as a data source for the design and integration of new buildings in the geospatial context. According to Hijazi et al. [12] the ability to integrate 3D models of buildings into the geospatial context is the crucial issue for facilitating interaction with 3D models of cities. These models can then be employed, for example, for navigation purposes. Also BIM and GIS cooperation for facility management (administration of a university campus) is mentioned in this article.

Another similar description of the BIM usability can be found in the work by Kolbe [22] which is focused on the CityGML standard. Kolbe states that BIMs in the IFC file format can be a very important data source for the LOD 4 CityGML city models. Such models can be utilized for disaster management (damage extent estimates, flood simulations, rescue teams navigation...), combined (indoor/outdoor) navigation and for 3D visualizations. If we speak about CityGML LOD4 and indoor navigation, the article by Isikdag et al. [16] is also very important. In this article the creation of graphs from primal geometric models for navigation purposes is analysed. Zlatanova [27] expands the 3D city model area of use in disaster management on training simulators based on real city models.

Benner et al. [2] also describe the utilization of high detailed city models. The QUASY data model described in his contribution should further extend the usability of such models in the areas of town planning and urban management, emergency and catastrophe planning or for traffic simulations. The BIM and GIS interconnection for traffic infrastructure planning in the surroundings of a high-rise building is described in [26]. Moreover, Bansal [1] employs the BIM and GIS cooperation in the construction safety planning.

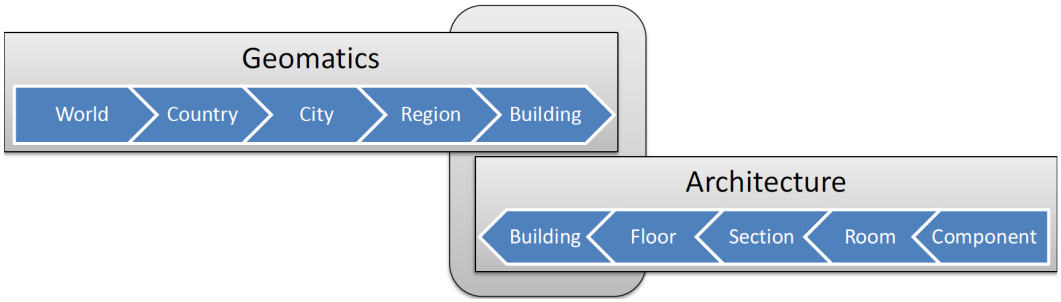

Figure 4: Overlap between the fields of Geomatics and Architecture [8]

4.2. Main obstacles

Building information models and geographic information systems were originally developed for different purposes and therefore significant differences can be found between them. Building information models and also their predecessors CAD systems are especially developed for the building design. That is for modelling of yet non-existent buildings. This models are to be maximally detailed in both geometry and semantics. Relationships between particular objects in a building are of utmost importance but absolute coordinates are not so relevant.

On the other hand geographic information systems mostly model the reality – already existing objects and phenomena around us. A great degree of abstraction is used in most cases and much emphasis is put on georeferencing (i.e. absolute coordinates of modelled elements) [15, 14].

With the use of the available literature the main obstacles of BIM and GIS integration were found as follows:

1. BIM (e.g. the IFC file format) uses more ways of geometry representation (CSG and sweeping in addition to B-Rep used in GIS)
2. BIM and GIS use different semantics
3. BIM and GIS use different coordinate systems

The first issue may be the most significant obstacle in the conversion from BIM (IFC) to GIS file formats such as CityGML. Whereas BIM models can use CSG or swept geometry, in GIS the geometry representation is limited to B-Rep and usually only straight lines and planar faces are used as the boundaries. In contrast to volumetric IFC models CityGML objects are only represented by visible surfaces. Therefore, the exterior shell of objects has to be extracted within the IFC to CityGML conversion. The exterior shell computation is not a trivial problem and a lot of existing conversion tools do not provide a fully valid results [8, 2].

Whereas BIM is focused on modelling detailed building models, in GIS whole cities and landscapes should be portrayed. Thus, it is logical that in BIM (e.g. IFC) and GIS (e.g. CityGML) objects do not correspond to each other completely. Semantic mapping which should eliminate the problems with different semantics during transformation is described in [15].

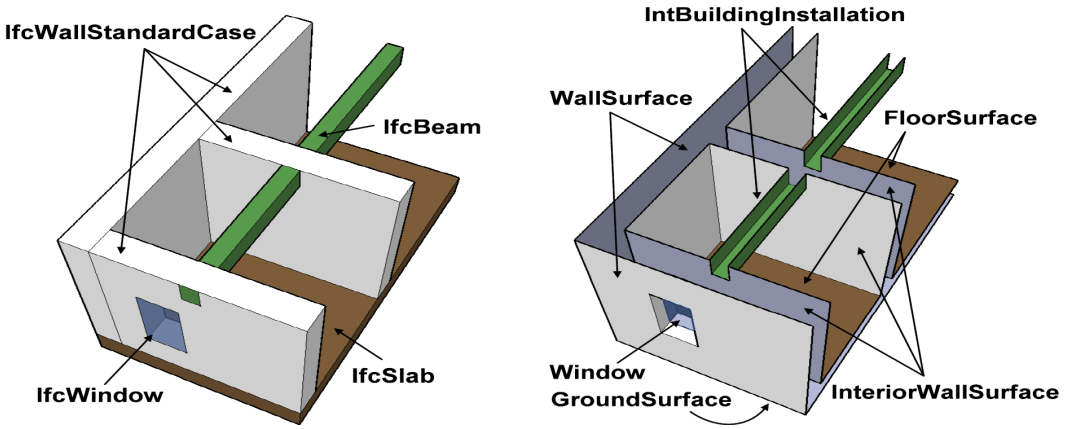

Figure 5: Differences between geometry representations in BIM and 3D GIS [23]

The difference between coordinate systems describes, for example, Černý [6]. In BIM the World Coordinate System (WCS) is used. WCS is a local rectangular coordinate system of a drawing. The origin and the orientation of its axes have to be defined to enable transformation into a global spatial reference system of GIS. These parameters should be listed in IFC (in WGS84) but they are not mandatory and they may only have an approximate precision. This problem is solved in IFC4 but, as said afore, this specification is still not widely supported.

5. Recent cooperation efforts

The most interesting found efforts dealing with the BIM and GIS collaboration are described in this chapter. At present it is clear that due to their differences the full integration (at the system level) is not reachable [6, 8, 13]. On the other hand Hijazi [12] states that it is possible to achieve integration at the data level, semantic level or within a web service. Academic debate aside some institutions are already using GIS tools for BIM tasks (see e.g. facility management of the University Campus Bohunice of the Masaryk University performed in ArcGIS).

5.1. IFC to CityGML transformation

According to Isikdag and Zlatanova [15] the transformation from IFC to CityGML has two parts: the conversion of semantics and the transformation of geometry. These parts cannot be realized separately due to the significant difference between both data models. One object might be mapped into a group of objects and vice versa. The paper contains theoretical framework to facilitate the transformation and describes specific objects and attributes of IFC which can be used to generate building models in CityGML LOD1 - 4.

Donkers deals in his thesis [8] mainly with the transformation of geometry. He states that a lot of today's IFC to CityGML conversion tools (Safe Software FME[4], BIMserver tools[5]) do not produce fully valid geometry. Therefore, his conversion is focused on the valid CityGML output. The already mentioned exterior shell computation is described as the most impor-

[4] http://www.safe.com/
[5] http://bimserver.org/

tant operation due to the differences in geometry representations. After semantic mapping and geometry transformation Donkers performs geometric and semantic refinement to ensure validity. The thesis contains a proposed framework and its testing implementation for LOD3 and experimentally for the most detailed LOD4 CityGML models.

5.2. CityGML extensions

The CityGML standard supports application specific extensions of its data model. These extensions can be created using the ADE (Application Domain Extension) mechanism. Every ADE can specify new properties of existing CityGML classes (e.g. the number of habitants of a building) or entirely new object types [7]. Most of the existing CityGML extensions can be found on the CityGML wiki.

Laat and Berlo [23] use the ADE mechanism to develop the GeoBIM extension. This ADE should increase the compatibility of the CityGML semantics with building models in the IFC file format. The extension adds new IFC compatible properties to CityGML classes (Room, Window, Door, Building...). Examples of these properties are the widths and heights of windows and doors. Furthermore, new classes are added, e.g. the Stair class. The GeoBIM ADE is implemented in the open source BIMserver.

5.3. BIM in the geospatial context

Isikdag et al. deal in [18] and [14] with the utilisation of the transformed IFC model in the geospatial context to facilitate site selection analysis and fire response management. The fire response application is the pivotal part of this effort. It is supposed that the information about the affected building should be acquired from the BIM model. This model ought to be transformed from BIM to GIS directly during the rescue operation. The conversion steps are very similar to the IFC to CityGML transformation described in [15] (5.1). However, the target destination is here the ESRI shapefile or the ESRI geodatabase.

The IFC to shapefile conversion performs also Černý as a part of his dissertation thesis [6] (see also 5.5).

5.4. Historic building modelling

In most cases, the information model is created for newly built buildings. Such model is produced and continuously updated during the whole process of the building design and construction. If all stakeholders take part in the model creation, the model is developed naturally. On the other hand, production of BIM of an already existing building can be highly time consuming. In this case existing documentation have to be revised and reprocessed or even geodetic survey of the actual state have to be performed. However, general consensus seems to be that the creation of BIMs of existing buildings can also pay off because the 3D BIM documentation is not much more time consuming than the 2D building passport (according to Černý [6] and the "BIM in Facility Management" panel discussion within the BIM DAY 2014).

The creation of models of historic heritage buildings is an even more special example of the BIM employment. Fai et al. [11] describe the N-dimensional modelling of a heritage building

in a BIM software where the building is modelled in multiple versions corresponding to different time periods. The contribution by Dore and Murphy [9] names such process Historic Building Information Modelling (HBIM). Within HBIM, historic buildings are modelled based on laser scanning and photogrammetry using BIM software (e.g. ArchiCAD). The resulting model is then integrated into the 3D GIS environment for storing and further analysis.

An approach similar to HBIM can also be found in the Czech Republic. The papers by Jedlička et al. [19] and Jedlička and Hájek [20] deal with the creation of a semantic 3D model of a heritage building. Although they do not use any BIM software for modelling, the process of the model integration into GIS and the focus on information-rich models is analogous with HBIM. Buildings are modelled using the SketchUp application, exported to CityGML and then imported into the ESRI geodatabase.

Speaking about the Czech Republic there exist a method of heritage building documentation whose origins date back to the 1940s or even further - the structural - historical investigation. The goal of this method is to gather maximum information about a heritage object. Objects are examined from different point of views by historians, architects, architectural historians, civil engineers or structural engineers. The results of the investigation are presented both textually and graphically. The textual part comprises outcomes of historical research, architectural analysis of the building and description of its structural development. Graphic part consists of historic maps, plans, photographs and paintings and is newly supplemented with plans and photographs of the current state. Finally, the very important graphical evaluation is provided which evaluates the development of the building structures and their historical value and uses floor plans as base layers [24]. It is obvious that this thorough investigation can be a very valuable data source for BIMs of heritage buildings and conversely BIM can be a suitable tool for the storage, presentation and analyses of these results.

5.5. GIS analyses in the BIM environment

Borrman [3] and Borrmann and Rank [4] deal with the development of a 3D spatial query language. 3D spatial queries can be useful for BIM (IFC) models and also in 3D GIS. The mentioned work contains description of metric, directional and topological spatial operators. To verify the concept, a prototype software was implemented to process models defined in the VRML language.

Černý in his thesis [6] analyses this topic in detail and focus on the implementation of spatial queries originating in GIS in the 3D BIM environment. His work first identifies several drawbacks of the GIS software (ArcGIS) utilisation (necessary degradation of geometry during the conversion to GIS, inability of ArcGIS to analyse geometrically complex objects and difficult promotion of results back to the original BIM model). Therefore, Černý chose another approach and developed his own tool which enables to analyse directly BIM models in IFC. This approach eliminates the mentioned issues but on the other hand works only with one IFC model with no geospatial context.

5.6. Server solution

The BIM4GeoA (BIM for Geo-Analysis) concept which is described in the article by Hijazi et al. [12] combines existing open source software to ensure efficient data management and analyses of building models in the broader geospatial context. The PostGIS spatial database,

the BIMserver model server, the Google Earth 3D viewer and IFC, CityGML and KML file formats are the key components of this effort. The system architecture is used to develop applications for management of a university campus (i.e. for facility management and indoor routing). This effort is another example of GIS utilization for the task of facility management.

6. Discussion

After the examination of the currently existing literature dealing with the BIM and GIS relationship it can be said that a lot of effort was spent to convert BIM models in IFC into the GIS file formats (i.e. CityGML or ESRI shapefile). The possible utilization is always presented but the description of the actual work with the model in the GIS environment is usually missing. This may be related to the fact that the BIM and GIS interrelationship as well as the BIM itself are relatively new fields of study and respective workflows are still in development. Therefore, up to date literature should be further sought and also development in the industry should be carefully monitored.

The very important thing is that BIM cannot be considered as one particular software but rather as a way of communication between programs of the building process stakeholders (e.g. with the use of exchange formats). From this point of view a GIS programs might serve as one of BIM tools and enable to consider the designed building in the broader geospatial context. According to the literature possible use cases can be found as follows: site selection analysis, visibility analysis, assessment of interaction between neighbouring buildings and their surroundings, construction safety planning and traffic planning. To facilitate this tasks, the aforementioned matter of conversions will have to be solved. We are talking here not only about the widely discussed topic of BIM to GIS transformation but also about the backward conversion. The difficult promotion of results back to BIM has been described [6] and only few papers mention this issue (minor reference about the derivation of IFC objects from CityGML found in [21]).

On the other hand, BIMs of finished buildings can be used to populate 3D models of cities. These models can be further employed for the tasks of disaster management, training simulators, indoor navigation, and last but not least for visualisation purposes. Moreover, speaking about finished buildings, GIS can also be used for the facility management. The database management of the building information and georeferencing are here the main advantages of GIS. Especially in the case of large building complexes (university campuses, factories), GIS might actually become a very powerful BIM tool. It is clear that GIS will have to compete with purely facility management software (e.g. Archibus). On the other hand, existing solutions – the aforementioned FM of Masaryk University, for instance, show that the utilization of GIS for facility management purposes can be advantageous.

A special field of study is the creation of models of already existing buildings. These models can be further used in the same way as the models which were developed during the design and construction process. Such information-rich models of existing (or even historic) buildings are worthy of attention because their creation involves geodetic survey, photogrammetry, laser scanning, measured data processing, model creation, database storage, administration of the resulting spatial model, its analyses and presentation all this being known to the field of geomatics. Moreover, in the Czech Republic, results of the mentioned structural-historical investigations would be probably used as a data source for models of historic buildings. It

is up to the experts of geomatics to emphasize their experience (and, where appropriate, the advantages of GIS) in this field of study.

A very important is also the question of safety of such BIMs. It is clear that especially heritage institutions will very carefully consider acquiring an information model which describe in detail a heritage building with very valuable movables inside. However, even so closely guarded objects such as banks are today provided with building information models[6] and, of course, not all information should be given available to the wide audience.

7. Conclusion

The main goal of this article was to search the fields where BIM and GIS could benefit from their cooperation and to introduce the most interesting examples of BIM and GIS collaboration efforts. The most promising fields of study were found as follows: the facility management of large building complexes and the creation of models of existing (or even historic) buildings. Nevertheless, the whole field of BIM should be carefully monitored by experts of GIS and geomatics in general to keep abreast of future developments.

References

[1] V.K. Bansal. "Application of geographic information systems in construction safety planning". In: *International Journal of Project Management* 29.1 (2011), pp. 66–77. DOI: 10.1016/j.ijproman.2010.01.007.

[2] J. Benner, A. Geiger, and K. Leinemann. "Flexible generation of semantic 3D building models". In: *Proceedings of the 1st international workshop on next generation 3D city models, Bonn.* 2005, pp. 17–22. URL: http://iai-typo3.iai.fzk.de/www-extern-kit/fileadmin/Image_Archive/Bauwerke/Geo-Informationssysteme/Veroeffentlichungen/NextGeneration3DCityModels.pdf (visited on 10/03/2014).

[3] A. Borrmann. "From GIS to BIM and back again – A Spatial Query Language for 3D building models and 3D city models". In: *International Archives of the Photogrammetry, Remote Sensing and Spatial Information Sciences – ISPRS Archives* 38.4 (2010), pp. 19–26. ISSN: 1574-0846.

[4] André Borrmann and Ernst Rank. "Topological analysis of 3D building models using a spatial query language". In: *Advanced Engineering Informatics* 23.4 (2009), pp. 370–385. DOI: 10.1016/j.aei.2009.06.001.

[5] Martin Černý et al. *BIM příručka*. Prague: Czech BIM Council, 2013. ISBN: 978-80-260-5296-8.

[6] Martin Černý. "GIS analýzy v prostředí informačních modelů staveb". PhD thesis. Brno University of Technology, Faculty of Civil Engineering, Institute of Geodesy, 2014.

[7] Open Geospatial Consortium. *City Geography Markup Language (CityGML) Encoding Standard, version: 2.0.0.* 2012. URL: http://www.opengis.net/spec/citygml/2.0 (visited on 11/17/2014).

[6] The case of ČSOB. Again information from BIM DAY 2014.

[8] S. Donkers. "Automatic generation of CityGML LoD3 building models from IFC models:" PhD thesis. Delft University of Technology, 2013. URL: http://oatd.org/oatd/record?record=oai%5C:tudelft.nl%5C:uuid%5C:31380219-f8e8-4c66-a2dc-548c3680bb8d (visited on 10/12/2014).

[9] C. Dore and M. Murphy. "Integration of Historic Building Information Modeling (HBIM) and 3D GIS for recording and managing cultural heritage sites". In: *2012 18th International Conference on Virtual Systems and Multimedia*. IEEE, 2012. DOI: 10.1109/vsmm.2012.6365947.

[10] ESRI. *The Multipatch Geometry Type – An Esri® White Paper*. 2008. URL: http://www.esri.com/library/whitepapers/pdfs/multipatch-geometry-type.pdf (visited on 05/13/2015).

[11] Stephen Fai et al. "Building Information Modeling and Heritage Documentation". In: *XXIII CIPA International Symposium, Prague, Czech Republic, 12th- 16th September*. 2011.

[12] I. Hijazi, M. Ehlers, and S. Zlatanova. "Bim for geo-analysis (BIM4GEOA): Set up of 3D information system with open source software and open specification (OS)". In: *International Archives of the Photogrammetry, Remote Sensing and Spatial Information Sciences – ISPRS Archives* 38.4 (2010), pp. 45–49. ISSN: 1574-0846.

[13] Ihab Hijazi et al. "IFC to CityGML transformation framework for geo-analysis: a water utility network case". In: *3D GeoInfo, Proceedings of the 4th International Workshop on 3D Geo-Information, Ghent: Ghent University*. Citeseer, 2009, pp. 123–127.

[14] Umit Isikdag, Jason Underwood, and Ghassan Aouad. "An investigation into the applicability of building information models in geospatial environment in support of site selection and fire response management processes". In: *Advanced Engineering Informatics* 22.4 (2008), pp. 504–519. DOI: 10.1016/j.aei.2008.06.001.

[15] Umit Isikdag and Sisi Zlatanova. "Towards Defining a Framework for Automatic Generation of Buildings in CityGML Using Building Information Models". In: *Lecture Notes in Geoinformation and Cartography*. Springer Berlin Heidelberg, 2009, pp. 79–96. DOI: 10.1007/978-3-540-87395-2_6.

[16] Umit Isikdag, Sisi Zlatanova, and Jason Underwood. "A BIM-Oriented Model for supporting indoor navigation requirements". In: *Computers, Environment and Urban Systems* 41 (2013), pp. 112–123. DOI: 10.1016/j.compenvurbsys.2013.05.001.

[17] Umit Isikdag et al. "Building information models: a review on storage and exchange mechanisms". In: *Bringing ITC Knowledge to Work* (2007). URL: http://itc.scix.net/data/works/att/w78-2007-020-068b-Isikdag.pdf (visited on 11/17/2014).

[18] U. Isikdag et al. "Investigating the role of building information models as a part of an integrated data layer: A fire response management case". In: *Architectural Engineering and Design Management* 3.2 (2007), pp. 124–142. ISSN: 1752-7589. URL: http://www.ingentaconnect.com/content/earthscan/aedm/2007/00000003/00000002/art00005 (visited on 10/12/2014).

[19] Karel Jedlička, Otakar Čerba, and Pavel Hájek. "Creation of Information-Rich 3D Model in Geographic Information System – Case Study at the Castle Kozel". In: *13th SGEM GeoConference on Informatics, Geoinformatics And Remote Sensing*. 2013. DOI: 10.5593/sgem2013/bb2.v1/s11.010. (Visited on 11/11/2014).

[20] Karel Jedlička and Pavel Hájek. *Large scale virtual geographic environment of the castle Kozel – best practice example*. 2014.

[21] Thomas H. Kolbe. "Representing and Exchanging 3D City Models with CityGML". In: *Lecture Notes in Geoinformation and Cartography*. Springer Berlin Heidelberg, 2009, pp. 15–31. DOI: 10.1007/978-3-540-87395-2_2.

[22] Thomas H. Kolbe, Gerhard Gröger, and Lutz Plümer. "CityGML: Interoperable Access to 3D City Models". In: *Geo-information for Disaster Management*. Springer Berlin Heidelberg, 2005, pp. 883–899. DOI: 10.1007/3-540-27468-5_63.

[23] Ruben de Laat and Léon van Berlo. "Integration of BIM and GIS: The Development of the CityGML GeoBIM Extension". In: *Advances in 3D Geo-Information Sciences*. Springer Berlin Heidelberg, 2010, pp. 211–225. DOI: 10.1007/978-3-642-12670-3_13.

[24] Petr Macek. *Standardní nedestruktivní stavebně-historický průzkum*. 2., doplněné vyd. Příloha časopisu Zprávy památkové péče, roč. 61. – Vydavatel: Státní ústav památkové péče v Praze. Praha: Nakladatelství Jalna, 2001. ISBN: 80–86234–22–3. URL: http://pamatky-facvut.cz/download/dokumenty/standardni.pdf (visited on 05/13/2015).

[25] Petr Matějka. "Lecture notes of the BIM – Informační modelování course". CTU in Prague, Faculty of Civil Engineering, Department of Economics and Management in Civil Engineering. 2014. URL: http://k126.fsv.cvut.cz/?p=45&cid=89 (visited on 11/29/2014).

[26] Jun Wang et al. "A Cooperative System of GIS and BIM for Traffic Planning: A High-Rise Building Case Study". In: *Cooperative Design, Visualization, and Engineering*. Springer International Publishing, 2014, pp. 143–150. DOI: 10.1007/978-3-319-10831-5_20.

[27] S. Zlatanova, J. Stoter, and U. Isikdag. *Standards for Exchange and Storage of 3D Information: Challenges and Opportunities for Emergency Response*. 2012. URL: http://resolver.tudelft.nl/uuid:a7d1e4a4-3155-43ce-81d4-6ad6cfc26617 (visited on 11/11/2014).

Temperature effects on the bridge structure during the all-day monitoring

Ondřej Michal, Rudolf Urban

Department of Special Geodesy, Faculty of Civil Engineering
Czech Technical University in Prague
Thákurova 7, 166 29 Prague 6, Czech Republic
ondrej.michal@fsv.cvut.cz, rudolf.urban@fsv.cvut.cz

Abstract

In current time the large amount of pre-stressed bridge structures is used. Their horizontal and vertical displacements are well predicted, but for verification of theoretical results is necessary to measure real displacements of these structures depending on external conditions. Given by the complexity of the design and by the inhomogenity of external influences (especially temperature of the atmosphere, insolation, wind speed, etc.) cannot yet be reliably determined the changes of the construction caused by the immediate state of the environment and to distinguish them from irreversible (permanent) deformation of the structure.

In this paper the deflection line of the bridge of general Chábera over river Labe during the all-day monitoring will be analysed. There is dense coverage of stabilized points enabling accurate approximation of the displacement of the bridge structure. The paper is focused especially on temperature effects on the bridge structure. The temperature changes cause the deformation of the construction not immediately, but with the time shift between change of temperature and structure deformation. Although the points are stabilized on both sides of the bridge deck, for the analysis of results were used only the points on the left side of the main span, where the biggest vertical displacements was detected. For testing of dependence of the time shift of the structure deformations and structure temperature the Pearson coefficient of correlation was used.

Keywords: Deflection line, Pearson correlation, time shift.

1. Introduction

Measurement of vertical displacement of building structures was usually solved by precise leveling, which has sufficient accuracy for significant determine of deformation according the standard ČSN 73 04 05. This standard is concerned with long-term displacements and the methodic respond that. Nowadays modern total station has almost the same accuracy and the measurement is faster than leveling. On the other hand, spatial polar method is more sensitive on outer conditions,especially atmospheric refraction. Therefore is still used less than leveling [6].

Spatial polar method is used in measurement of vertical and longitudinal deformation of bridges. In [1] was used trigonometric method for the determination of longitudinal deformations with very high (sub-millimeter) accuracy. The determination of the vertical deformation

from the changes of zenith angle was used in [10], where the influence of refraction was investigated.

The results from [11] and [9] demonstrate that spatial polar method has sufficient accuracy for determining of vertical displacements of bridges respecting correct procedures suppressing the atmospheric refraction.

The measured points can be difficult to access during the measurement of deflection. Therefore new methods with passive reflection are used. Displacements with high frequency can be measured by Ground-Based (GB) radar interferometry. This new technology can be effectively used for measuring of steel bridges with high accuracy, because there is no need to stabilize and signalized the measured points [2]. GB radar interferometry can be used for concrete structures also. In this case the observed points have to be signaled by the corner reflectors. Accuracy of measurement stays still very high [8].

Deformations of complex structures can be measured by laser scanning with advantage. This method provides large amount of data, after the statistical processing can be obtained the displacements of parts of structure. Unfortunately, the accuracy is still worse than in case of the other methods [3].

The aim of this paper is investigating of the vertical displacements in relatively short time. The measurement has to be fast, so the spatial polar method was used. The structure was monitored for 24 hours in 24 epochs. Temperature of the air and the structure was observed during measurement. Linear dependence was expected between temperature changes and displacements with unknown time shift between temperature and structure change. The time of the experiment was chosen carefully, the weather conditions were the same several days before and after the monitoring. Temperature changed continuously during day and night period and the same periodicity was expected in displacements.

1.1. General Chabera bridge

The bridge crosses the river Elbe near the town Litoměřice in Czech Republic. The bridge (Figure 1 and Figure 2) is the part of the road II/247 – connection of the industry area Prosmyky to D8 highway. The superstructure is designed as a continuous beam with box girder cross-section. Total length of the structure is 584.5 m. It is divided to 7 spans with lengths 43 + 64 + 72 + 90 + 151 + 102 + 60 m – [4].

2. Material and methods

The Trimble S6 Robotic instrument (standard deviation of the horizontal direction and zenith angle measurement is $\sigma_\phi = \sigma_\zeta = 0.3\,mgon$, standard deviation of the distance measurement is $\sigma_D = 1\,mm + 1\,ppm \times D$) with a relevant omnidirectional reflection prism was used for the measuring (on Figure 3). S6 is a robotic total station with automatic targeting system. Range pole has special flat heel, which ensures the same height of the target in all epochs. The bridge structure was measured by the space polar method. Automatic targeting on omnidirectional prism was used.

For deflection line time and temperature analysis it was necessary to determine its shape in time during the day. There was monitored 16 points on the left side of the main span during

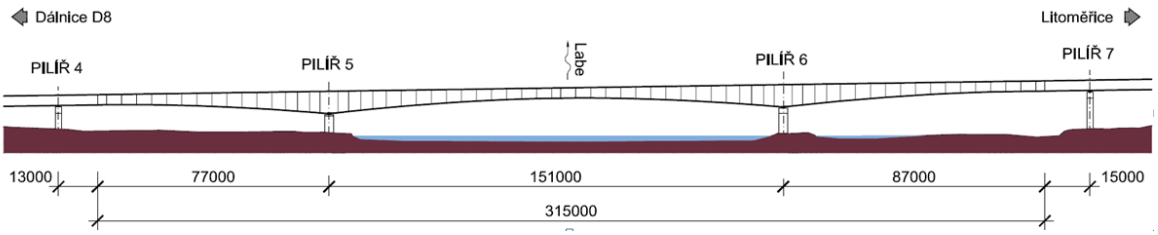

Figure 1: Longitudinal section of superstructure

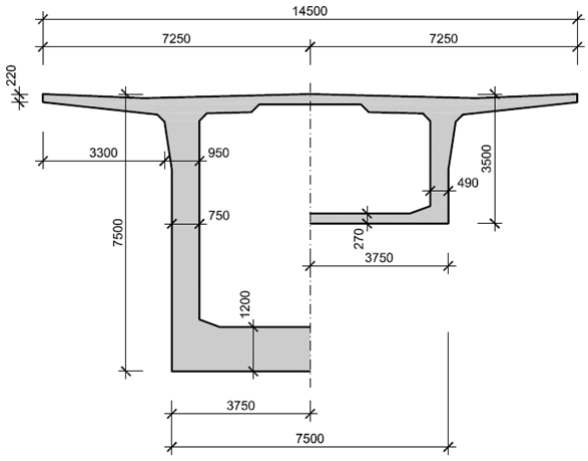

Figure 2: Cross section of superstructure

the period of 24 hours. Points are stabilized by metal leveling nails in bridge structure. The spacing between them is ten meters, it is sufficient for deflection line approximation.

Atmospheric conditions during measurement were extreme and so were the expected vertical changes of the monitored points, it was good for experiment. The difference between maximum and minimum structure temperature was over 20° C. Weather conditions are summarized in Figure 4.

The deflection line of the main span was measured by spatial polar method. There was one connecting point on the left bank of the river and two control points at the end of the bridge construction – situation during measurement is shown on Figure 5.

The predicted displacements were less than 10 millimeters. The standard deviation of determined vertical point's displacement of 1 mm was then required, therefore the maximum horizontal distance to observed point was reduced to 80 m [7].

Temperature of the atmosphere at various heights above the bridge was measured to verify of the refraction influence. Measurement of all points took forty minutes, so deflection line was intended in epoch every one hour, whole experiment lasts 24 hour and therefore 24 epochs were

Figure 3: Trimble S6 Robotic

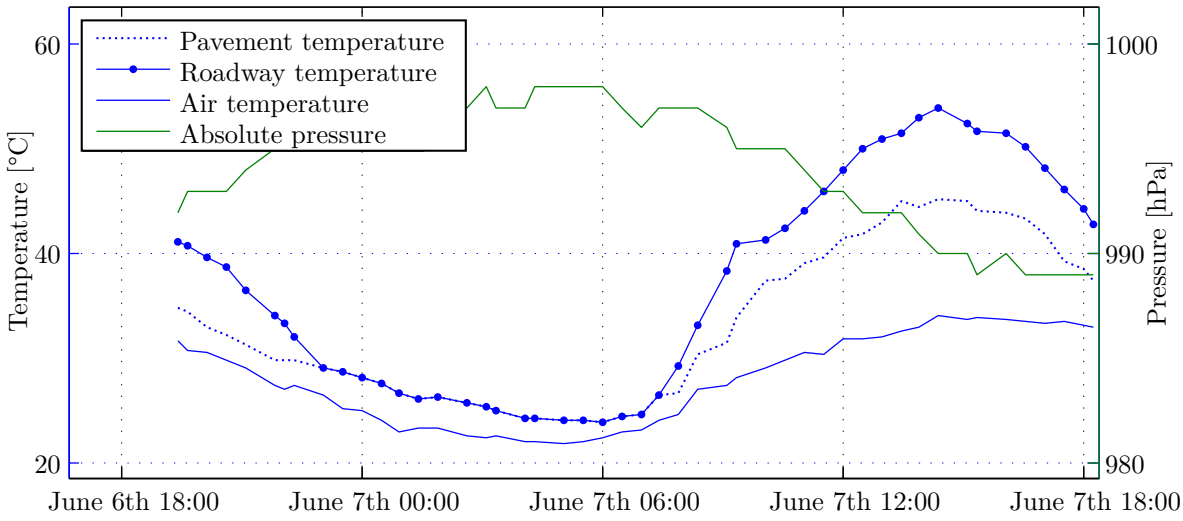

Figure 4: Weather conditions during measurement

Figure 5: Configuration of measurement (Areal Image © Geodis)

measured. First epoch was measured at 19:00, June 6th 2013, last epoch at 18 o'clock next day [5]. The heights of all points were calculated in local vertical datum (correction for Earth curvature was included) using simple trigonometric functions:

$$h_i = h_{pb} + S_{pb} \cos z_{pb} - S_i \cos z_i \tag{1}$$

h_i ..... height of point i.
h_{pb} ..... height of connecting point.
S_{pb} ..... slope distance to connecting point.
S_i ..... slope distance to point i.
z_{pb} ..... zenith angle to connecting point.
z_i ..... zenith angle to i-point.

3. Results

Vertical displacements reached values up to 10 millimeters maximally on points in the middle of the main span. Presentation of all values from all epochs would be unclear and not very interesting, only one epoch with biggest displacements is presented here for idea about their values - Table 1. In next section the relation between displacements and temperature will be demonstrated.

3.1. Relation between displacement and temperature in the same time

First were calculated Pearson correlation coefficients between vertical displacements and temperature of air and structure in the same time. Calculation was applied only on eight points in the middle of main span, where the displacements were the biggest, all over 6 mm. The result, however, was not according to the expectations.

Correlation coefficients of these eight points are close to zero – Table 2, therefore they was not calculated for the remaining points. Very low values of correlation coefficients were caused by unknown time shift between temperature and structure changes. The time shift is visible in Figure 6. Extremes of both quantities are in different time – maximum of displacement is circa 5 hours after minimum of temperature. This time shift will be investigated.

Table 1: The epoch with biggest displacements

$\sigma_d = 1.1mm$	**Point number**															
Epoch 14	13	14	15	16	17	18	19	20	21	22	23	24	25	26	27	28
Displacement [mm]	2.4	2.3	3.3	4.5	5.2	6.2	6.7	7.3	7.0	6.6	5.8	4.9	4.0	2.9	2.1	2.3

Table 2: Correlation coefficients between displacements and temperature

Point	**24**	**23**	**22**	**21**	**20**	**19**	**18**	**17**	
Correlation coeficients	0,10	0,08	0,05	0,05	0,02	0,04	0,01	0,03	**With air temperature**
Correlation coeficients	0,10	0,08	0,05	0,05	0,02	0,04	0,01	0,03	**With structure tempertature**

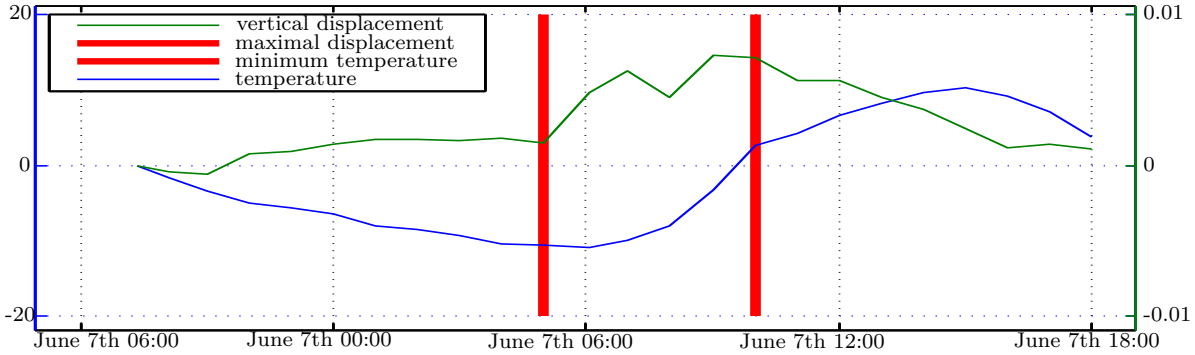

Figure 6: Time shift between displacements and temperature changes

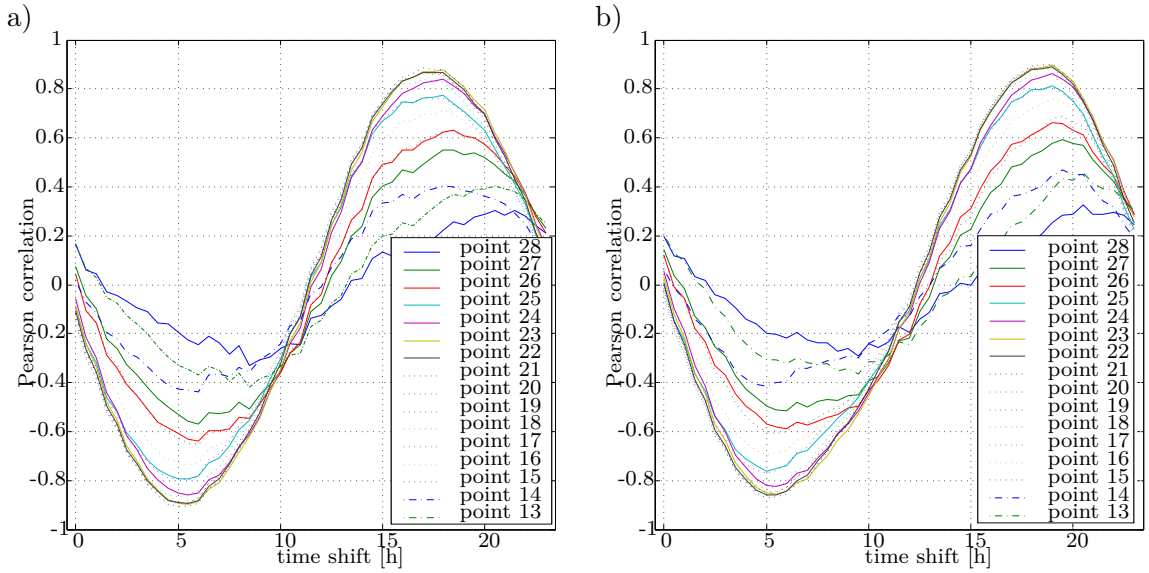

Figure 7: Time shift between displacements and a) air temperature changes b) structure temperature changes

3.2. Time shift between temperature and vertical displacement

Correlation function (from correlation coefficients) was used for determination of time shift between temperature changes and displacements of structure. The displacements were measured every hour, while the temperature was monitored almost continually. Correlation coefficient was calculated with time shift from 0 to 24 hour with step 0.5 hour. The course of correlation function depending on the time shift was obtained.

For both air temperature and structure temperature were correlation functions calculated. Graphs of functions were presented in Figure 7. These graphs are point symmetric and seem to be periodical, which corresponds to the assumptions.

The same functions are presented in Figure 8 in 3D graph. Here we can see that extremes of correlation function are greater in the middle of the main span, where displacements were greater, too.

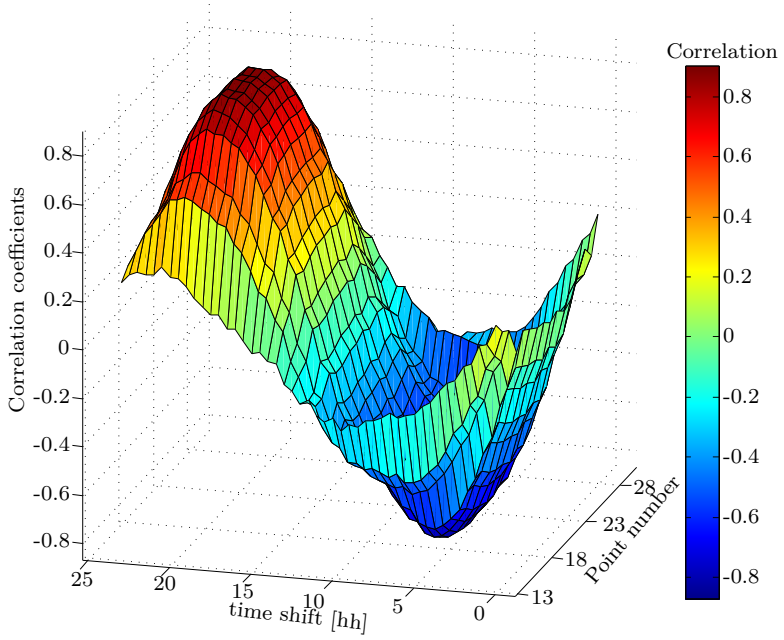

Figure 8: Time shift between displacements and temperature changes in 3D figure

Assuming, that correlation function is a period function with the period one day long we get two extremes of correlation function. If we compute exact time of both extremes, we get time shift and its supplement to one period. That gives us 2 values of time shift for each point.

Values of correlation function in its extremes were compared with critical value of Pearson correlation coefficient - (2).

$$r_k = \left(\frac{F_k}{n - 2 - F_k} \right)^{\frac{1}{2}} \tag{2}$$

r_k ..... critical value of correlation coefficient.
n ..... degrees of freedom.
F_k ..... critical value of F distribution.

For $n = 24$ (24 epochs of measurement) is $r_k = 0,413$.

If the value of correlation function was lower than its critical value, time shift from this point was not used for next computations. Correlation coefficient was significant at all points except point 28, which is situated above the support and its displacement was very small.

In Table 3 are values of extremes of correlation function and appropriate time shift for relation with temperature of air and structure both. There are both extremes of correlation functions and appropriate time shift. The time shift from minimum of correlation function fluctuate around five hours and the time shift from maximum of correlation function around 19 hours, which is supplement to 24 hours.

The time shift from all points is very consistent. Its values fluctuate between 5 and 6 hours. Only on point 13 the time shift is 8 and a half hour. But point 13 is situated identically like point 28 above the support and maximum of correlation function only slightly outperforms the critical value.

Table 3: Determining of time shift between temperature and structure deflections

	Point number	28	27	26	25	24	23	22	21	20	19	18	17	16	15	14	13	Average shift [h]
Air	r	0.30	0.55	0.63	0.77	0.84	0.88	0.87	0.88	0.87	0.87	0.84	0.77	0.71	0.63	0.40	0.40	5.4
	r	-0.33	-0.57	-0.64	-0.79	-0.86	-0.90	-0.89	-0.91	-0.89	-0.89	-0.87	-0.80	-0.74	-0.66	-0.44	-0.42	5.6
	Shift [h]		18.5	18.5	18.0	18.0	18.0	17.0	17.0	17.0	17.0	17.0	17.0	18.0	18.0			**5.5**
	Shift [h]		6.0	6.0	5.0	5.5	5.5	5.5	5.5	5.0	5.5	5.0	5.5	5.5	6.0	6.0	8.5	
Structure	r	0.33	0.59	0.66	0.81	0.86	0.90	0.89	0.90	0.89	0.89	0.86	0.81	0.76	0.69	0.47	0.46	4.9
	r	-0.29	-0.51	-0.59	-0.76	-0.82	-0.86	-0.86	-0.87	-0.86	-0.85	-0.84	-0.77	-0.70	-0.61	-0.42	-0.37	5.0
	Shift [h]		19.5	19.0	19.0	19.0	19.0	19.0	19.0	19.0	19.0	19.0	19.0	19.0	19.5	19.5	20.5	**5.5**
	Shift [h]		6.0	6.0	5.0	5.5	5.5	5.0	5.0	5.0	5.0	5.0	5.0	5.0	5.5	5.0		

Resultant time shift was calculated as a weighted average. The values of extremes of correlation functions were used as weight. The time shift between displacements of structure and their cause is five hours.

4. Conclusion

The direct correlation was found between vertical displacements and changes of both the air and structure temperature using Pearson correlation coefficient.

It was found that structure reacts to temperature changes with quite a delay. This time shift was calculated using course of the correlation function. Its values significantly outperform the critical value and are close to 1, which indicates functional dependency.

This time shift depends on the thermal transmittance of the structure and temperature difference and is not generally valid. It is necessary to consider the effect of this delay during precise measurement of bridges with large span like load tests. It may cause major inaccuracies and completely invalidate otherwise properly conducted measurement.

Acknowledgement

The article was written with support of the internal grants of Czech Technical University in Prague SGS15 “Optimization of acquisition and processing of 3D data for purpose of engineering surveying“

References

[1] Jaroslav Braun and Martin Štroner. “Geodetic Measurement of Longitudinal Displacements of the Railway Bridge”. In: *Geoinformatics FCE CTU* 12 (June 2014), pp. 16–21. DOI: 10.14311/gi.12.3.

[2] Ján Erdélyi et al. “Monitoring of a concrete roof using terrestrial laser scanning”. In: *Geoinformatics FCE CTU* 13 (Dec. 2014), pp. 25–30. DOI: 10.14311/gi.13.3.

[3] Ján Erdélyi et al. “Určovanie posunov a pretvorení železobetónových konštrukcií pomocou TLS”. In: *Geodézia, kartografia a geografické informačné systémy*. Košice: Technical University, BERG Faculty, 2012. ISBN: 978-80-553-1173-9.

[4] Václav Kvasnička. "Bridge over Elbe river in Litoměřice". In: *Structural concrete in the Czech Republic 2006-2009: national report of the Czech Republic : 3rd fib Congress Washington*. Prague: Czech Concrete Society, c2010, pp. 34–37. ISBN: 978-80-903806-0-8. URL: http://www.metrostav.cz/pdf/reference/CBS_NZ2010_06_PRINT.pdf.

[5] Ondřej Michal. "Analysis of deflection of the bridge construction". Master thesis. Czech Technical University in Prague, 2015. URL: http://geo.fsv.cvut.cz/proj/dp/2015/ondrej-michal-dp-2015.pdf.

[6] Ondřej Michal and Rudolf Urban. "Analýza technologie pro určování průhybové čáry mostních konstrukcí". In: *Grant Journal* 2.2 (2013). ISSN: 1805-062X. URL: http://www.grantjournal.com/issue/0201/PDF/0201urban.pdf.

[7] Martin Štroner and Miroslav Hampacher. *Zpracování a analýza měření v inženýrské geodézii*. Praha: CTU Publishing House, 2011, p. 313. ISBN: 978-80-01-04900-6.

[8] Milan Talich. "Přesné monitorování svislých průhybů mostních konstrukcí metodou pozemní radarové interferometrie". In: *XII. mezinárodní konference Geodézie a kartografie v dopravě, Olomouc 4.-5.9. 2014*. Český svaz geodetů a kartografů, 2014, pp. 75–88. ISBN: 978-80-02-02553-5.

[9] Rudolf Urban and Martin Štroner. "Measurement of deflection line on bridges". In: *Reports on Geodesy and Geoinformatics* 95.1 (Jan. 2013). DOI: 10.2478/rgg-2013-0013.

[10] Rudolf Urban, Martin Štroner, and Václav Jurga. "Development of Bridge Deflections in the 24-hours Cycle". In: *INGEO 2014*. Vol. 1. České vysoké učení technické v Praze, 2014, pp. 155–160. ISBN: 978-80-01-05469-7.

[11] Lukáš Vráblík, Martin Štroner, and Rudolf Urban. "Measurement of bridge body across the river Labe in Melnik". In: *Acta Montanistica Slovaca* (2009), pp. 79–85. ISSN: 1335-1788.